Streamflow reduction due to *Eucalyptus* plantations in the St. Lucia Catchment

C Viviers

22825606

Dissertation submitted in fulfilment of the requirements for the degree *Magister Scientia* in Environmental Sciences (specialising in Hydrology and Geohydrology) at the Potchefstroom Campus of the North-West University

Supervisor: Prof I Dennis

Co-supervisor : Dr SR Dennis

May 2017

Summary

Lake St. Lucia is an internationally recognized, vital estuary lake system that is the core feature of the iSimangaliso Wetland Park, a UNESCO World Heritage Site. Lake St. Lucia is situated within the study area. W32 is a tertiary catchment with extensive afforestation, most dominant in E32G and W32H. Inappropriate management of coastal aquifers may result in irreversible damage and destroy freshwater resources (Vaeret *et al.,* 2009). *Eucalyptus* tree roots will increase in depth if the soil moisture is more reliable at the increased depth and is not restricted by confining geology. Where the soil is deep and the groundwater table is approximately eight meters below the surface, a three year old *Eucalyptus* tree is most likely extracting water directly from the groundwater and the total evapotranspiration may likely exceed total precipitation (Benyon *et al.,* 2006; Von Roeder, 2014). Reference evapotranspiration (ET_0) and potential evapotranspiration (PET) are the same in the absence of water restrictions, which is the case where trees have tapping roots mining groundwater from an aquifer (Karisson & Pomade, 2004).

The ET_o rate of the *Eucalyptus* trees in the Lake St. Lucia study area were calculated using the Shuttleworth-Wallace (S&W) model (1985) as per example by Zhou *et al.* (2006), using 2014 and 2015 meteorological data. The S&W model quantified viable time variant data comparable to literature data, and with little variance within monthly simulated ET_o. The maximum average daily ET_o for 2014 and 2015 months' as simulated using the S&W model, is 6 mm/day, while the minimum average daily ET_o is 3.4 mm/day. The average monthly total ET_o for 2014 and 2015 has an 85 % correlation to the monthly ET estimated by the WRC (2016) for quaternary catchment W32H and an 84 % correlation to that of quaternary catchment W32G. The average annual simulated ET_o exceeds the annual average MAP, by a factor of 1.67.

Drawdown increases at a 3 % greater rate per year during drought in comparison to years with normal MAP. The drawdown continues to increase, without exception for every sequential year - for both normal rainfall and drought scenario's, correlating to the results from S&W that the annual ET exceeds the annual precipitation.

After six years of afforestation, the impact of afforestation, only considering normal rainfall circumstances, decreased streamflow most by 14.45 m^3/day at Zone 8. Zone 8 has afforestation along the whole western streamflow zone boundary. Zone 2 is reduced by 4 m^3/day and Zone 7's streamflow is reduced by 3 m^3/day when subjected to forestry's water needs - irrespective of receiving the MAP. Zones 4 and 9's streamflow do not reduce when receiving normal rainfall and is subjected to afforestation. Streamflow Zone 4 has no afforestation situated along it. Zone 9 flows out of Lake St. Lucia which is recharge by regional groundwater, precipitation and the inflow from the other streamflow zones; zone 9 does not have reduced streamflow even when subjected to drought and afforestation. The streamflow reduction ascribed to afforestation's impact is generally constant and not significantly greater due to drought, but adds to the steamflow reduction from the drought.

Key words

Lake St. Lucia; Shuttleworth-Wallace; Evapotranspiration*; Eucalyptus*; MODFLOW

Acknowledgements

All glory to our Heavenly Father. You never left me, and all success is only a product of Your undeserving mercy.

The following list, in no particular order, I acknowledge for they all have one common character - I found that they often believed in me, more than I did in myself, and that has made all the difference.

My greatest rock and without whom I would not be a fraction of who I am, my pappa

My best friend and the person that has to suffer the consequences of my entire Master's stress - my husband

My greatest mentor and supporter, my late godfather

My greatest prayer, my grandmother

My greatest examples, I can only strive to know as much, and one day juggle family and career so elegantly and loving as you, but you are examples that it can be done, my study promoters

"Failure is not because of a lack of knowledge, but a lack of will"

Vince Lombardi

Table of Contents

Chapter 1 Introduction 1

1.1. General Introduction 1

1.2. Research aims and objectives 4

1.3. Dissertation Layout 5

Chapter 2 Literature Review 6

2.1. Afforestation 6

2.1.1. Streamflow Reduction Activity Classification 6

2.1.2. Forestry establish in South Africa 6

2.1.3. *Eucalyptus* Trees 7

2.1.4. Hardwood and softwood rotation cycle 10

2.1.5. Timber trees' roots mine groundwater 11

2.1.6. Previous studies on *Eucalyptus* forestry's impact 13

2.1.7. Previous studies on forestry in the Lake St. Lucia study area 16

2.2. Analytical evapotranspiration methods 18

2.2.1. Pan-coefficient-based methods 20

Class A Pan Method 21

Pereira Model (1995) 21

FAO-based Pan Method (1996) 21

2.2.2. Temperature-based methods 22

FAO-24-Blaney-Criddle Method 22

Hargreaves Method (1975) 24

2.2.3. Mass-transfer-based methods 24

Rohwer Method (1931) 24

2.2.4. Radiation-Based Methods 24

Priestley-Taylor Model (1972) 24

FAO-24-Makkink Method (1957) 25

2.2.5. Combination Methods 26

Penman-Monteith-FAO-56 model (1998) 26

Shuttleworth-Wallace model (1985) 27

2.3. Numerical Groundwater Models Introduction 28

2.4. Groundwater Recharge 31

Chapter 3 Study Area Characterisation 33

3.1. Study Area Setting 33
3.2. Rainfall 35
3.3. Topography 38
3.4. Soil 39
3.5. Geology 40
3.6. Hydrological Setting 44
3.7. Ground- and surface water interaction 50
3.8. Conceptual Model 51
Chapter 4 Method of Investigation 54
4.1. Analytical Models 54
4.1.1. Saturated Volume Fluctuation Recharge Calculation Method 54
4.1.2. Chloride Mass Balance 55
4.1.3. Shuttleworth-Wallace analytical model 58
Climate-related parameters 58
Aerodynamic Resistances 60
Bulk stomatal, boundary layer and surface resistances 62
Net radiations over vegetation canopy, substrate soil surface and soil heat flux 63
Vegetation parameters 65
Simulating ET_0 with the S&W model 65
4.2. Numerical Modelling 66
Finite Difference Network generation 66
Boundary conditions 67
Initial hydraulic head 69
Sources and sinks 69
Aquifer parameters 71
Assumptions summary 71
Calibration steady state 73
Calibration transient state 75
Scenarios 77
Chapter 5 Results and Discussion 78
5.1. Shuttleworth and Wallace Model 78
5.2. MODFLOW Numerical Model 83
ET_o's impact on groundwater drawdown at observation point and regionally 83
ET_o's impact on groundwater flow quantities west and south of lake 88
ET_o's impact on each streamflow zone 89

Chapter 6 Conclusions 97
6.1. Shuttleworth - Wallace Analytical Model 97
6.2. Numerical Modelling 98
Bibliography 100

List of Figures

Figure 1:1: Distribution of land use types across South Africa (DAFF, 2016) 1
Figure 1:2 KZN's land use for different practices (DAFF, 2016) 2
Figure 1:3 Afforested areas per province (DAFF, 2016) 2
Figure 2:1 Predicted *Eucalyptus* tree heights per age according to Singh *et al.* (2014) 9
Figure 2:2 Afforestation's areas of softwood and hardwood species per tree age for 2011/2012 (DWA, 2014) 11
Figure 2:3: Lake St. Lucia's water levels and immediate vegetation cover change as visual from NDVI (Esri, 2016) 17
Figure 2:4: Water body boundary and land development with time (Esri, 2016) 18
Figure 3:1: Locality Map 34
Figure 3:2: MAP comparison for the different rain stations as well as monthly, average minimum and maximum temperatures of station 684910 36
Figure 3:3: Data stations and surface hydrology across topography 37
Figure 3:4 Linear correlation between topography and groundwater hydraulic head 38
Figure 3:5: Surface geology and cross section locality map (Esri, 2016) 42
Figure 3:6 Geological cross section along line in Figure 3:5 44
Figure 3:7 Localities of time series boreholes over magnetic regional imagery 47
Figure 3:8 Time Series Groundwater Level Data for boreholes in study area (NGA and DWS data) 49
Figure 3:9 Groundwater flow direction, forestry, river and lake locations, and unconsolidated layer over confined layer 52
Figure 4:1 SVF Recharge Simulation for Alluvium Surface Geology 55
Figure 4:2 MODFLOW grid and boundary conditions 68
Figure 4:3 Initial regional hydraulic heads and observation borehole localities 70
Figure 4:4 Simplified recharge and hydrological zones for steady state calibration 72
Figure 4:5 Correlation between observed and simulated groundwater hydraulic heads (steady state) 74
Figure 4:6 Pattern similarity between the hydraulic heads measured and those simulated in steady state calibration 74
Figure 4:7 Transient state groundwater recharge and geo-hydrological zones 76
Figure 4:8 Correlation between observed and simulated groundwater hydraulic heads (transient state) 77
Figure 4:9 Pattern similarity between the hydraulic heads measured and those simulated in transient state calibration 77
Figure 5:1Simulated ET_o to mean daily temperatures correlation 78
Figure 5:2Simulated ET_o to mean daily wind speed correlation 79
Figure 5:3 S&W daily ET_0 for 2014 and 2015 80
Figure 5:4 Correlation between monthly S&W ET_o and that from WRC (2016) for W32G and W32H 83
Figure 5:5 Observation point A's drawdown for the normal and drought scenario 84
Figure 5:6 Drawdown distributions across study area 2 years since afforestation 85
Figure 5:7 Drawdown distribution across study area 4 years since afforestation 86
Figure 5:8 Drawdown distribution across study area 6 years since afforestation 87
Figure 5:9 Water flow quantity difference for sequential year of afforestation from previous year 88

Figure 5:10 Zone 1 streamflow for scenario's across six years duration 90
Figure 5:11 Zone 2 streamflow for scenario's across six years duration 91
Figure 5:12 Zone 3 streamflow for scenario's across six years duration 91
Figure 5:13 Zone 4 streamflow for scenario's across six years duration 92
Figure 5:14 Zone 5 streamflow for scenario's across six years duration 92
Figure 5:15 Zone 6 streamflow for scenario's across six years duration 93
Figure 5:16 Zone 7 streamflow for scenario's across six years duration 93
Figure 5:17 Zone 8 streamflow for scenario's across six years duration 94
Figure 5:18 Zone 9 streamflow for scenario's across six years duration 94
Figure 5:19 Zones for quantification of afforestation's impact on streamflow 95
Figure 5:20 The difference between streamflow subjected to afforestation and not subjected to afforestation (sixth year of afforestation) 96

List of Tables

Table 3:1 Average monthly precipitation per rain station 36
Table 3:2: Average monthly river and lake water level per monitoring station and percentile of annual precipitation for month 46
Table 3:3 Groundwater contributions to river flow according to Herold Method (Baseflow) 50
Table 4:1 Percentage groundwater recharge per geological unit in each quaternary catchment 57
Table 4:2 Initial hydraulic parameters input data for the different geological units (steady state) 71
Table 4:3 Transient state calibrated parameters 75
Table 5:1 Average monthly ET_0, data completeness and coefficient of variance 81
Table 5:2 Monthly and annual S&W simulated and WRC (2016) ET_0 82
Table 5:3 Average monthly ET_o from 2014 and 2015 S&W calculated model applied to MODFLOW 82
Table 5:4 Water flowing from Lake St. Lucia to afforested areas 88
Table 5:5 Factors by which the quantity decreased since the previous year of afforestation 89

List of Mathematical Equations

Equation 2:1 Pereira model evapotranspiration (Racz *et al.*, 2013) 21
Equation 2:2 Pereira model pan coefficient (Racz *et al.,* 2013) 21
Equation 2:3 FAO-56 pan coefficient (1998) (Allen *et al.,* 2006) 22
Equation 2:4 Primitive Blaney-Criddle reference evapotranspiration (1950) 23
Equation 2:5 FAO-56-model refined with Blaney-Criddle (Xu & Singh*,* 2002*;* Racz *et al.,* 2013*)* 23
Equation 2:6 Blaney-Criddle FAO-56 modification parameter a_1 (Racz *et al.,* 2013) 24
Equation 2:7 Blaney-Criddle FAO-56 modification parameter b_1 (Racz *et al.,* 2013) 24
Equation 2:8 Hangreaves and Samani improved method (Xu & Singh, 2002) 24
Equation 2:9 Rohwer's adaption of the Daltonian method for estimating evaporation (Xu and Singh, 2002) 24
Equation 2:10 Priestley and Taylor reference evapotranspiration model (Racz *et al.*, 2013) 25
Equation 2:11 Dimensionless coefficient for Priestley and Taylor model (Racz *et al.*, 2013) 25
Equation 2:12 Makkink (1957) original model 25
Equation 2:13 Makkink-FAO-24 reference evapotranspiration method 25
Equation 2:14 Correction factor for Makkink-FAO-24-Method 26
Equation 2:15 Correction factor for Makkink-FAO-24-Method 26
Equation 2:16 Hansen's version of Makkink-Model (1984)984) 26
Equation 2:17 Penman-Monteith-FAO-56-model (Racz *et al.*, 2013) 27
Equation 2:18 Shuttleworth-Wallace Model 27
Equation 2:19 Steady state groundwater flow equation 31
Equation 2:20 Transient state groundwater flow equation 31
Equation 4:1 Saturated Volume Fluctuation (Van Tonder & Xu, 2000; Adams *et al.,* 2004) 55
Equation 4:2 Groundwater's recharge calculation CMB Method (Adams *et al.*, 2004) 56
Equation 4:3 Recharge in m/d (Adams *et al.,* 2004). 56
Equation 4:4 Latent heat of vaporization (Racz *et al.,* 2013) 59
Equation 4:5: Saturation vapour pressure at the specific temperature 59
Equation 4:6 Saturation vapour pressures 59
Equation 4:7 Slope vapour pressure curve (Raes, 2009) 59
Equation 4:8 Psychometric constant (Raes, 2009) 59
Equation 4:9 Mean air density at constant pressure 59
Equation 4:10 Atmospheric pressure (Raes, 2009) 60
Equation 4:11 Aerodynamic resistance from the soil to canopy 60
Equation 4:12 Aerodynamic resistance from the canopy to the reference height 60
Equation 4:13 Eddy diffusion coefficient at the top of canopy 61
Equation 4:14 Friction velocity 61
Equation 4:15 Zero plane displacement of the canopy 61
Equation 4:16 Preferred roughness length of the canopy 61
Equation 4:17 Wind speed at the reference height 61
Equation 4:18 Height of observation 61
Equation 4:19 Bulk stomatal resistance of the canopy method 1 62
Equation 4:20 Shielding factor for Equation 4:19 62
Equation 4:21 Bulk stomatal resistance of the canopy method 2 62
Equation 4:22 Bulk resistance of the boundary layer 63
Equation 4:23 Hydraulic resistance of the concentrated boundary layer 63

Equation 4:24 Net radiation above canopy 64
Equation 4:25 Net radiation to soil surface 64
Equation 4:26 Albedo of land surface 64
Equation 4:27 Net loss of long wave radiation energy to atmosphere 64
Equation 4:28 Actual vapour pressure 64
Equation 4:29 Radiation reaching soil surface 64
Equation 4:30 Leaf area index 65
Equation 4:31 Ratio of hemispheric reflectance for near infrared light to that for visible light 65
Equation 4:32 Fraction of photo-synthetically active radiation 65
Equation 4:33 Reference evapotranspiration (S&W) 66
Equation 4:34 Evaporation from soil 66
Equation 4:35 Transpiration from canopy 66
Equation 4:36 Closed canopy transpiration weighting coefficients 66
Equation 4:37 Bare substrate evaporation weighting coefficients 66

List of Mathematical Variables

Variable	Symbol	Applicable Equation No.	Unit
Reference evapotranspiration	ET_0	2.1;2.4;2.5;2.8;2.9;2.10;2.12;2.13; 2.16;2.17;2.18;4.33	mm/d
Pan coefficient	K_p	2.1;2.2;2.3	-
Pan measured evapotranspiration	E_p	2.1	mm/day
Slope vapour pressure curve	Δ	2.2;2.10;2.11;2.12;2.13;2.16; 2.17;4.7;4.34;4.35	kPa/°C
Psychometric constant	γ	2.2;2.10;2.11;2.12;2.13;2.16;2.17; 4.8;4.34;4.35	kPa/°C
Daily mean wind speed at reference height 2 m above ground surface	u_2	2.2;2.3;2.9;2.17	km/day
Specific heat at constant pressure	C_p	4.8;4.34;4.35	MJ/kg/°C
Atmospheric pressure assuming 20 °C for a standard atmosphere	P	4.8;4.9;4.10	kPa
Ratio molecular weight of water vapour/dry air	ε	4.8	-
Latent heat of vaporization	λ	2.10;2.12;2.13;2.16;2.18;4.4;4.8; 4.33	MJ/kg
Elevation above sea level	z	4.10	m.a.m.s.l.
Average daily relative humidity	RH_{mean}	2.3;2.15;4.28	%
Fetch; Distance of the identified surface type	FET	2.3	-
Relative sunshine duration	$(\frac{n}{N})$	2.6; 2.7;	-
Daily minimum of relative humidity	RH_{min}	2.6; 2.7	%
Mean wind speed of daylight hours	u_2d	2.7;2.15	m/s
Mean daily temperatures	T_{mean}	2.4; 2.5; 2.8; 2.17;4.4;4.5;4.7; 4.9	°C
Mean daily percentage of annual daytime hours	p	2.5	%
Parameters for equations	a_1 and b_1	2.5;2.6 ;2.7	-
Hangreaves parameter	a	2.8	-
Extra-terrestrial radiation expressed in equivalent evaporation units	R_a	2.8	-
Maximum daily temperature	T_{max}	2.8;4.6;4.27;4.28	°C/K
Minimum daily temperature	T_{min}	2.8;4.6;4.27;4.28	°C/K
Saturation vapour pressure	e_s	2.9;2.17;4.6;4.34;4.35	mmHg or kPa
Actual vapour pressure	e_a	2.9;2.17;4.27;4.28;4.34;4.35	mmHg or kPa
Priestley-Taylor Coefficient	α	2.10; 2.11	-
Net radiation	R_n	2.10;2.17;4.34;4.35	$MJ/m^2/day$
Soil heat flux	G	2.10;2.17;4.34;4.35	$MJ/m^2/day$
Canopy resistance	r_c	2.11	s/m
Aerodynamic resistance	r_a	2.11	s/m
Parameters for equations	a_2 and b_2	2.13;2.14;2.15	-
Parameters for equations	c_0, c_1, c_2, c_3, c_4, c_5	2.15	-
Global radiation	R_g	2.12;2.13;2.16	$cal/m^2/day$
Head in month i	h[i]	4.1	m

Variable	Symbol	Applicable Equation No.	Unit
Head in previous month	h[i-1]	4.1	m
Recharge percentage in month i	Recharge	4.1;4.2;4.3	%
Fraction of precipitation	Precip[i]	4.1	m
Inflow in month i	Inflow [i]	4.1	m^3/month
Outflow in month i	Outflow[i]	4.1	m^3/month
Abstraction in month i	Abstract[i]	4.1	m^3/month
Area of aquifer	Area	4.1	m^2
Specific Yield	S_y	4.1	-
Saturation vapour pressure at temperature	e^0	4.5;4.6;4.28	kPa
Mean air density at constant pressure	ρ	4.9;4.34;4.35	kg/m^3
Specific gas constant	R	4.9	kJ/kg/K
Air virtual temperature	T_{kv}	4.9	Kelvin
Aerodynamic resistance from soil to canopy	r^s_a	4.11;4.34	-
Aerodynamic resistance from canopy to reference height	r^a_a	4.12;4.34;4.35	-
Vegetation height	h_c	4.11;4.12;4.13;4.15;4.16	m
Eddy diffusivity decay constant of the vegetation	n	4.11;4.12;4.23	
Eddy diffusion coefficient at the top of canopy	K_h	4.11;4.12;4.13	m^2/s
Von Karman's constant	κ	4.12;4.13;4.14	-
Friction velocity	u_*	4.12;4.13;4.14	m/s
Zero plane displacement of the canopy	d_0	4.12;4.13;4.14;4.15;4.16;4.17	m
Reference height 2 m above vegetation	z_a	4.12;4.14;4.17	m
Wind speed observed at the weather station	u_w	4.17;	m/s
Preferred roughness length of the canopy	z_0	4.12;4.14;4.17;	m
Wind speed at the reference height	u_a	4.14;4.17	m/s
Roughness length of a closed canopy	z_{0c}	4.11;4.15;4.16	m
Roughness length of the ground	z_{og}	4.11	m
Preferred zero plane displacement	d_p	4.11;4.12	m
Height of internal boundary layer	z_b	4.17;4.18	m
Fetch at the weather stations	F_w	4.18	m
Roughness length	z_{0w}	4.17;4.18	m
Height of observation	z_w	4.17	m
Bulk resistance of canopy stomatal	r^c_s	4.19;4.21;4.35	s/m
Bulk resistance of boundary layer	r^c_a	4.22;4.34;4.35	s/m
Hydraulic resistance of the concentrated boundary layer	r_b	4.22;4.23	s/m
Shielding factor	$σ_b$	4.22	-
Canopy characteristic leaf width	w_{max}	4.23	m
Wind speed at top of canopy	u_h	4.23	m/s
Soil surface resistance	r^s_s	4.34	s/m
Net radiation above canopy	R_n	4.24;4.29;4.34	MJ/m^2/d
Albedo of land surface	α	4.25;4.26	-

Variable	Symbol	Applicable Equation No.	Unit
Solar radiation	R_{solar}	4.25;4.27	$MJ/m^2/d$
Net radiation to soil surface	R_{ns}	4.24;4.25	$MJ/m^2/d$
Net loss of long wave radiation energy to atmosphere	R_{nl}	4.24;4.27	$MJ/m^2/d$
Clear sky solar radiation	R^0_{solar}	4.27	$MJ/m^2/d$
Albedo corresponding to the closed canopy	α_m	4.26	-
Albedo corresponding to the bare soil	α_s	4.26	-
Stefan-Boltzmann constant	σ	4.27	$MJ/K^4/m^2/d$
Extinction coefficient of vegetation for net radiation	C_r	4.29	-
Radiation reaching soil surface	R^s_n	4.29;4.34;4.35	$MJ/m^2/d$
Maximum LAI when the vegetation develops fully	LAI_{max}	4.30	-
Fraction of photo-synthetically active radiation	FPAR	4.30;4.32	-
Fraction of photo-synthetically active radiation maximum	$FPAR_{max}$	4.30;4.32	-
Fraction of clumped vegetation	F_{cl}	4.30	-
Ratio of hemispheric reflectance for near infrared light to that for visible light	SR	4.31;4.32	-
Normalized Difference Vegetation Index	NDVI	4.31	-
5 % of NDVI population	SR_{min}	4.32	-
98 % of NDVI population	SR_{max}	4.32	-
Leaf area index	LAI	4.19;4.20;4.22;4.26;4.29;4.30	-
Fraction of photo-synthetically active radiation minimum	$FPAR_{min}$	4.32	-
Evaporation from soil	ET_s	2.18;4.33;4.34	mm/day
Transpiration from canopy	ET_c	2.18;4.33;4.35	mm/day
Bare substrate evaporation weighting coefficients	C_s	2.18;4.33;4.37	-
Closed canopy transpiration weighting coefficients	C_c	2.18;4.33;4.36	-
S&W weighing coefficients input parameters	R_s; R_a; R_c	4.36;4.37	-
Mean stomatal resistance	r_{ST}	4.19;4.21	s/m
Shielding factor	σ_c	4.19;4.20	-
Effective leaf area index	LAIe	4.21	-

Variable	Symbol	Applicable Equation No.	Unit
Mean air temperature in previous month	T_{i+1}		°C
Mean air temperature in next month	Ti-1		°C
Hydraulic head	h	2.19;2.20	m
Hydraulic conductivity in spatial coordination	K_x, K_y, K_z	2.19;2.20;	m/d
Storage coefficient	S	2.20;	-
Time	t	2.20;	days
Source/Sink	W	2.19;2.20	m^3/day
Spatial coordination	x, y, z	2.19;2.20	-

List of Acronyms

2D	Two Dimensional
3D	Three Dimensional
3DFEMFAT	Finite Element Model of Flow and Transport
ASCE	American Society of Civil Engineers
CDM	Camp Dresser & McKee
CMB	Chloride Mass Balance
CSR	Climatologically Solar Radiation
DAFF	Department of Agriculture, Forestry and Fishing
DNI	Direct Normal Irradiation
DWA	Department of Water Affairs
DWAF	Department of Water and Forestry
DWS	Department of Water and Sanitation
ESRI	Environmental Systems Research Institute
ET	Evapotranspiration
ET_o	Reference Evapotranspiration
FAO	Food and Agricultural Organization
GDP	Gross Domestic Product
GHI	Global Horizontal Irradiation
GRA	Groundwater Resource Assessment
KZN	KwaZulu-Natal
LAI	Leaf Area Index
LAI_e	Effective Leaf Area Index
LAI_{max}	Maximum Leaf Area Index
MAP	Mean Annual Precipitation
NDVI	Normalized Difference Vegetation Index
NGA	National Groundwater Database
NREL	National Renewable Energy Laboratory
NWA	National Water Act
NWRS	National Water Resources Strategy
PET	Potential Evapotranspiration
PMWIN	Processing MODFLOW for Windows
RASA	Regional Aquifer System Analysis
S&W	Shuttleworth and Wallace
SA	South Africa
SAPPI	South African Pulp and Paper Industries
SAWS	South African Weather Service

SFRA	Streamflow Reduction Activity
SVF	Saturated Volume Fluctuation Method
UCOSP	uMfolozi Sugar Planters
UNESCO	United Nations Educational, Scientific and Cultural Organization
USGS	United States Geological Survey
VPD	Vapour Pressure Deficit
WARMS	Water Authorisation and Registration Management System
WCDMS	Water Conservation and Demand Management Strategy
WRC	Water Research Commission
ZFP	Zero Flux Plane

Chapter 1 Introduction

1.1. General Introduction

Forestry in South Africa (SA) dates back to 1656 when Jan Van Riebeeck imported various trees to be planted for settler's firewood when the Cape Region's natural forests had already been depleted. (Campbell & Moll, 1977). In 1663, the settlers started to exploit regions for forestry, and in 1711 they discovered the now known Knysna Woods (Zahn & Neetling, 1926). The Knysna woods were depleted to the extent that by 1883 the first regulations were issued for the systematic management of the forests (Zahn & Neetling, 1926). In 1875, the appointed superintendent ordered that the first *Eucalyptus* tree plantation be developed in Worcester in 1876. The first 408 ha of trees were planted in 1889 in the Cape Colony (Campbell & Moll, 1977).

Present reports by Department of Agriculture, Forestry and Fishery (DAFF) (2016) indicate that of the 122.3 million hectares of land being used in SA, only 1% is being occupied by forestry (Figure 1:1). In KwaZulu-Natal (KZN) 5.5% of the total land is being used for forestry (DAFF, 2016) (Figure 1:2). Forestry accounts for 1 % of SA's gross domestic product (GDP), and 40.6 % of this 1 %, is from KZN alone (Figure 1:3).

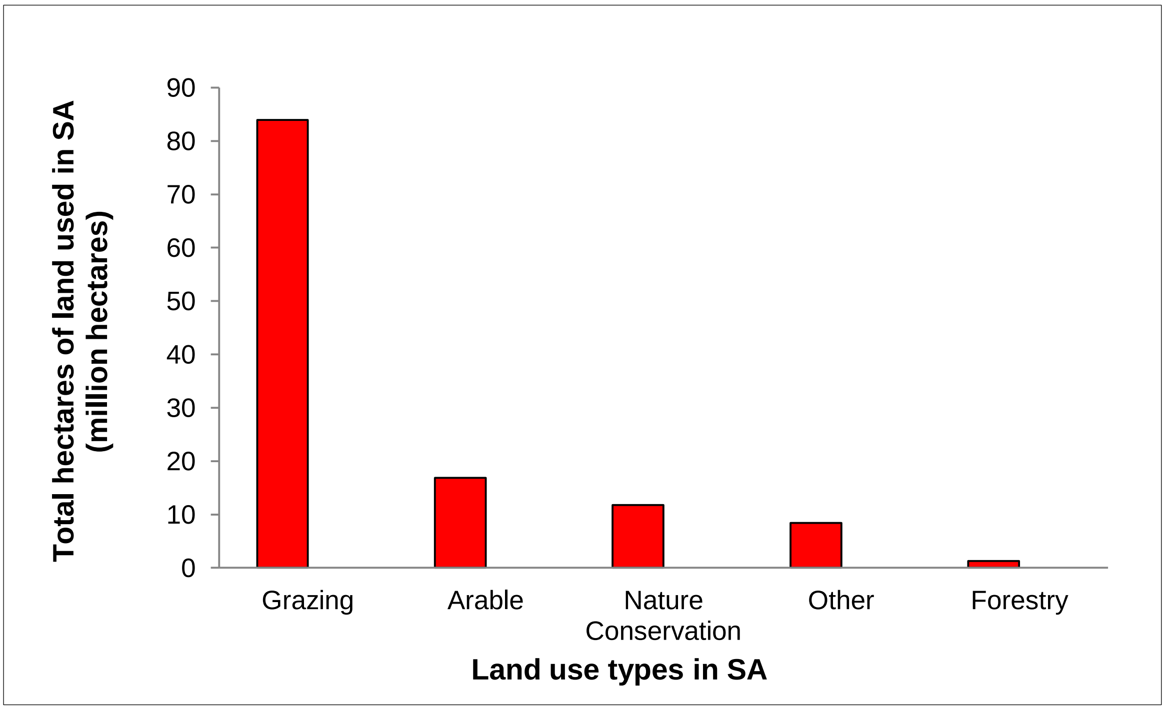

Figure 1:1: Distribution of land use types across South Africa (DAFF, 2016)

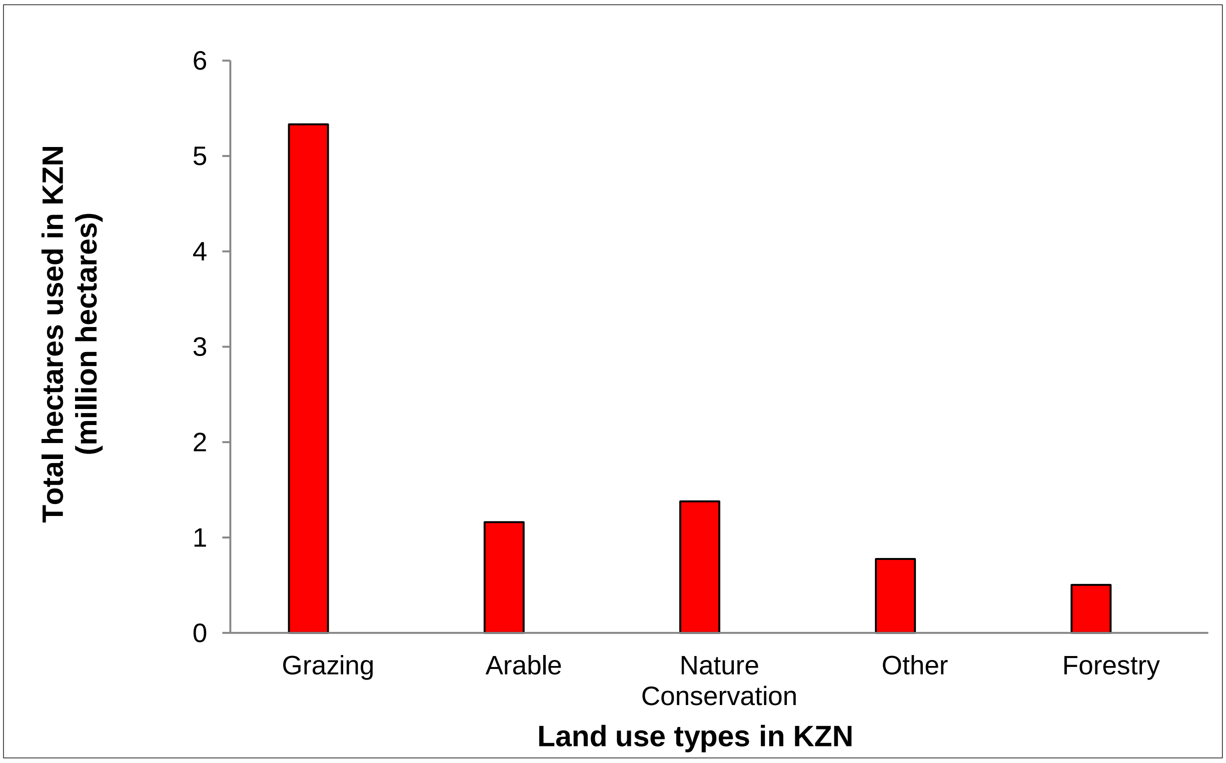

Figure 1:2 KZN's land use for different practices (DAFF, 2016)

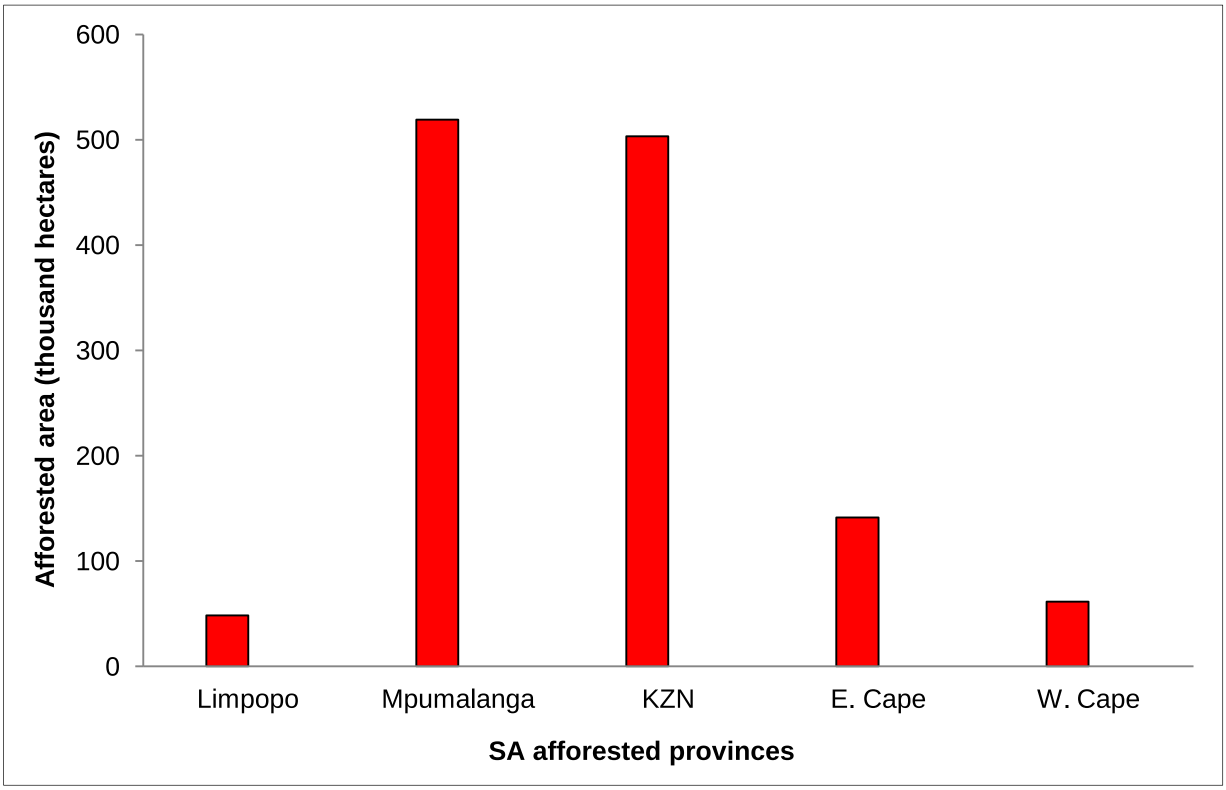

Figure 1:3 Afforested areas per province (DAFF, 2016)

Eucalyptus trees are one of the most popular trees being planted in SA due to its vigorous growth and heat tolerant capabilities (Meadows, 1999).

Eucalyptus evapotranspiration (ET) is dependent on the atmospheric demand (maximum potential evapotranspiration), while the actual ET is a function of the availability of water to meet the atmospheric demand (Kelbe and Germishuyse, 2010). In KZN specifically, the deep sinker roots commonly extent into the primary aquifer, accessing a groundwater resource for ET to meet the maximum potential evapotranspiration rate (Coppen, 2002; Von Roeder, 2014). A model by Kiezle and Schulze in 1992, simulating the impact of *Eucalyptus* afforestation on the groundwater in northern KZN, concluded the water table's drawdown to be 4 m, 6 m, and 12 m as dependent on the maximum root depths of the trees as reported by Von Roeder (2014).

In 2004, South Africa was listed the eleventh out of 150 countries with the least amount of renewable water available per person (Kelbe *et al.*, 2013a; Kelbe and Germishuyse, 2010). South Africa receives an average annual rainfall of 450 mm (Von Roeder, 2014).

The magnitude and distribution changes in ET, has the greatest direct impact on a catchment's eco-hydrology, and consequently streamflow and water quality (Lu *et al.*, 2003). Cyrus *et al.* (2011) report that high ET rates further reduced water levels during the estuary mouth closure in 2002 for almost 5 years. Water resource management regarding forestry is essential as sufficient water serves as a method of poverty mitigation and the storage thereof is a limiting factor to economic growth (Weitz and Demlie, 2014). Water is the key constraint to SA's economic growth, and thus an increase in pressure for efficient and sustainable management of this resource is experienced (Le Maitre *et al.*, 2002). The Department of Water Affairs and Forestry (DWAF) (2000) reports that forestry multiplies downstream activities by a factor of six. Forestry serves as an excellent rural development catalyst - while only 10 % of the output is unbeneficial (DWAF, 2000).

The potential evapotranspiration (PET) of *Eucalyptus* trees are quantified using the analytical Shuttleworth-Wallace (S&W) model, while groundwater recharge is calculated using the Saturated Volume Fluctuation (SVF) and Chloride Mass Balance Method (CMB). These analytically calculated parameters are then used as input to a single layered, numerical model, which is calibrated to the measured field groundwater levels. The rivers and regional groundwater is simulated as head dependent to quantify the change in groundwater levels in reaction to the ET for *Eucalyptus* trees.

1.2. Research aims and objectives

1. Limit assumptions in the numerical model through the implementation of analytical models:
    - research various analytical ET_0 models to select the most relevant model as dependent on the model's input data requirements, - sensitivity and historical evaluations
    - simulate viable transient (monthly) ET_0 rates for *Eucalyptus* plantations
    - evaluate the selected ET_0 model's viability/stability/sensitivity
    - quantify the most accurate spatial variant groundwater recharge rates by using the SVF method where sufficient data is available and the CMB method where groundwater chemical analysis are available
2. Conceptualize a model for quaternary catchment W32H within which Lake St. Lucia is situated, and the immediate catchments enclosing catchment W32H for a regional approach:
    - interpolate NGA borehole log data, literature examples and surface geology maps to compose a cross section
3. Simulate a numerical model (with analytical simulated, transient input data where possible) representative of the geohydrological environment of the Lake St. Lucia catchment:
    - numerical model calibrated to a correlation accuracy greater than 70 % between the simulated hydraulic heads and the observed hydraulic heads for steady state and transient state
4. Simulate numerical modelling scenario's to quantify the impacts of *Eucalyptus* plantations' ET_0 on:
    - regional and local drawdown when recharged assuming normal annual precipitation as appose to only 30 % of the normal annual precipitation during drought, across 6 sequential years of afforestation
    - regional groundwater flow when recharged assuming normal annual precipitation as appose to only 30 % of the normal annual precipitation during drought, across 6 sequential years of afforestation
    - streamflow for 9 distinctive surface drainage zones, when recharged assuming normal annual precipitation as appose to only 30 % of the normal annual precipitation during drought across 6 sequential years of afforestation

1.3. Dissertation Layout

Chapter 2, Introduction, reviews the following:

- Afforestation's:
  - History, relevance and characterisation of afforestation in South Africa;
  - Previous studies specific to *Eucalyptus*' impact on ground - or surface water and
  - Previous studies specific to afforestation's impact in the study area.
- Analytical evapotranspiration method's:
  - Data input requirements (different model types) and
  - Efficiency and relevance of different methods
- Numerical groundwater model's:
  - Model's advantages and
  - Model's disadvantages
- Groundwater recharge estimation method's:
  - Data input requirements;
  - Accuracy level and applicability and
  - Required data's costs and availability

Chapter 3, Study Area Characterisation, reviews the:

- The study area's
  - Setting;
  - Meteorological character;
  - Topography, soil and geology environment;
  - Hydrological setting;
  - Groundwater and surface water interaction relevant to the study area and
  - Conceptual model in consideration of the review.

Chapter 4, Method of Investigation, reviews the following:

- S&W analytical model's:
  - S&W analytical model - daily and monthly average simulated ET_o results
- Numerical model's
  - Drawdown during drought and normal precipitation years in afforested study area
  - Water flow from lake to afforested areas during drought and normal precipitation years
  - Streamflow during drought and normal precipitation years
  - Streamflow during drought and normal precipitation years when subjected to afforestation

Chapter 5 reviews the Results and Discussion and Chapter 6 the Conclusions.

Chapter 2 Literature Review

2.1. Afforestation

2.1.1. Streamflow Reduction Activity Classification

Forestry is declared a Streamflow Reduction Activity (SFRA) in Section 36 of the National Water Act (NWA). Prior to 1998, groundwater rights were reserved exclusively for the land owner as groundwater was not recognized for the significant resource it truly is. As a result, little research regarding forestry's impact on groundwater, its importance and the management thereof was conducted prior to 1998 (Kelbe *et al.*, 2013a). The South African National Water Policy acknowledges that water resources cannot be managed in isolation. The NWA of 1998 recognises water as part of the hydrological system, belonging to the nation as regulated by the central government on a regional level (Kelbe *et al.*, 2013a; Scott & Lesch, 1997). The NWA (1998) obligates the Ministry of the Department of Water and Sanitation (DWS) to develop a National Water Resources Strategy (NWRS). The implementation success of this strategy, and other strategies such as the Water Conservation and Demand Management Strategy (WCDMS) for the forest sector in SA, is dependent upon our understanding of forests' interaction with water resources (Calder, 2007; Clulow *et al.*, 2011; Kelbe *et al.*, 2013a).

A SFRA is "*any dry land use practice which reduces the yield of water (with reference to yield from natural veld in undisturbed condition) from that land to downstream users. Such activities may be declared as SFRAs if found to be significant."* SFRAs require licensing. Although afforestation development has been controlled through limited licence allocation during the last decade, it has still increased (Kelbe *et al.*, 2013a).

2.1.2. Forestry establish in South Africa

The DAFF describes forest plantations as "*a man-made forest which provides industrial timber products including saw logs and mining timber*" (DAFF, 2011).

In 1828, the first *Eucalyptus* tree (*Eucalyptus globulus*) was introduced to SA by the Cape Colony's Governor, but it was not until 1875 that the first timber plantations were established in SA (Campbell & Moll, 1977; Sappi, 2005; Von Roeder, 2014). Sir David Hutchins introduced *Pinus patula* into SA in 1907 by planting a block in the Western Cape Province (Sappi, 2005 & Von Roeder, 2014).

More than 21 *Eucalyptus* species had been introduced into the Cape Colony by 1875. Eucalypts expanded from the Cape Province to the then Transvaal (Limpopo -, Mpumalanga -, Gauteng - and North-West Province), the Orange Free State (Free State Province) and to Lesotho by 1881 (Campbell & Moll, 1977; Sappi, 2005). The first economical employment of *Eucalyptus* trees, in SA, is only documented in 1953 (Rawlins, 1991; Von Roeder, 2014). *Eucalyptus* species are indigenous to the Australasian region, and while the first tree was only described in 1788, 80 years later already 135 different species of the genus were known. Since then, more than 600 species have been added to the *Eucalyptus* genus list, of which 20 have become internationally important due to its timber practicality and suitability as reported by South African Pulp and Paper Industries (Sappi) (2005). Many species that were once favoured, have been disregarded due to pest and disease vulnerability, poor environmental adaptation or inadequate wood properties (Sappi, 2005). *E. grandis* has been favoured as the most important hardwood for SA's industry (Sappi, 2005).

The maximum plantation productivity capacity is dependent on the locality's ability to supply the resources required for maximum tree growth, combined with the tree's ability to obtain these resources (Battaglia *et al.*, 1997). Cloning and hybrid programs have made it possible for companies like Sappi and Mondi to expand tree plantations in SA to previously unfavourable geographic sites (Meadows, 1999; Sappi, 2005 & Sappi, 2012). *Pinus patula* and *Pinus elliotii* are the most abundant softwood species cultivated while *Eucalyptus grandis* is the predominant hardwood specie planted in SA (Meadows, 1999; Sappi, 2005 & Sappi, 2012).

Pine plantations cover 52.5 % of the South African afforested land surface, *Eucalyptus* 39.1 % and Wattle trees comprise 7.6 % of the total afforested area (Dye, 2013). According to the Department of Water Affairs' (DWA) South African Forestry and Forest Products Industry Facts published in 2014, the majority of KZN's afforested area, 72.2 % (362 540 ha) is afforested by hardwood species and only 27.8 % is afforested by softwood species (DWA, 2014). Off the total KZN afforested area, 169 774 ha (46.8%) is *Eucalyptus grandis* (DWA, 2014).

2.1.3. *Eucalyptus* Trees

Eucalypts grandis' flourishes in a humid to sub-humid environment with annual temperatures higher than 17 °C and an annual rainfall higher than 900 mm, along with minimum frost occurrences (Sappi, 2012). Eucalypts trees are adaptable to various climates and have a high tolerance to sodicity, salinity and water logging (Singh *et al.*, 2014). *Eucalyptus* trees can grow in a sandy soil with a high pH of around 11, a clay soil with a pH of around 9.2 and in a loamy soil with a pH of 8.8 (Singh *et al.*, 2014).

Eucalypts trees are classified as angiosperms meaning that they flower and produce fruits with seeds, while Pines are gymnosperms, meaning that the seeds produced are not inside a fruit but outside attached to a pine cone (Sappi, 2012).

Eucalypts trees are the most valuable and widely planted forest planted tree species in the world because they are fast growing. Eucalypts have an average annual growth rate of $100m^3$/ha/year (Von Roeder, 2014). *Eucalyptus* trees are not indigenous to SA, and consequently free from threats or growth reduction from native diseases and pests (Scott & Lesch, 1997).

The *E. grandis*' tree bark is characterised as rough and persistent at the base while becoming more flaking and thinner to the top of the bark. *E. grandis* has a high bark stripping yield, while having a low susceptibility to defects such as forks which make them more susceptible to environmental damage (Sappi, 2005 & Singh *et al.*, 2014). Stumps are commonly left to sprout, after which about one to three of the sprouts would be left on each stump to grow for the next harvest. The yield from the first coppice is usually the highest while it declines with every cropping (Von Roeder, 2014).

Eucalypts are suitable for products such as tissue paper, mine props, sawn timber, charcoal, firewood, fuel, firewood, ply wood, construction, tannin extracts, industrial chemical additives, poles, essential oils, tannin and Kraft pulping and cellulose purposes (Sappi, 2012; Singh *et al.*, 2014 & Von Roeder, 2014).

Lowering the water table to below the root zone may be required for successful crop production under water logged conditions (Singh *et al.*, 2014). While the water use of Eucalypts is a worldwide ecological issue, it has served as a useful attribute in managing water logging and salinity through bio-drainage (Benyon *et al.*, 2006; Singh *et al.*, 2014). Bio-drainage includes growing certain plants to consistently tap their main water supply. Eucalypts trees are of the popular species recommended for bio-drainage in salt affected localities (Singh *et al.*, 2014). *Eucalyptus* species are effective for groundwater level reduction due to high ET rates, and that *Eucalyptus*' water use exceeds that of the Acaia, the Albizia and the Azadirachta tree species (Bilal *et al.*, 2014).

Eucalyptus trees continue to grow in height until the age of eight to ten years (Singh *et al.*, 2014). The ET demand increases with the age of the plantation as the trees grow, height increases and consequently canopy cover increases (Singh *et al.,* 2014). *Eucalyptus*' height growth continues independent of competition from plant stand density. The trees' diameter growth is more sensitive to plant stand density than the height growth. The diameter growth of the trees reduces more severely in dense plantation than the height growth, resulting in high height to diameter ratios in dense plantations. The reverse is also true as studies indicate that an increase in inter-tree spacing (less dense plantations) results in lower height to diameter ratios as the additional space allows residual trees to maintain rapid diameter growth rates (Wonn and O'Hara, 2001). Where old trees experience thinning, their growth rates recover to that of coexisting younger trees (Martinez-Vilalta *et al.*, 2006). The water use by an isolated tree is more variable than the water use of a uniform forest stand, and generally the isolated trees have higher water uses as ascribed to their larger canopy and exposure (Nisbet, 2005). Sappi's

(2005) tree farming guidelines recommend planting hardwood species according to a 2 m by 3 m grid in warm and cool environments, but only planting every 2.7 m by 2.2 m in sub-tropical environments. Thus in a warm and cool environment, 1666 stems can be planted per hectare and 1683 stems can be planted per hectare in sub-tropical environments (Sappi, 2005). A study by Bernardo *et al.* (1998), conducted in southeastern Brazil, assessed the influence of three different plant spacing intervals (3 m x 1.5 m; 3 m x 3 m and 4 m x 3 m) on the *E. urophylla, E. pellita* and *E. camaldulensis* species at ages 15-, 31- and 41 months. The study concluded that while the highest total biomass per individual tree is obtained using the 4 m x 3 m spacing grid, the highest growth rate per hectare occurred at the 3 m x 1.5 m spacing (Bernardo *et al.,* 1998).

Battaglia *et al.* (1997) have reported *Eucalyptus* trees in Australia with heights of 15.6 m, 12.6 m, 9.0 m and 5.9 m, and all at different localities and altitudes, but all aged seven. The *Eucalyptus* trees aged six had heights of 16.3 m and 13.6 m. This indicates the importance of the environmental circumstances on tree productivity (Battaglia *et al.,* 1997). Singh *et al.* (2014) predicted the expected *Eucalyptus* tree height and differentiating tree height growth rate for the first ten years of growth. The results from Singh *et al.* (2014) were graphed as tree height per age class to assess the trend at which *Eucalyptus* trees grow (Figure 2:1). The *Eucalyptus* tree height growth rate has a polynomial correlation of 0.9937. Polynomial regression is a linear regression where the dependent "y" variable and independent "x" variable is modelled to an n^{th} degree, in this case to the degree of 2. The predicted growth rate has a linear regression correlation of 0.8413, with a logarithmic correlation of 0.9608. The *Eucalyptus* trees' vertical growth rate only decreases from 5 years of age.

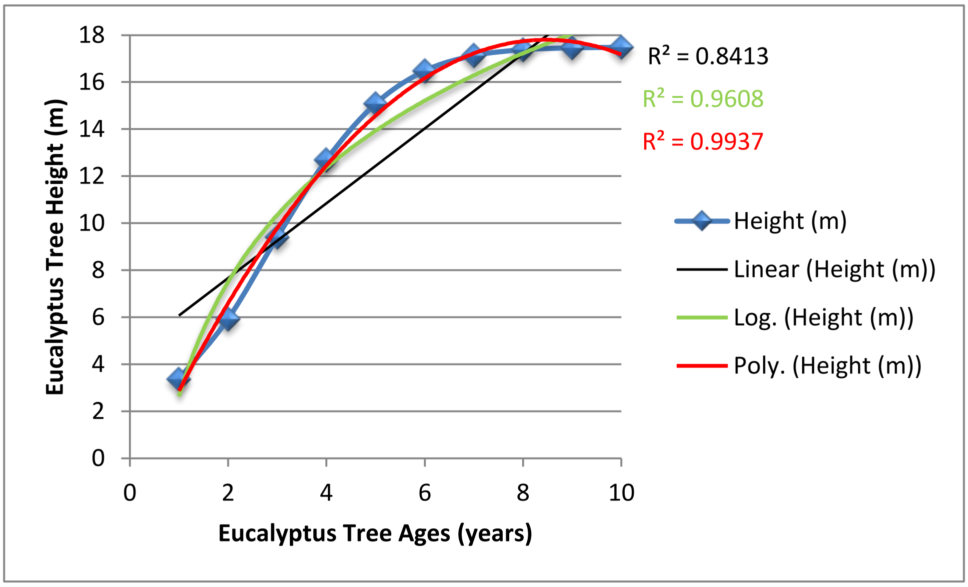

Figure 2:1 Predicted *Eucalyptus* tree heights per age according to Singh *et al.* (2014)

Calder *et al.* (1997) report that the rate at which *Eucalyptus* species' roots penetrate the soil, is roughly equivalent to the annual growth in tree height from 2.5 meters, and *Eucalyptus* tree roots will have exceeded 7.4 meters within three years of age (Calder *et al.,* 1997).

2.1.4. Hardwood and softwood rotation cycle

Eucalypts trees require a lot of water and obtain their water needs with deep tap roots (Meadows, 1999). *Eucalyptus* trees have an efficient water turn-over (Singh *et al.*, 2014). *Eucalyptus* trees use an average 15 - 30 % more water than Pine trees growing at the same age and in the same environment - but the rotation length for the two tree species are different (Sappi, 2005 & Singh *et al.*, 2014). Plantation's harvest time is dependent on the climate and the desired final product. Near the coast, the production cycle might only be six years, while it could take up to eight years inland (Von Roeder, 2014).

Steven Rennis, a commercial forestry farmer located in southern KZN, states that if trees are to be used for poles, it takes 5 - 7 years before they are harvested, while taking 10 - 15 years if the trees are to be used for pulp (Meadows, 1999; Von Roeder, 2014). There is a relationship between the age of tree harvest and the application of the trees. KZN timber numbers for soft- and hardwood species are graphed by age class in Figure 2:2 according to data available from DWA (2014).

Eucalyptus are more efficient water users than Pine trees as supported by Australian data that indicate that the harvest index of *Eucalyptus* trees are higher than that of Pine trees (Sappi, 2012). In comparing the hardwood and softwood species' harvest age, in the same region/environment, it is clear that hardwood species are usually harvested at a younger age than softwood species (Figure 2:2). Hardwood species are harvested within 14 years after plantation, while the softwood plantations have a greater life span of up to almost 40 years (typically 25 years). Sappi on average harvests *Eucalyptus* trees at ten years, while harvesting Pine trees at eighteen years (Sappi, 2012).

Hardwood species in Northern KZN are harvested from the age of 6 years and then again at a greater rate from the age of 10 years (Figure 2:2). The softwood species' hectares in Northern KZN, initially declines at a sharp rate after 5 years planted, but is then only harvested again after 10 and 21 years of age. In the KZN Midlands, hardwood species are harvested from 5 years after planting and again more drastically after 9 years of planting, while the softwood species are only harvested after 6 years and more drastically after 20 years. The hardwood species in Southern KZN are harvested after 8 years, while there is a sharp decline in softwood species in Southern KZN from the age of 9 years up until the age of 12 years, and then again at the age of 18 years the hectares of softwood trees in this age class declines dramatically.

It can be concluded from the DWA (2014) data that softwood plantations have a greater lifespan than hardwood plantations as hardwood species are generally harvested at least a year younger than softwood species. Softwood and hardwood species in Northern KZN and its Midlands, are harvested an average 2 years younger than the species in South KZN. The area of hardwood plantations in Northern KZN, are almost three times more than the area of softwood plantations. In Southern KZN and its Midlands, the areas of hardwood plantations exceed the areas of softwood plantations by a factor of 3.

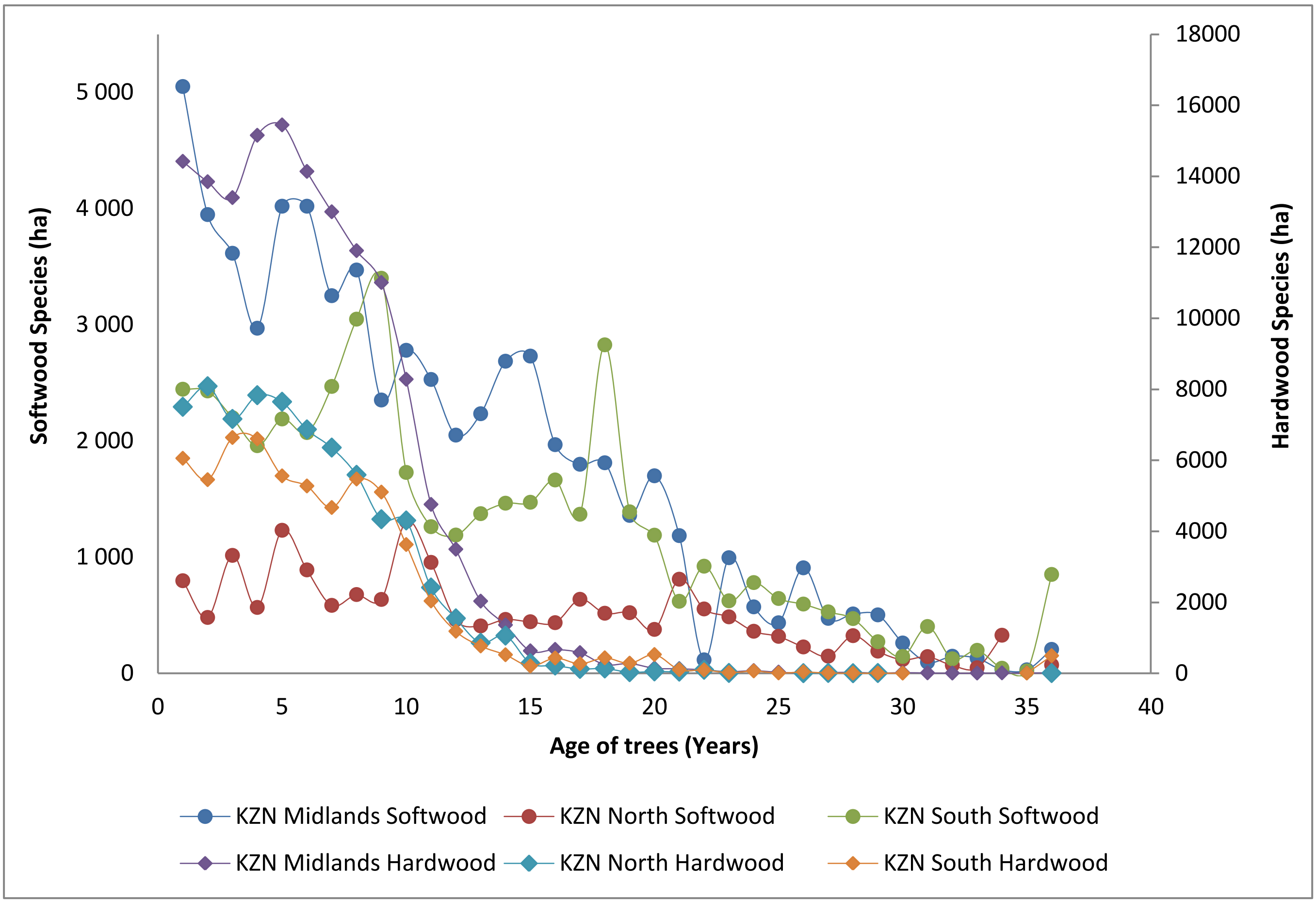

Figure 2:2 Afforestation's areas of softwood and hardwood species per tree age for 2011/2012 (DWA, 2014)

2.1.5. Timber trees' roots mine groundwater

The impact of the "modern land use" as described by the Sappi and Mondi forestry companies, on a catchment's hydrology is dependent on the rooting depth and the depth to the groundwater level (Coppen, 2002; Von Roeder, 2014). *Eucalyptus* trees have deep rooting systems and therefore their ET is not limited to the annual rainfall as with the dominant/indigenous vegetation scenario where groundwater is unreachable to the roots (Coppen, 2002; Von Roeder, 2014). Indigenous vegetation's roots do not have access to the groundwater, and water availability is limited to the soil moisture replenished by rainfall. *Eucalyptus*' roots can however grow to access the groundwater and mine the groundwater instead of suffering from droughts (Le Maitre *et al.*, 1999). Throughout droughts, air humidity is usually lower and air temperatures higher, consequently the atmospheric ET demand can be greater during drought circumstances. During droughts, the trees with roots extending into the groundwater resource can obtain the increased required quantities from the resource with little restraint as long as the groundwater table is within the reach of the tree's tapping roots (Coppen, 2002; Von Roeder, 2014).

Dye (1997) conducted a study in the Sabie area (Mpumalanga) and found that although soil water recharge was prevented, the trees didn't develop high stress levels. Plastic sheeting was applied to exclude soil water recharge, but still the trees did not experience a high degree of water stress. Dye *et al.* (1997) concluded that the trees did not experience water stress because of the trees' ability to obtain water at greater depths. Root system studies on the Zululand sand plain established that both Pine and *Eucalyptus* trees develop strong sinker roots that reach the in-situ shallow water table. The root diggings confirmed that it is common for *Eucalyptus* trees to have root depths of six meters. The diggings concluded that on average, three year old *E. grandis* trees have roots up to eight meters in depth and the nine year old *E. grandis* trees have living roots up to 28 m below ground (Dye, 1997; Von Roeder, 2014).

Dye *et al.* (2004) report that it is widely accepted that tree roots will increase in depth into the soil if the water supply is more reliable at the increased depth in comparison to the shallow soil horizons. Dye *et al.* (1995) explained that if the *Eucalyptus* trees are rooted in thick, unconsolidated material, the roots are most likely very deep in the absence of a confining formation. Dye *et al.* (1995) also add that even when sinker roots do not extent to the groundwater table, *Eucalyptus* trees may still impact the groundwater level through water extraction from the unsaturated zone and consequently decrease groundwater recharge (Dye *et al.*, 1995; Von Roeder, 2014). Underestimations of trees' water use in previous studies support the use of groundwater by trees (Dye & Jarmain., 2004; Le Maitre & Versfeld, 1997).

Thus where the soil is deep and the groundwater table is approximately eight meters below the surface, a three year old *Eucalyptus* tree is most likely extracting water directly from the groundwater and the total ET may likely exceed total precipitation (Benyon *et al.,* 2006; Von Roeder, 2014). Accessibility of groundwater is a function of soil type and the depth of the groundwater table from the ground surface (Benyon *et al.,* 2006). A reduction in base flow has resulted in degradation of the Siyaya Estuary due to the *Eucalyptus* plantations having much deeper rooting systems than the sugar cane plantations (Kelbe & Germishuyse, 2010).

Trees experiencing stress at a regular timescale will adapt physiologically over time compared to those in high rainfall and deep soil areas (Dye, 1997; Zahid & Nawaz, 2007). A comparative analysis of the stomata conductance, leaf area index (LAI) and sap flows of trees situated in rainfall and soil profile depth contrasting areas, indicate that even when soil water is available, the trees from the low rainfall area, use less water (Dye, 1997). The comparative study concluded that the LAI of the tropical, deep soiled Mpumalanga area's trees are almost twice that of the drier, shallower soiled Legogote North East (White River) area's trees. Trees cannot obtain substantial water requirements from the groundwater at Legogote and thus the wetter Mpumalanga area has greater sap flow (Dye, 1997). The overall daily water use of the Legogote area's trees was less than half of the Sabie (Mapumalanga) area's trees. The Legogote trees were surviving on soil water (unsaturated zone) during the winter, and therefore experienced a high degree of stress when soil water recharge was prevented. The Legogote site's trees experienced an increase in sap flow immediately after the plastic sheeting was removed and soil water recharge permitted (Dye, 1997). The sap flow and LAI of trees in areas with shallower and root accessible groundwater supply, is greater in comparison to areas with regular water stress. Zahid and Nawaz (2007) confirm that because Eucalypts are native to Australia where arid climates dominate, Eucalypts have drought avoidance mechanisms such as changes in LAI, almost vertical leave arrangements, air saturation shortage stomatal sensitivity, osmotic manipulation and deep rooting abilities.

A sandy terrain allows for Pine trees to develop deep roots which extend below the water table and are branched in the unsaturated zone. Thus, the Pine trees are able to extract moisture available in the unsaturated zone as well as tap water from the saturated zone (Rawlins, 1991).

It can thus be said that groundwater is most likely mined by the *Eucalyptus* plantations' roots where the soil profile is deep, groundwater recharge high and the groundwater level shallow. The absence of a confining layer almost ensures that roots will sink till it taps from the unconfined groundwater aquifer. In case the groundwater level is outside the reach of the sinker tree roots, the aquifer cannot be penetrated and trees are reliant on water in the unsaturated soil profile and recharge episodes for water supply.

2.1.6. Previous studies on *Eucalyptus* forestry's impact

The water table under *Eucalyptus* plantations are generally deeper than the water table in areas without timber plantations (Singh *et al.*, 2014). Groundwater can provide water to a stream by means of inflow through the streambed, making the stream a gaining stream. A losing stream is where a stream loses water to groundwater through the streambed (Feyen, 2005). A combination is also possible where a single stream loses water in some reaches, while gaining water in other reaches (Feyen, 2005). Whether a stream is a gaining or losing stream is dependent on the water table elevation in the vicinity of the stream and that of the stream. For a stream to be a gaining stream, the stream's immediate groundwater level's head must be higher than the water level elevation of the stream itself. Flow direction can alter in short timeframes due to focused recharge near the stream bank caused by individual storms. Other possible causes of flow direction alterations include flood peaks or transpiration by riparian vegetation (Feyen, 2005).

The quantity of water Pine and *Eucalyptus* forests use more than short vegetation, have been estimated to be 300 to 400 mm per year by Scott and Lesch (1997) in the Mokobulaan study. An afforestation experiment at Mokobulaan, initiated in 1956 provides statistical information of the effect of afforestation on water supplies in SA's eastern escarpment (Scott & Lesch, 1997). The Mokobulaan study concluded that Eucalypts afforestation caused a streamflow reduction, considered to be significant, from the third year since afforestation, during both the dry (low flows) and wet seasons (Scott & Lesch, 1997). The field data indicates that during the first six years after plantation, monthly streamflow reduced by an average of 51 % during the wet season and 52 % during the dry season. After six years since afforestation, the stream dried up periodically during the dry season, but dried up completely nine years after *Eucalyptus* plantation (Scott & Lesch, 1997).

Base flow refers to the streamflow fraction that originates from groundwater/subsurface flow and storage. It is dependent on the recharge rate of the groundwater/intermediate zone's water storage. The coefficient at which groundwater/stored water is released to the stream is dependent on geology, slope and area (Stretch & Maro, 2013). Base flow for rivers, is a slow, consistent release of groundwater that ultimately increases the river flow period after a groundwater recharge event. Groundwater's contribution to streamflow might be small under average hydrological conditions, but quickly becomes more significant and contributes a greater proportion to streamflow during droughts (Kelbe *et al.*, 2013b; Von Roeder, 2014). Bredenkamp *et al.,* (1992) identified groundwater off great importance during the low flow periods, stating that groundwater seepage contributes significantly to the streams.

Streamflow reduction was found to be dependent on the age of the tree but more so, on the annual rainfall (Scott & Lesch, 1997). The flow reduction was less during the drier years than during the wetter years, and the state of flow reduction is dependent on the available water in the catchment (Scott & Lesch, 1997). Removing the actual streamflow reduction variability by expressing the flow reduction as a percentage of the expected flow, indicated a clear relation between the progressive desiccation of the catchment and the increase in the tree's age (Scott & Lesch, 1997). Sixteen years after afforestation, the plantation was clear felled, but the stream only flowed as a short-lived response to large storms three years after clear felling. The stream was again perennial five years after clear felling (Scott & Lesch, 1997).

Mokobulaan data only indicates a significant total and wet season streamflow reduction four years after Pine afforestation. Only during the fifth year of Pine afforestation did significant streamflow reduction occur during the dry season. The stream however did only dry up completely 12 years after afforestation started (Scott & Lesch, 1997). The highest streamflow reductions correlate to that of the Eucalypts in that once the tree is mature; the highest reductions were experienced during the wettest years (Scott & Lesch, 1997). The *Eucalyptus* afforestation led to streamflow reduction in the third year, compared to only the fifth year when Pine afforestation led to streamflow reduction - ascribed to the *Eucalyptus* species developing canopy cover faster and having a general faster growth rate (Dye, 2013). Sappi (2012) supports these findings by declaring that *Eucalyptus* trees use between 15 to 30 % more water than Pine trees.

Nisbet (2005) reports that transpiration loss for broadleaf land cover is typically in the range of 300-390 mm/a, the interception losses are typically 100 - 250 mm/a, while the total evaporation losses are typically 400 - 640 mm/a for an area receiving 1000 mm/a.

An Australian study, conducted in the Green Triangle (south-eastern Australia) concluded that average ET rates for eight *E. globulus* plantations with water tables 6 meter below ground surface or shallower, were 1090 mm/year (MAP was 630 mm/year; ET exceeding MAP by a factor of 1.7) (Benyon *et al.,* 2006). The plantations were estimated to use groundwater at a rate of 108 to 670 mm/year. The ET rates of eight plantations with groundwater tables deeper than 6 meter below ground surface, were faintly less or equal to the MAP (Benyon *et al.,* 2006). Benyon *et al.* (2006) further concluded that in areas with shallow groundwater tables (< 3 m.b.g.l.), but with high clay contents and saline subsoils, the *E. grandis* trees used little to no groundwater. The *E. grandis* trees did however use groundwater for 41 % (380 mm/year) of the total annual ET where the water table was shallow, but soils more sandy and salinity lower (Benyon *et al.,* 2006). *Eucalyptus camaldulensis* obtains 67 % of its total water use from groundwater and the upper vadose zone (the vadose zone supplied the groundwater) (Bilal *et al.,* 2014).

A study in southern India, with a MAP of 800 mm and soil depth of 3 m at Devabal and Puradal, and a soil depth greater than 8 m at Hosakote was initiated in 1987 to quantify the environmental impacts of fast growing tree plantations, specifically *Eucalyptus* species. The study concluded that the water use of the plantations on soils no deeper than 3 m, were no greater than that of the indigenous, dry deciduous forest and equal to the MAP. The water use of plantations in soils deeper than 8 metres exceeded the annual precipitation. The cumulative ET_0 was 3400 mm for the three year study duration period (1133 mm/annum), compared to the cumulative precipitation of only 2100 mm (700 mm/a) (Calder *et al.,* 1997). ET_0 thus exceeds MAP by a factor of 1.6.

2.1.7. Previous studies on forestry in the Lake St. Lucia study area

The most significant water loss from the St. Lucia catchment (W32) is due to ET. ET is spatial specific as it is dependent on the water level depth, the vegetation type and its root depth. ET losses projected due to Pine and *Eucalyptus* plantations are up to 300 % of the atmospheric demand (Kelbe *et al.*, 2013a). ET rates are high in the Lake St. Lucia area; especially in drier winters and early springs, and are estimated to be 1300 mm/annum. Afforestation has led to a major reduction in runoff, estimated to be 25 million m^3/annum (Stretch & Maro, 2013).

Dye and Jarmain (2004) conducted a study on a 44.7 ha black wattle plantation on Mistley-Canema Estate (Mondi Forests) in the Seven Oaks district, KZN for four complete years from 1997 to 2001. Dye and Jarmain's (2004) study concluded total ET of the black wattle plantation to be 1240 mm, 1364 mm, 1239 mm and 1048 mm respectively for the four years. The total annual rainfall however was only 874 mm, 616 mm, 1016 mm and 860 mm for each respective year. This negative input and output difference indicates that the black wattle trees were using soil water accumulated prior to rainfall/forestation. The study concluded a streamflow increase/recovery immediately after tree felling (Dye & Jarmain, 2004).

Clulow *et al.* (2011) conducted a study on the Two Streams catchment located 70 km from Pietermaritzburg near Seven Oaks. Their study concluded that after complete catchment clearing in 2004, a significant increase in streamflow followed in the subsequent years. While the runoff: rainfall ratios were 0.03, 0.04, 0.01 and 0.02 for 2001 to 2004 for the afforested area before clear felling, the new runoff: rainfall ratios were 0.08, 0.07, 0.08 and 0.08 from 2005 to 2008 after complete clearing. Replanting late 2006 had not reduced streamflow by 2011 (Clulow *et al.*, 2011). Peak streamflows occurred in January 2005 as reaction to the 2004 clear felling. The relationship between the accumulation of rainfall and that of streamflow, were significantly influenced by riparian vegetation clearing in 2000 and catchment clear felling in 2004 (Clulow *et al.*, 2011).

Rawlins (1991) has reported that aerial photograph evaluation revealed that afforestation has reduced the wetlands frequency and size in Maputuland. Rawlins (1991) reports that while the wetlands are present during the early years of the forest development, the wetlands dried sufficiently as the plantations matured and ET rates increase accordingly. Wetlands are only visible for short periods after sufficient heavy precipitation (Rawlins, 1991).

The Environmental Systems Research Institute's (ESRI) (2016) normalized difference vegetation index (NDVI) indicates an increase in vegetation, especially since 2005, while the Lake St. Lucia's water level decrease visible from the NDVI data since 2000 (Figure 2:3).

NDVI Change (1975-1990)	NDVI Change (1990-2000)	NDVI Change (2000-2005)	NDVI Change (2005-2010)

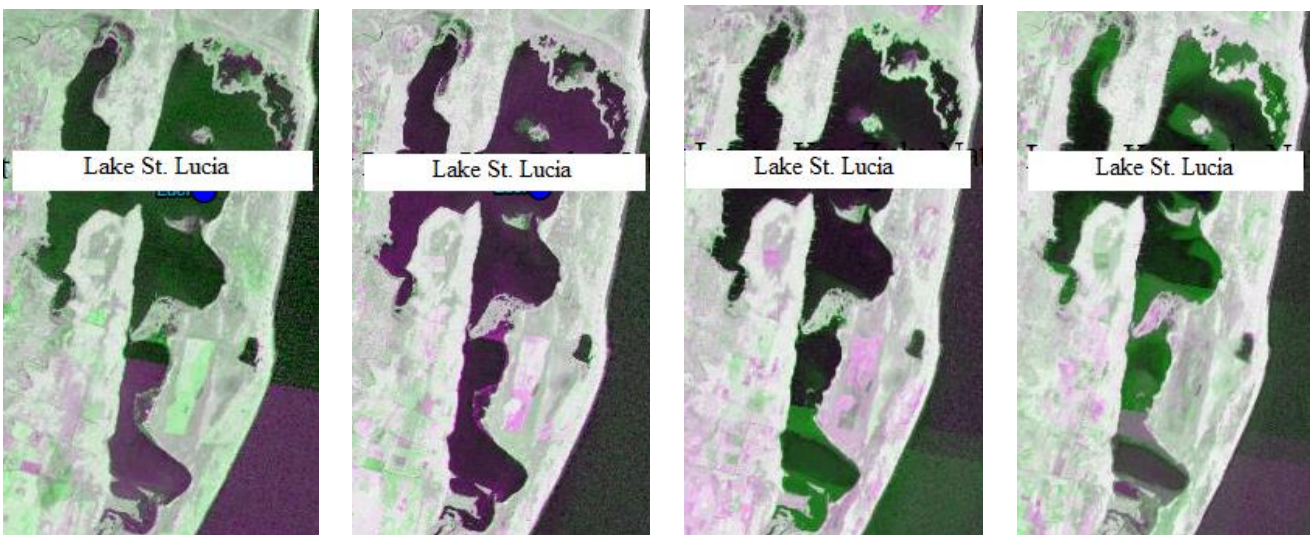

Vegetation Increase/ Decrease in water level of water body

Vegetation decrease/ Increase in water level of water body

Figure 2:3: Lake St. Lucia's water levels and immediate vegetation cover change as visual from NDVI (Esri, 2016)

The NDVI data supports Rawlins (1991) statement that wetland's size reduction can be connected to increasing afforestation. NDVI is a graphical indicator of the live, green vegetation present as determined using remote sensing analysis. The land and water boundary imagery (Figure 2:4) correlate to the NDVI data, as a decline in the lake's water surface area is clear, with an increase in land use, from 2000. Since a lake water level increase in 1990 - 2000, the lake's water level has been decreasing.

Rawlins concluded that the average lake inflow will be decreased by 10 to 12 %, with an increase to 30 % during extreme dry periods (Rawlins, 1991).

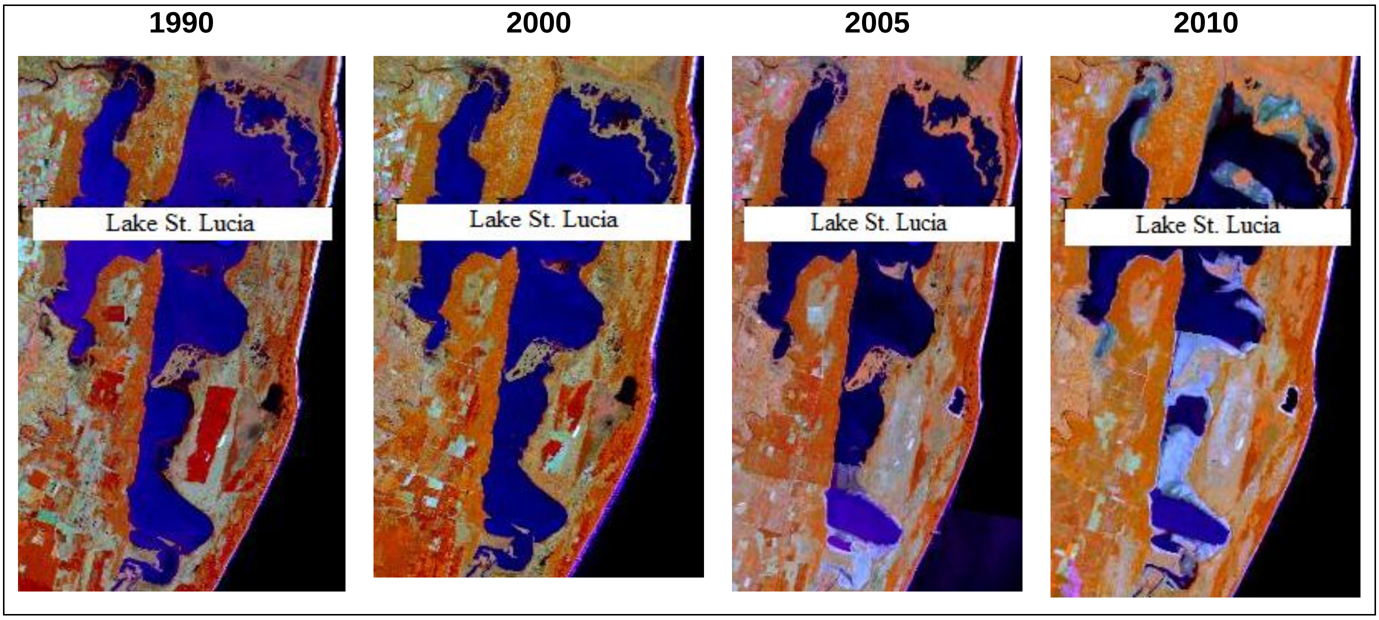

Figure 2:4: Water body boundary and land development with time (Esri, 2016)

2.2. Analytical evapotranspiration methods

Dye and Jarmain (2004) have identified the need for practical and affordable methods for predicting streamflow response to afforestation and clear felling. The value of long-term monitoring, improved conceptual models and numerical models are emphasized by the unanswered questions of Lake St. Lucia (Dye *et al.*, 2004; Kelbe *et al.*, 2013a). Rao *et al.* (2011) is of opinion that modelling ET is not an easy task.

Evaporation is defined as the conversion process of water from a liquid state to a water vapour state, from an evaporating surface such as lakes, rivers, other water bodies or any other material with water content such as soil (Allen *et al.*, 2006; Jovanovic *et al.*, 2012). The liquid to vapour state transformation is driven by direct solar radiation and the ambient air temperatures. The process is driven by the difference in water vapour pressure between the evaporating surface and the immediate surrounding atmosphere. The lowest layer becomes increasingly saturated, but water molecules are continuously carried from the area through wind (Shuttleworth & Wallace, 1985; Zhou *et al.,* 2006). An increase in saturation of the surrounding air decreases the evaporation rate (Allen *et al.*, 2006).

Transpiration is the vaporization/removal process of liquid water enclosed in plant tissue, to the atmosphere in liquid state as explained by the United States Geological Survey (USGS) (2016) and Jovanovic *et al.* (2012). Plants obtain water using their roots and carry this moisture through their vascular system, to the small pores (stomata) underneath their leaves, from which it is released to the atmosphere as vapour (USGS, 2016). USGS (2016) report that 10 % of atmospheric moisture is supplied by plant transpiration, while the rest (90 %) is supplied by evaporation from water bodies (oceans, lakes, rivers).

ET is the combination of the evaporation and transpiration processes. Water is lost from the land/soil/water surfaces through evaporation, while transpiration is responsible for the water loss from plants (Jovanovic *et al.*, 2012; Karisson & Pomade, 2004; Racz *et al.*, 2013). Through ET, water and nutrients move from the soil, into the root hairs, within the plant, to the plant leaves. ET sanctions the continuous cycle of water returning to the atmosphere for the formation of clouds (Ramirez-Builes, & Harmsen, 2011). These two processes occur simultaneously and clear distinguishing is next to impossible, thus the common, collaborating term (Jovanovic *et al.*, 2012).

ET is complex to quantify as it is the deliverable of different, interactive processes. Processes influencing ET include evaporation from the soil, transpiration from the plant leaves and water intercepted by the canopy, off which every one of these processes are again dependent of the in-situ physiological (crop type, root depth, leaf surface, life cycle stage), climatic (weather) and soil variables (Ramirez-Builes, & Harmsen, 2011). Agricultural management practices, such as the presence of soil salinity, absence of soil fertilizers and disease or pest control or the presence of impermeable soil horizons can limit/influence plant development, and thus reduce ET (Ramirez-Builes, & Harmsen, 2011).

Nisbet (2005) reported that trees use and loose water through two separate processes. One process is the physiological process where water is tapped by the roots from the soil and evaporated through the stomata as a function of soil and atmospheric factors. The second process is the interception of water by leaves, branches and trunks during rainfall, and the subsequent evaporation from these surfaces. Interception losses are increased by atmospheric turbulence accredited to canopy height and roughness (Nisbet, 2005). Broadleaf interception losses are estimated to be 10 - 25 % of the mean annual precipitation (MAP) (Nisbet, 2005).

The reference crop evapotranspiration (ET_0) rate refers to the ET rate from a specific reference surface, namely the ET rate of a short green crop (grass) in the absence of water shortage and direct sunlight. ET_0 is sometimes incorrectly referred to as PET (Jovanovic *et al.*, 2012; Pandey *et al.*, 2016). The PET is the ET rate of a crop grown in ideal agronomic and soil water environments - the evaporative quantity in the absence of water restrictions (Jovanovic *et al.*, 2012).

The relationship between ET_0 and PET depends on the soil moisture content and in this case, whether the plant roots can tap from alternative groundwater resources. If the vegetation is unable to abstract water from the soil, then the ET_0 becomes less than the PET (Karisson &

Pomade, 2004). ET_0 and PET are the same in the absence of water restrictions, which is the case where trees have tapping roots mining groundwater (Karisson & Pomade, 2004).

ET is a critical component in the forest water balances, and thus the importance of model choice should not be underestimated (Lu *et al.*, 2003). The methods and models for measuring or rather simulating the ET have increased extensively due to its relevance in various fields such as hydrology, geohydrology, climatology and agricultural science (Ramirez-Builes & Harmsen, 2011). ET might be one of the greatest components for water budgeting, but is also the least understood - resulting in the extensive quantity of models, all an attempt to accurately account for this component of the water balance (Ramirez-Builes & Harmsen, 2011).

The simulated ET rate often differs by hundreds of millimetres per growing season dependent on the method applied (Racz *et al.*, 2013). The applicable method is greatly determined by the relevant data, which was dominantly restricted to weather data obtained from the South African Weather Service (SAWS) for this study. The weather data available from the SAWS station, 684910, included minimum and maximum daily temperatures, daily relative humidity percentages and daily wind speed measurements. The choice of analytical model has to account for the accuracy of that model for the relevant climatic conditions (Racz *et al.*, 2013).

A study conducted by Racz *et al.* (2013) identified the need to compare various ET determination/quantification methods. The analysis was performed using daily 2005-2010 data, neglecting winter periods and using estimated net radiation values. Research conducted by Racz *et al.* (2013) concluded that temperature and radiation based methods give the highest PET rate values. In comparison, the pan-coefficient based methods yield the lowest PET rate results in both humid and arid environments (Racz *et al.,* 2013). The most popular ET models, which were considered and from which the S&W method was selected as most ideal for the study, will be discussed in the following sections.

2.2.1. Pan-coefficient-based methods

Pan coefficient based methods include the Pereira model and the Food and Agricultural Organization (FAO) 56 model as examples. Calculating the ET_0 using evaporation pan data, is considered fairly reliable and common by Ramirez-Builes & Harmsen (2011), although Racz *et al.* (2013) state that the pan-coefficient based methods result in the most under-estimated ET_0 values. The little input data required, namely the measured daily evaporation pan data, which can be obtained with little effort, makes this method very popular (Racz *et al.*, 2013).

Smith *et al.* (1996) report that during comparative studies by the American Society of Civil Engineers (ASCE), the performance of twenty different methods were comparatively evaluated (Smith *et al.*, 1996).

Class A Pan Method

The evaporation pan is installed in a grassy field, filled with a known water quantity of which the exposed surface and filled dimension (depth) is recorded. A Class A pan is usually 1 cm in height and 12,06 cm in diameter. The remaining water quantity is measured after evaporation was permitted for a certain time elapse. The pan evaporation is expressed as the amount of evaporation per time, usually over 24 hours. It is this evaporation measurement which is multiplied by a pan coefficient to calculate the ET_0 rate (Eijkelkamp, 2009). Input data required is on a daily time step. Eijkelkamp (2009) estimates that a pan coefficient between 0.35 and 0.85 (average 0.7) is applicable to a Class A evaporation pan for calculating the ET_0. The pan coefficient tends to be higher if the pan is situated in an un-cultivated area, an area with high humidity or an area with low wind speed (Eijkelkamp, 2009).

Pereira Model (1995)

The Pereira model simulates the ET_0 using a calculated pan coefficient (K_p), multiplied by the direct measured pan evaporation (E_p in mm/day) (Equation 2:1). The pan coefficient is site specific (Equation 2:2) as Δ refers to the slope of the vapour pressure curve (kPa/°C), γ refers to the psychrometric constant (kPa/°C) and u_2 to the daily mean wind speed at reference height 2 m above ground surface (km/day). The pan coefficient can be seen as a correction factor accounting for in-situ conditions (Racz *et al.*, 2013; Ramirez-Builes, & Harmsen, 2011).

Equation 2:1 Pereira model evapotranspiration (Racz *et al.*, 2013)

$$ET_0 = K_p \, . \, E_p$$

Equation 2:2 Pereira model pan coefficient (Racz *et al.,* 2013)

$$K_p = \frac{0.85\ (\Delta + \gamma)}{[\Delta + \gamma(1 + 0.33u_2)]}$$

FAO-based Pan Method (1996)

FAO-24 refers to the ET_0 quantification methodology first published in the Food and Agricultural Organization Irrigation and Drainage Series, in 1974 and revised in 1977 (Smith *et al.*, 1996). The introduction of standardized crop coefficients for the calculation of crop water requirements across all growth stages, for the FAO-24-method, was vital for simplifying and standardizing the then accepted and standard method. The FAO-24-method has developed since then as illustrated in the FAO-56 pan coefficient formula (Equation 2:3) (Smith *et al.*, 1996). A coefficient expressing the relationship between the crop and the ET_0, is calculated and expressed as a single coefficient or two separate coefficients of which one describes the effect of evaporation and the other the effect of transpiration (Ramirez-Builes, & Harmsen, 2011; Racz *et al.*, 2013).

The coefficient has been extended to a crop development coefficient which is the sum of a basal crop coefficient and a soil evaporation coefficient, each coefficient calculated independently of each other. The crop coefficient has also been modified to include a water stress coefficient where 1 indicates no water limitation/stress, and non-standard conditions (Ramirez-Builes, & Harmsen, 2011).

Katerji and Rana (2006) found an approximate 40 % difference between the FAO-56-model crop coefficients and the coefficients experimentally obtained. The large difference is accredited to the complexity represented by the coefficient. The crop coefficient is ideal to account for aerodynamic factors (crop height), biological factors (leave surface), physical factors (soil moisture; stomata response to relative humidity (RH_{mean}) and average daily wind speed (u_2) and agronomic crop management practices (Ramirez-Builes, & Harmsen, 2011; Xu & Singh, 2002).

Equation 2:3 FAO-56 pan coefficient (1998) (Allen *et al.,* 2006)

$$K_p = 0.61 + 0.00341.RH_{mean} - 0.000162.u_2.RH_{mean} - 0.00000959.u_2.FET + 0.00327.u_2.\ln(FET) - 0.00289.u_2 \ln(86.4.u_2) - 0.0106.\ln(86.4.u_2)\ln(FET) + 0.00063[\ln(FET)]^2 \ln(86.4.u_2)$$

2.2.2. Temperature-based methods

ET_0 estimation methods which only require temperature measurements as input data, are classified as temperature based methods. Temperature based methods date back to the 1920s as some of the first attempts to quantify ET_0, and were all based on temperature measurements (Xu & Singh, 2002). The Blaney-Criddle and Hargreaves methods were selected as the best ET_0 methods in the temperature-based category according to Xu and Singh's comparative study (2002). Both methods concluded estimations acceptable relative to the results obtained from the FAO recommended Penman-Monteith Method. In comparison of the different method types, the radiation based methods, yielded better results than the temperature based methods, which again had estimations more accurate than the mass-transfer based method relative to the FAO-recommended Penman-Monteith Method (Xu & Singh, 2002). Temperature and radiation based methods are relatively simple and require little input data, but the calculations for the required empirical coefficients are complex (Racz *et al.*, 2013).

FAO-24-Blaney-Criddle Method

The initial Blaney-Criddle theoretical equation (1950) is simple and easy, although not very accurate. The primitive version, which is not integrated with other methods to form a combination, requires only measured temperature data (Eijkelkamp, 2009). The initial Blaney-Criddle method is known to underestimate ET_0 in windy, sunny or dry environments, while overestimating ET_0 by over 40 % in humid, clouded and calm climatic conditions. The original method can in reality only serve as an order of magnitude estimation/indication (Eijkelkamp, 2009).

The parameter "mean daily percentage of annual daytime hours", is locality specific as related to the geographical latitude degree. The percentage increases with a decrease in latitude degrees, while being greatest in January and lowest in June for the southern hemisphere (Eijkelkamp, 2009; Xu & Singh, 2002). The Blaney-Criddle model is still relevant when combined with other models, to make the approximation more accurate.

The FAO-24 methodology was adapted for a wider range of climatic condition by incorporating the Blaney-Criddle method. The FAO-24-Blaney-Criddle combination method includes a correction factor estimated from humidity, wind and sunshine conditions, but the method always still required post-calibration (Smith *et al.*, 1996). The FAO-24 model, modified with the Blaney-Criddle model, has been classified as less likely to overestimate ET_0. The FAO-24-Blaney-Criddle model can be applied to different climates, requiring data input of a monthly time step or even longer (Pandey, *et al.*, 2016; Smith *et al.*, 1996).

The FAO-24-Blaney-Criddle has been reported as a model capable of estimating ET_0 with reasonable accuracy, and the best, if not the only, of the temperature-based models applicable to estimating viable ET_0 values (Pandey, *et al.*, 2016). In comparison to four equations which can be supplemented as a suitable option for the FAO-56-Penman-Monteith model, the FAO-24-Blaney-Criddle model ranked third. The first and second ranked models were radiation-based (Pandey, *et al.*, 2016). The monthly consumptive use coefficient recommended by Blaney and Criddle (1950) varies from 0.5 for an orange tree to 1.2 for dense vegetation, and from 0.85 in the growing season to 0.45 in the non-growing season respectively (Xu & Singh, 2002). The FAO-56 refined Blaney-Criddle equation (Equation 2:5), multiplies and includes in addition to the single mean daily percentage of annual daytime hours (p in Equation 2:4), two separate calculated coefficients which are summed to be multiplied with the original *Blaney-Criddle* (1950). The two separate coefficients (Equation 2:6 (a_1) and Equation 2:7 (b_1)) account for the minimum daily relative humidity (RH_{mean}) as well as the relative sunshine duration ($\frac{n}{N}$) and the mean wind speed (u_2d) but still only of daytime hours' data (u_2d).

Equation 2:4 Primitive Blaney-Criddle reference evapotranspiration (1950)

$$ET_0 = p\ (0.46\ T_{mean} + 8)$$

Equation 2:5 FAO-56-model refined with Blaney-Criddle (Xu & Singh*, 2002; Racz et al.,* 2013*)*

$$ET_0 = a_1 + b_1\ [p(0.46\ T_{mean} + 8.13)]$$

Equation 2:6 Blaney-Criddle FAO-56 modification parameter a_1 (Racz *et al.,* 2013)

$$a_1 = 0.0043\ \mathrm{RHmin} - \left(\frac{n}{N}\right) - 1.41$$

Equation 2:7 Blaney-Criddle FAO-56 modification parameter b_1 (Racz *et al.,* 2013)

$$b_1 = 0.82 - 0.0041\ \mathrm{RHmin} + 1.07\left(\frac{n}{N}\right) + 0.066u^2d - 0.006\ \mathrm{RHmin}\left(\frac{n}{N}\right) - 0.0006\mathrm{RHmin}.u_2d$$

Hargreaves Method (1975)

Equation 2:8 Hangreaves and Samani improved method (Xu & Singh, 2002)

$$ET_0 = a\,.\,R_a\,.\,(T_{max} - T_{min})\ \exp 0.5\,.\,(T_{mean} + 17.8)$$

2.2.3. Mass-transfer-based methods

Rohwer Method (1931)

The Rohwer Method was selected as the best ET_0 method in the mass-transfer-based methods category and concluded estimations acceptable relative to the estimation results obtained from the FAO recommended Penman-Monteith Method (Xu & Singh, 2002). The ET_0 is calculated to account for wind (u_2) (Equation 2:9), and the difference between the saturation (e_s) and actual vapour pressure (e_a) (these components makes it a mass-transfer based method).

Equation 2:9 Rohwer's adaption of the Daltonian method for estimating evaporation (Xu and Singh, 2002)

$$ET_0 = 0.44\ (1 + 0.27\ u_2)(e_s - e_a)$$

2.2.4. Radiation-Based Methods

The Priestley-Taylor and Makkink methods were selected as the best ET_0 method in the radiation-based method's category according to the Xu and Singh (2002) study which compared ET_0 estimation methods to the simulated results of the FAO recommended Penman-Monteith Method.

Priestley-Taylor Model (1972)

Priestley and Taylor (1972) introduced a dimensionless coefficient in their method of 1972, in attempt to disregard the aerodynamic term and fix the radiation term required as input for calculating ET_0 (Racz *et al.*, 2013; Ramirez-Builes, & Harmsen, 2011; Xu and Singh, 2002). The Priestley and Taylor combined version of the Penman method (*Equation 2:10*), was formulated for estimating ET_0 from specifically a wet surface area. The adapted formula's aerodynamic component was erased, while the energy component was multiplied by the dimensionless coefficient, reported as 1.26. Net radiation (R_n) and the soil heat flux (G) are included as radiation parameters and are in unit $MJ/m^2/day$ (Xu & Singh, 2002). The Priestley-Taylor's coefficient (α calculated according to Equation 2:11) accounts for the vapour pressure curve's slope (∆) and the psychometric constant (γ) just like the pan coefficient for example. As with the S&W model, the equation is divided by the latent vaporization heat (λ).

Equation 2:10 Priestley and Taylor reference evapotranspiration model (Racz *et al.*, 2013)

$$\mathrm{ET_0} = \frac{\propto \frac{\Delta}{\Delta + \gamma}\left(\mathrm{R_n} - \mathrm{G}\right)}{\lambda}$$

Equation 2:11 Dimensionless coefficient for Priestley and Taylor model (Racz *et al.*, 2013)

$$\propto = 1 + \frac{\gamma}{\Delta + \gamma} . \frac{\mathrm{r_c}}{\mathrm{r_a}}$$

FAO-24-Makkink Method (1957)

This FAO-Penman method was later extended to account for radiation data as based on the Makkink method. The Makkink-FAO-24-method was made applicable worldwide with the addition of a wind and humidity correction coefficient. The Makkink-FAO-24 method is more restricted to humid climates as its results are underestimated and erratic in arid conditions (Racz et al., 2013; Smith et al., 1996; Xu & Singh, 2002). The Makkink equation (Equation 2:12, Equation 2:13 and Equation 2:16) accounts for radiation by including global radiation over latent heat as a factor. The vapour pressure slope (∆) over the sum of the vapour pressure slope and psychometric constant ($\Delta + \gamma$) is included as a factor as with the Priestley and Taylor ET_0 quantification method. The Makkink coefficient or correction factor, is the greatest variable between the different versions thereof. The FAO-24 Makkink (Equation 2:13) version attempts to account for transient, in-situ relative humidity (RH) and wind speed ($\mathrm{u_2 d}$) by including Equation 2:15 instead of an invariable factor such as Equation 2:12 and Equation 2:16.

Equation 2:12 Makkink (1957) original model

$$\mathrm{ET_0} = 0.61\left(\frac{\Delta}{\Delta + \gamma}\right)\left(\frac{Rg}{\lambda}\right) - 0.12$$

Equation 2:13 Makkink-FAO-24 reference evapotranspiration method

$$\mathrm{ET_0} = \mathrm{a_2} + \mathrm{b}_2\left(\frac{\Delta}{\Delta + \gamma}\right)\left(\frac{Rg}{\lambda}\right)$$

Equation 2:14 Correction factor for Makkink-FAO-24-Method

$$a_2 = -0.3$$

Equation 2:15 Correction factor for Makkink-FAO-24-Method

$$b_2 = c_0 + c_1 RH_{mean} + c_2 . u_2 d + c_3 . RH_{mean} . u_2 d + c_4 . RH_{mean}{}^2 + c_5 . u_2 d$$

Equation 2:16 Hansen's version of Makkink-Model (1984)984)

$$ET_0 = 0.7 \left(\frac{\Delta}{\Delta + \gamma}\right)\left(\frac{Rg}{\lambda}\right)$$

2.2.5. Combination Methods

Although combination methods are considered more accurate and dynamic models, and have consequently become widely used, it also requires a high variance of input data. The S&W model is a modification of the Pennman-Monteith-FAO-56 model (Racz *et al.*, 2013).

A more recent comparative study conducted by Racz *et al.* (2013) found a greater difference in annual ET_0 between different types of methods and to a lesser extent between methods of the same type (based on the same parameter). They concluded that the highest ET_0 sums were calculated using the Blaney-Criddle, the Makkink-model, Penman-Monteith-FAO-56 model and S&W model. The Pereira and FAO-56 models showed the greatest correlation to the pan evaporation measurements, but the S&W model showed the greatest correlation to the Penman-Monteith-FAO-56 model (Racz *et al.*, 2013).

In contrast to the Penman-Monteith-FAO-56-model, the S&W model's ET_0 is more sensitive to ET's response to wind, global radiation, temperature and air humidity according to Racz *et al.* (2013). This was considered important as these parameters that the S&W model is more sensitive to, are the measured in-situ parameters obtainable from weather stations. This characteristic was prioritized as favourable in combination with being one of the models with the highest ET_0 annual sums in attempt to have rather worst-case scenarios. Racz *et al.* (2013) identified the S&W model as one of the best performing models, calculating proper, accurate estimations for ET_0. Other adequate performing models identified included the Priestley-Taylor and Penman-Monteith-FAO-56 method (Racz *et al.*, 2013).

Penman-Monteith-FAO-56 model (1998)

The original Penman Method was adjusted to include a revised wind function obtained from lysimeter data recorded at various locations worldwide, but still required calibration of the wind function for viable results (Racz *et al.*, 2013; Smith *et al.*, 1996; Xu & Singh, 2002). The

Penman-Montheith (Equation 2:17) model accounts for the difference between the net radiation (R_n) and soil heat flux (G) typical from the radiation based methods, for the vapour pressure deficiency (e_s-e_a) typical from the mass transfer based methods, and for temperature (T) and wind speed (u_2).

Equation 2:17 Penman-Monteith-FAO-56-model (Racz *et al.*, 2013)

$$ET_0 = \frac{0.408\,\Delta\,(R_n - G) + \gamma\,(\frac{900}{T_{mean} + 273})\,u_2\,(e_s - e_a)}{\Delta + \gamma\,(1 + 0.34\,u_2)}$$

Shuttleworth-Wallace model (1985)

Shuttleworth and Wallace extended the popular Penman-Monteith method to include the transpiration from vegetation as well as that from the substrate soil. Vorosmarty *et al.*, (1998) and Stannard (1993) concluded that the S&W model performs best in representing ET_0 in hydrological modelling. The Penman-Monteith method neglects evaporation from interception, while the S&W model accounts for this evaporation and accounts for varying surface conditions more accurately (Zhou *et al.*, 2006). The quantification of the canopy (C_c) and soil (C_s) weighing coefficients for the transpiration (ET_c) and evaporation (ET_s) are discussed in greater detail in Chapter Method of Investigation.

Equation 2:18 Shuttleworth-Wallace Model

$$ET_0 = \frac{Cc\,.\,ETc + Cs\,.\,ETs}{\lambda}$$

Racz *et al.* (2013) concluded that the S&W, Priestley-Taylor, Penman-Monteith-FAO-56, Szasz and Makkink methods performed the best in calculating ET_0.

The scope of possible methods was limited to those which calculate the highest ET_0 values, as to rather overestimate and simulate worst case, than underestimate the impact of forestry ET. This decreased the model choices to the S&W model, the Penman-Monteith-FAO-56 model and the Makkink methods. The Pereira and FAO-56 models showed the best correlation to the pan ET measurements, while the S&W model showed the most similarity to the Penman-Monteith-FAO-56 method. Considering systematic error however, the S&W and Makkink model's simulations were the closest to the pan ET measurements (Racz *et al.*, 2013). The S&W, Mahringer, WMO-1966, the pan measurements and the Pereira models were found to be rather sensitive in comparison to the rest of the analysed models which showed lower fluctuations to alterations in atmospheric variables (temperature, radiation, humidity and wind). The sensitivity of the selective model to the changing climatic parameters, which are the measured parameters in this case, were important to improve the simulated accuracy and model relevance (Racz *et al.*, 2013).

Zhou *et al.* (2006)'s study concluded that the S&W model is sensitive to specific land uses and vegetation and that the simulated ET_0 changes with vegetation types and climate variables. Zhou *et al.* (2006) also applied literature values combined with NDVI data from satellite images and weather station climate data as input data. Zhou *et al.* (2006) confirmed that the simulated ET_0 values can serve as direct input to a hydrological model without requiring conversion and found the simulations to be accurate. Thus, the S&W model was chosen as is considered accurate using literature input data as well as because it differentiates between vegetation types (Zhou *et al.*, 2006).

2.3. Numerical Groundwater Models Introduction

The demand for predicting the impact of human activities on groundwater and associated environments, have driven the advancement of groundwater models as well as the extensive increase in model variability (Zhou and Li, 2011). The first analytical groundwater simulation, dating back to 1963, is accredited to Toth, who investigated groundwater flow for hypothetical small drainage basins (Toth, 1963). In 1966, Freeze and Witherspoon applied the first numerical simulations to steady state regional groundwater flow patterns for hypothetical layered aquifers, simulating 3D groundwater flow in anisotropic and heterogeneous groundwater basins (Freeze and Witherspoon, 1967). In 1978, the Regional Aquifer System Analysis Program (RASA) of USGS kick-started the application of groundwater models to large scale aquifer simulation. The program extended over 18 years and consisted of intensively studying 25 regional aquifer systems. The program outcomes include regional hydrogeological database compilation, conceptual model construction, insight into response of aquifer systems to stress/human interference and national groundwater atlas cartography. The USGS 3D finite difference model and the USGS MODFLOW models were two of the models constructed and used for characterization of the groundwater systems and the impact of human development (Zhou and Li, 2011). Since the release of MODFLOW in 1988, MODFLOW has extended to be the industrial standard groundwater model worldwide, progressively updated to MODFLOW-2000 and again MODFLOW-2005 (Zhou and Li, 2011).

A groundwater flow model is a conceptual description of the physical system, described by mathematical equations as made possible by certain simplified assumptions (Feyen, 2005). Different boundaries need to be assessed differently - evaporation involves the change in phase while seepage through a boundary is direct water flow. An appropriate large scale, regional groundwater model accounts for groundwater discharge and recharge as well as the areal distribution of multiple aquifer systems according to Zhou & Li (2011). Basin scale groundwater flow models are characterised by differences in the topographic elevations, serving as the driving force for regional groundwater flow (Zhou & Li, 2011). A regional scale groundwater model is to account for major regional aquifers and aquitards, thus geological compartmentalisation characterised by varying hydraulic properties should be computed. Intensive groundwater and surface water resources are essentially the single resource and the river and water body heads are to be simulated as head-dependent or constant head model boundaries (Zhou & Li, 2011). Groundwater models have respective advantages and disadvantages in relation to the models accessibility, the model's cost, the user easiness and pre-required knowledge and off course the applicability (Feyen, 2005). In attempt to understand the present effect of groundwater withdrawal/loss through ET, a calibrated model is required. Common 3D groundwater flow models include the 3D Finite Element Model of Flow and Transport (3DFEMFAT), AQUA3D, FEFLOW and MODFLOW and then abundant MODFLOW extensions/enhanced versions (Kumar, 2002).

3DFEMFAT's primarily applied for simulating groundwater flow of the saturated and unsaturated/vadose zone, as well as groundwater quality as reported by Camp Dresser & McKee (CDM) (2001). Advantages 3DFEMFAT has over conventional finite-element and finite-difference models, as stated by Kumar (2002), include that 3DFEMFAT eliminates numerical fluctuation ascribed to advection terms. The 3DFEMFAT model is ideal when using a large time step size to significantly reduce numerical diffusion. 3DEMFAT is described as ideal for large scale scenarios and flexible to simulating a wide range of real world scenario's (Kumar, 2002). AQUA3D is a 3D groundwater flow and contaminant transport model, limited to the groundwater flow and water quality modelling of the saturated zone. AQUA3D uses the Galerkin finite-element method to solve transient groundwater flow with inhomogeneous and anisotropic glow (CDM, 2001).

FEFLOW is able to simulate groundwater system (phreatic aquifers/perched groundwater tables/moving meshes) scenario's in saturated as well as unsaturated zones (Kumar, 2002). In defining the numerical model domain in FEFLOW, the super element mesh, the 2D horizontal mesh and the 3D slice elevations are to be defined using horizons, independent of geology (Hesch, 2009). FEFLOW can account for complex geological features. FEFLOW has built in features for fracture modelling, but limited capabilities for groundwater balance evaluations. FEFLOW can simulate drying and/or wetting of cells and the newest FEFLOW versions can compute groundwater age (Kumar, 2002). The code's flexibility makes FEFLOW ideal for simulating complex scenarios, but significant modelling expertise is required to use these model capabilities (Wels et al., 2012). FEFLOW does not permit for the pinching out of model layers and convergence issues arise if the groundwater table intersects with the layer interface with large contrast (Wels et al., 2012). Generally, FEFLOW is more expensive financially and in time

- the license is expensive, but also in time FEFLOW simulations are considered more time consuming to learn and setup, even for experienced modellers (Kumar, 2002).

MODFLOW is reported to be the most widely used numerical groundwater flow model (Feyen, 2005 & Kumar, 2002). Originally developed by the USGS, the developers named the modular three-dimensional groundwater flow model, MODFLOW. MODFLOW is a physically based model and combines mass balance and Darcy's Law for groundwater flow simulations (Kim et al., 2008). Physically-based models solve a form of the groundwater flow equation, initial conditions and given boundary conditions as based on the full description of the aquifer. The aquifer system is described by the geological information and hydraulic parameters of each block/grid cell in the area. MODFLOW subdivides the region into cells/a grid in which the medium properties are assumed to be homogeneous across that cell. The grid is made up of lines that may be variably spaced (Feyen, 2005). Numerical MODFLOW model set up entails defining the horizontal grid resolution, refining the grid and again defining the vertical layers (Feyen, 2005 & Hesch, 2009).

MODFLOW is capable of representing various aquifer conditions such as confined, unconfined, leaky, steady state and transient conditions, and common boundary conditions like variable or constant head boundary conditions, fixed or pressure head boundary conditions, drains and point withdrawals (Feyen, 2005; Kim et al., 2008). MODFLOW is capable of simulating one-dimensional, two-dimensional and full three dimensional models (USGS, 1997). MODFLOW is extended to simulate river channels by using the MODFLOW stream package. The stream package simulates channel-aquifer interaction and channel state using the Manning's equation (Feyen, 2005; Kim et al., 2008). MODFLOW can account for multiple hydrologic processes in addition to the basic finite difference groundwater flow equation solutions. Additions include abstractions, surface water gain/loss and ET (Valerio, 2000). MODFLOW requires estimations of the maximum rooting depth of the vegetation and assumes that no evapotranspiration will take place where the water table is below the reach of the roots. MODFLOW generally simulates water tables which are independent of the topography, except in areas with streams (Feyen, 2005). MODFLOW's data input instructions and theory is extensively documented (documentation available to public) and capable of simulating a wide variety of systems as thoroughly reviewed by USGS (USGS, 1997). MODFLOW is considered less complex to set up and process pre/post files. MODFLOW includes many facilities for preparing data of which the data is transferable in standard form with little effort (Feyen, 2005; USGS, 1997). The code permits for simple modification and adaptation for a particular application, while still having great flexibility for a wide scope of complexity (Feyen, 2005). MODFLOW versions, such as Processing MODFLOW for Windows (PMWIN), are free to use, with new packages added frequently. MODFLOW runs on many different, common computer systems (Kumar, 2002).

The MODFLOW steady state groundwater flow quantification is expressed using Equation 2:19 in comparison to Equation 2:20 which is applied for groundwater flow quantification in transient state. The difference is obvious as the steady state simulation assumes that the difference between the inflow and outflow is zero, thus equilibrium is reached. Equation 2:20 expresses that the dynamic within the aquifer system is not zero and that water can be entered and removed from storage, thus a storage coefficient (S) is included. The other parameters present in both quantification of steady – and transient state include the hydraulic head (h in length unit; meter in this model), the hydraulic conductivities in an x, y and z direction (K_x, K_y and K_z expressed in m/day for the relevant model), the time (day) and W, the addition (source) or removal (pumping) per unit area (m^3/day). The x, y and z refer to the spatial coordination (meters).

Equation 2:19 Steady state groundwater flow equation

$$\frac{\partial}{\partial x}\left(K_x\frac{\partial h}{\partial x}\right)+\frac{\partial}{\partial y}\left(K_y\frac{\partial h}{\partial y}\right)+\frac{\partial}{\partial z}\left(K_z\frac{\partial h}{\partial z}\right)\pm W=0$$

Equation 2:20 Transient state groundwater flow equation

$$\frac{\partial}{\partial x}\left(K_x\frac{\partial h}{\partial x}\right)+\frac{\partial}{\partial y}\left(K_y\frac{\partial h}{\partial y}\right)+\frac{\partial}{\partial z}\left(K_z\frac{\partial h}{\partial z}\right)\pm W=S\frac{\partial h}{\partial t}$$

2.4. Groundwater Recharge

Groundwater recharge is defined as the rainfall portion which reaches the saturated zone. This can be through direct contact with the riparian zone, or just downward percolation through the unsaturated zone to the saturated zone, or lateral groundwater relocation from adjacent aquifers. Recharge is fundamental for continuous aquifer replenishment (DWA, 2010). Effective recharge is often one of the main “unknowns” when determining the regional groundwater balance for catchments. Better estimations of the effective recharge will results in more accurate forecasts of potential groundwater exploitation. Groundwater recharge determination is dependent on data accessibility and distribution, the characteristics of the area under investigation and the capability to apply available data to quantify recharge.

Groundwater recharge estimation methods can be classed as surface water data, unsaturated zone or saturated zone physical methods, chemical tracer type or heat tracer type methods (Healy, 2010). All recharge estimation methods, have advantages and disadvantages related to the data requirements, the estimation accuracy, and the relative cost for that level of estimation accuracy. Methods based on surface water data include stream water-budget methods, streambed seepage determination methods, streamflow duration cure and physical streamflow hydrograph analysis (Healy, 2010). Stream gauging has a relative low cost for moderate accuracy recharge estimations as it only requires streamflow hydrographs. The stream gauging technique is most ideal for humid and temperate climates, with perennial streams connected to a shallow aquifer (Adams *et al.*, 2004).

Physical based methods can be divided into those based on the unsaturated zone and those based on the saturated zone. The zero flux plane (ZFP) method and the Darcy methods are classified as unsaturated zone physical based methods (Healy, 2010). The ZFP refers to the horizontal depth, in the unsaturated zone/soil profile, where the vertical hydraulic gradient is 0. The ZFP marks the separation in groundwater movement direction. Water located above the ZFP is assumed to move only upwards in response to processes such as ET, while water situated beneath the ZFP is assumed to drain downward and replenish groundwater (Healy, 2010). The ZFP thus requires soil water potential profiles and water content changes in relation to time. The moderate accuracy of this method comes at a relatively moderate to high price. The method is most ideal for temperate and semi-arid to arid climates, although applicable to any soil type (Adams *et al.*, 2004). The ZFP method fails during periods of higher precipitation and consequential periods of higher infiltration. Higher infiltration results in a positive hydraulic gradient with an increase in depth below surface (Adams *et al.*, 2004). The Darcian Gradient Method requires hydraulic gradient and unsaturated hydraulic conductivity data input. Although the technique is relevant to any site condition, the estimations are considered low to moderate at a low to moderate cost (Adams *et al.*, 2004). The ZFP and the Darcian Method require hydraulic gradient measurements/estimations which can be measured with instruments such as tensiometers or heat-dissipation probes. The ZFP method is not applicable to steady flow conditions, although the Darcian Method can be adjusted for application in steady flow and transient flow conditions (Healy, 2010).

Physical recharge estimation methods dependent on the saturated zone include water table fluctuation methods and methods based on the Darcy Equation (Haely, 2010). The water level fluctuation methods' estimations range from low to high accuracy at a low cost, but are optimally limited to unconfined aquifers with well characterised flow regimes and recharge areas (Adams *et al.*, 2004).

Chemical tracer methods such as the Tritium profiling, Chlorine-36 profiling, the CMB method, the stable isotope profile and the groundwater age dating method all estimate groundwater recharge to a high accuracy. The groundwater age dating method's accuracy comes at a higher cost in relation to the other chemical tracer methods. The groundwater age dating method is more ideal for shallow unconfined aquifers with vertical hydraulic gradients near the groundwater table, but is applicable to any climate (Adams *et al.*, 2004). The SVF and CMB method is discussed in greater detail in Chapter Method of Investigation.

Chapter 3 Study Area Characterisation

3.1. Study Area Setting

The study area is the quaternary catchment (W32H) within which Lake St. Lucia is located, and the immediate surrounding catchments (W32B, W32C, W32F, W32G and W23D). The study area is located in the north-eastern SA coastal region, in the KZN Province (Stretch & Maro, 2013). The Province is bordered by the Eastern Cape, Mpumalanga and Free State Provinces and the States of Lesotho, Swaziland and Mozambique (Von Roeder, 2014). The relevant catchments are situated in Umkhanyakude District Municipality, predominantly extending across the Big Five False Bay and Mtubatuba Local Municipalities (Figure 3:1).

Lake St. Lucia is an internationally recognized, vital estuary lake system that is the core feature of the iSimangaliso Wetland Park. The iSimangaliso Wetland Park is a United Nations Educational, Scientific and Cultural Organization (UNESCO) World Heritage Site (Vaeret *et al.*, 2009). Inappropriate management of coastal aquifers may result in irreversible damage and destroy freshwater resources (Vaeret *et al.*, 2009). The St. Lucia Estuary links the largest wetland in Africa to the Indian Ocean (Mallory, 2002). In June 2002, the estuary mouth closed for 4 years and 9 months due to drought (Cyrus *et al.,* 2011).

The study site is located within the Mfolozi/Pongola Primary catchment. Lake St. Lucia is located within the Mkhuze drainage area and Mhlathuze Water Management Area (Mallory, 2002). The Lake St. Lucia system stretches roughly 70 km parallel to the southeast coast of Africa and is located in the southern end of the Maputuland coastal plain, which extends north into Mozambique (Vaeret *et al.*, 2009). Despite Lake St. Lucia being an internationally recognised wetland of fundamental environmental importance - extensive forest developments within the lake catchment have continued (Rawlins, 1991). Catchment W32's forestry is predominantly located in catchment W32G and catchment W32H. It is estimated that forestry in W32 results in 18 million m^3/annum runoff reduction and an overall 3 million m^3/annum reduction in yield (Mallory, 2002).

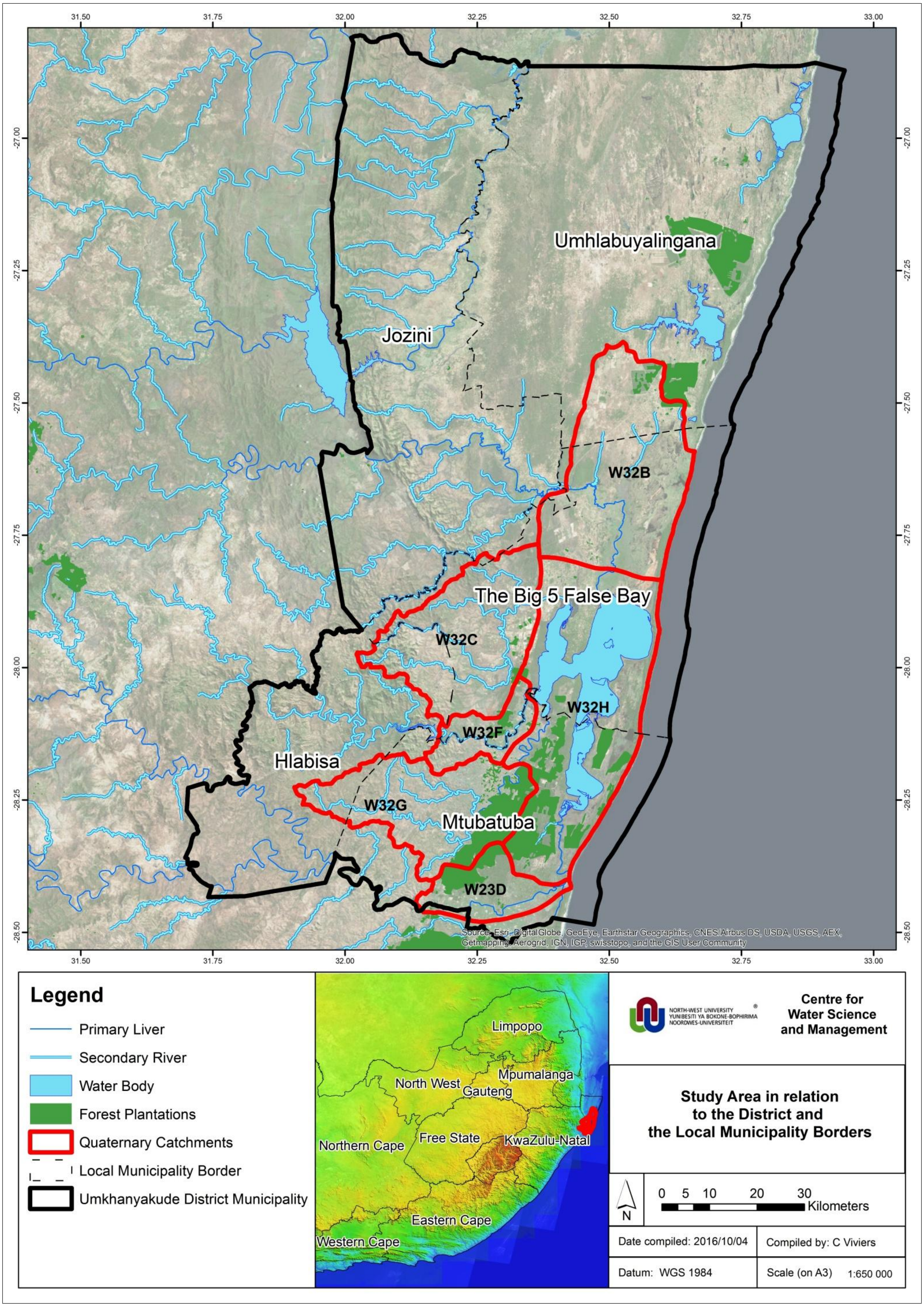

Figure 3:1: Locality Map

3.2. Rainfall

The region is strongly influenced by the warm Agulhas current offshore to the east. Southward migrations of the Inter-tropical Convergence Zone and the El Nino Southern Oscillation have been blamed for quasi-periodic drought/flood periods in the study area (Stretch & Maro, 2013). The well-known rainfall gradient of SA, highest to the east, while decreasing further inland to the west, is clear from the MAPs for the quaternary catchments. The quaternary catchments most east have the highest MAP. The MAP decreases from quaternary catchments most east (W23D, W32H and W32B) to those further inland (W32G, W32F and W32C). The MAP for the respective catchments, in the same order, are 1039 mm/a, 958 mm/a and 901 mm/a bordering the coastline, while decreasing to 846 mm/a, 783 mm/a and 686 mm/a further inland according to the Water Research Commission (WRC) (2016).

There are four rain stations situated in the quaternary catchments relevant to this study. The DWS rain stations are W3E001, W3E002 and W3E003, while the SA Weather Services (SAWS) station, 684910, is situated at DWS station W3E001 (Figure 3:3). The summer temperatures are typically around 30 °C, while the minimum temperatures range from 10 °C during the winter to almost 20 °C during the summer months. Precipitation is greatest during the summer months, when the air temperatures are also the highest.

A temperature and rainfall comparison is shown in Figure 3:2, indicating that almost 75 % of Lake St. Lucia's annual rainfall is from October till March. The average monthly rainfall and MAP was calculated for each rain station, as based on the number of monthly measurements across the relevant timeframes specified (Table 3:1). The rainfall gradient and relation between the monthly precipitations of the different rain stations are displayed in Figure 3:2. Rainfall Stations 684910 and W3E001, situated most east have the highest MAP (941.24 mm/a and 944.48 mm/a respectively), while W3E002 west of the lake and W3E003 further inland, have lower MAPs (693.03 mm/a and 696.72 mm/a respectively).

In summer, rainfall is short of duration and high intensity - vegetation/canopy interception is unlikely to result in a significant recharge loss. In the winter, rainfall is long of duration and low intensity- vegetation/canopy cover is more likely to result in a significant rainfall available for recharge loss (Kelbe et al., 2013b).

Table 3:1 Average monthly precipitation per rain station

		684910	W3E001	W3E002	W3E003
Monthly Measurement Counts		60	285	306	308
Time Frame	**From**	**Jan-10**	**Jul-90**	**Oct-90**	**Oct-90**
	Till	**Dec-14**	**Sep-14**	**Mar-16**	**May-16**
January		128.36	111.54	94.75	101.08
February		72.64	116.36	83.40	101.55
March		145.48	94.75	100.53	59.73
April		48.48	81.68	40.76	43.59
May		19.08	45.77	32.78	26.99
June		24.76	43.65	26.12	23.68
July		41.48	35.92	16.36	16.79
August		22.96	36.83	19.46	19.01
September		71.80	46.64	34.06	38.61
October		127.96	120.43	85.08	88.79
November		114.76	123.17	82.82	95.10
December		123.48	87.75	76.92	81.81
Total mm/a		941.24	944.48	693.03	696.72

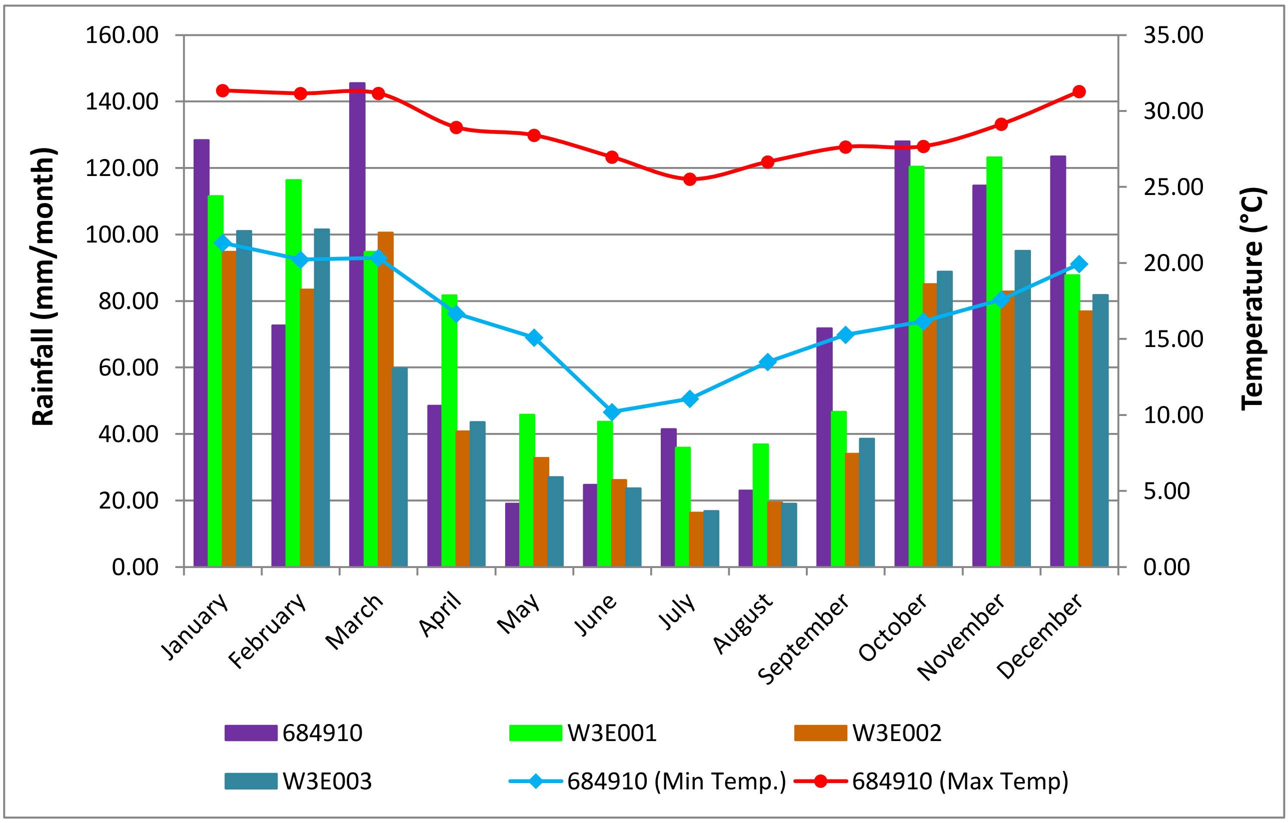

Figure 3:2: MAP comparison for the different rain stations as well as monthly, average minimum and maximum temperatures of station 684910

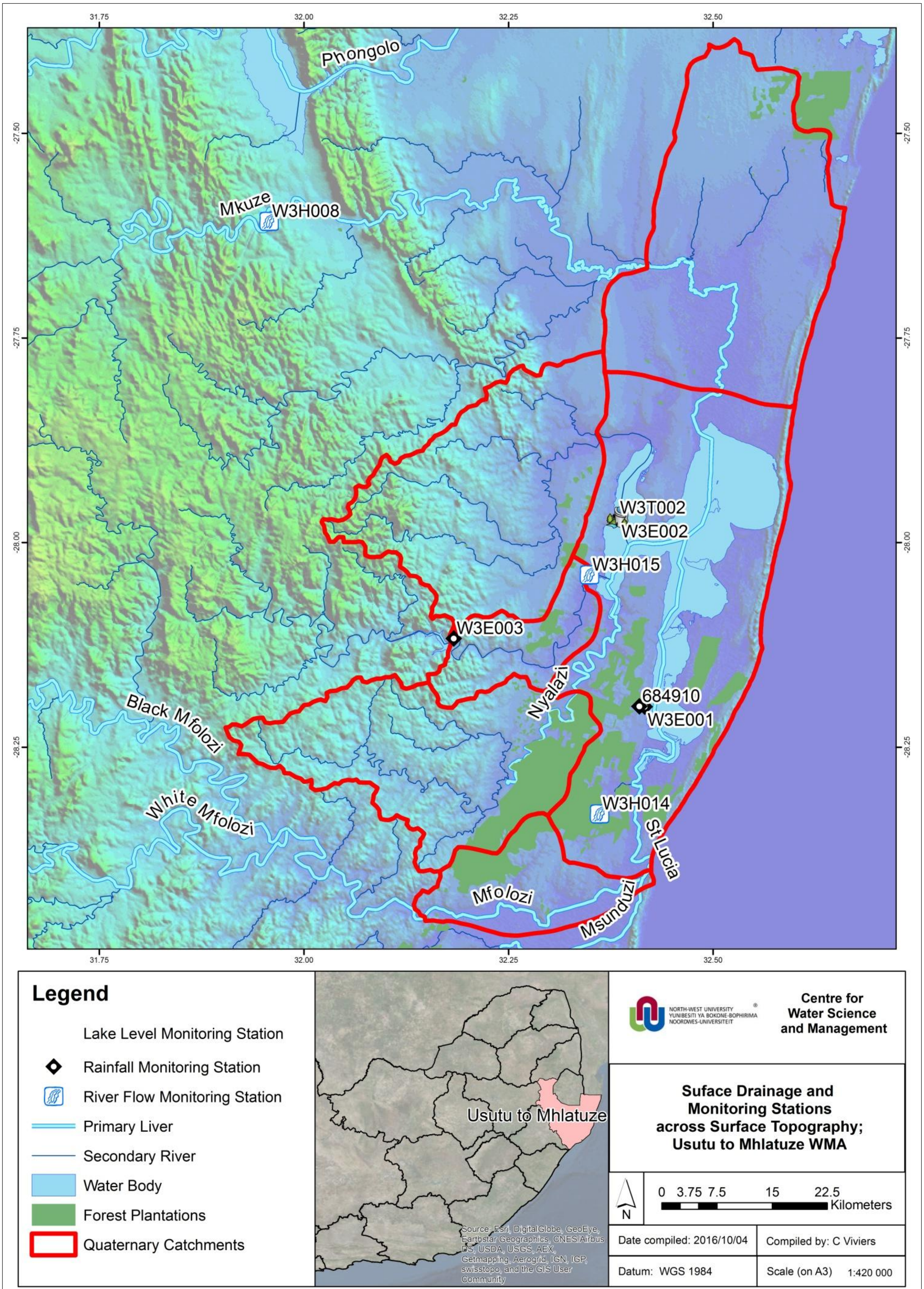

Figure 3:3: Data stations and surface hydrology across topography

3.3. Topography

Topography (Figure 3:3) on the west of Lake St. Lucia is characterised by a low lying plain, while the east is characterised by the high coastal dune belt. To the north red sand dunes form a central dune belt (Rawlins, 1991). The topography gradients in the St. Lucia catchment (excluding the Mfolozi catchment) are small (Stretch & Maro, 2013). Elevations do not even increase by a 100 m in the first 30 km inland from sea level, however elevations quickly increase and so the gradients to around a 1000 m within the next 120 km inland (Stretch & Maro, 2013). The elevations decrease from 1 600 m in the west to sea level in the east.

There is a strong (98 %) linear correlation between the topography and the groundwater hydraulic head (Figure 3:4). Unconfined aquifers are associated with high surface topography and groundwater correlations as explained by Haitjema and Mitchell-Bruker (2005). The water table in unconfined aquifers, is most often assumed to be a replica of the topography (Haitjema and Mitchell-Bruker, 2005). Groundwater and topography are always related in a general sense since shallow water tables occur near surface water, and surface waters occur in topographically low areas (Haitjema and Mitchell-Bruker, 2005).

The Haitjema and Mitchell-Bruker (2005) study indicates that the difference between the topography and water levels are dependent on recharge, hydraulic conductivity, aquifer thickness and the distance between surface water features.

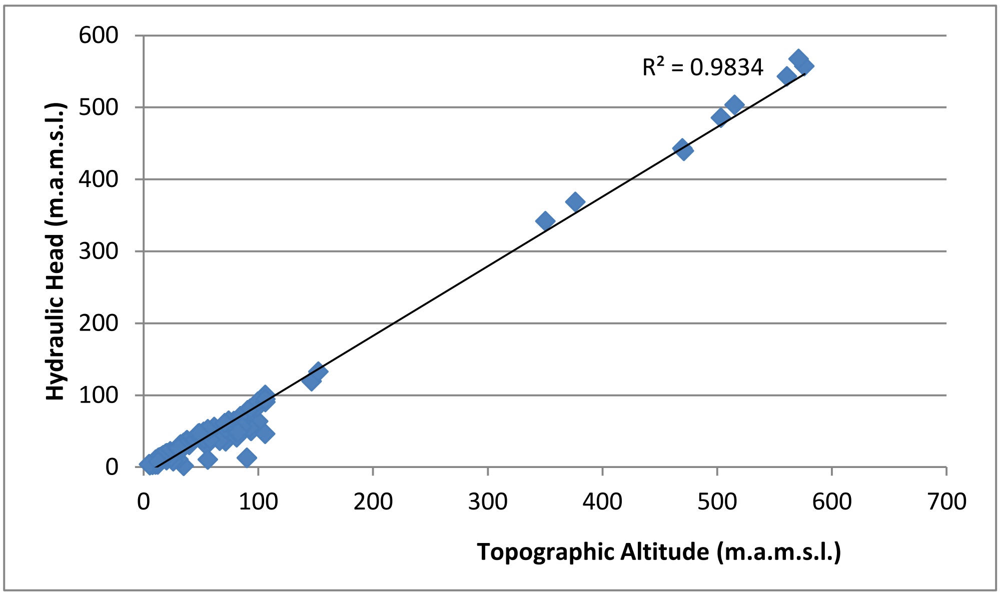

Figure 3:4 Linear correlation between topography and groundwater hydraulic head

3.4. Soil

Soil profiles reveal that the surface layer is almost completely sand, and has a low organic content. Organic material is seldom detected at a depth greater than 0.5 m. Except for the immediate surface layer in a dense vegetated area, the organic content is generally low (Rawlins, 1991). The sand fraction results in a high infiltration rate, and consequently minimal surface runoff. The area is comprised of unconsolidated alluvium, aeolian and estuarine sands and clays (Rawlins, 1991). Soil types vary from sandy soils at low elevations in the east, to loam soils at higher elevations to the west of the catchments. The dominant soil types, in catchments W32H is loamy sand, while the dominant soil type in catchment W32G is loam soil (Stretch & Maro, 2013).

While the coastal dunes have a maximum height of 100 m, this thickness decreases to only 3 m on the plains (Rawlins, 1991). The unconsolidated sands, silts, organic material and clays have various hydraulic properties that can alter expected groundwater flow rates and directions (Rawlins, 1991). The high permeability of the sand layers, increases water movement, while clays and silts restrict and redirect water movement. Water infiltration can be restricted to the formation of a shallow perched aquifer in the case of high clay and silt (Rawlins, 1991).

The soils are classified as Arenosols as they are deep, have a great sand fraction and have a low fertility combined with a high porosity resulting in a low water capacity (Von Roeder, 2014; Rawlins, 1991). These soils are part of the Quaternary deposits. The dunes are mainly comprised of quartz, while the younger dunes from the east are white and become more reddish to brown to the west as the dunes become older (Von Roeder, 2014). Where dunes are covered by woody vegetation, soils are a darker greyish-brown as explained by the higher humus content. Alluvials are classified near the wetlands and rivers as they are made up of sands with organic material (Rawlins, 1991; Von Roeder, 2014). The impermeable Pleistocene Port Dunford Formation is responsible for the shallow water table. The high rainfall combined with the permeable soils, results in leaching that contributes to the soils being infertile. While soil moisture deficiencies are expected during the winter, it is worsened by the high permeability of the quaternary sandy soils (Von Roeder, 2014).

Soil and geology impact the ET rate by influencing the quantity of water available for ET (Nisbet, 2005).

3.5. Geology

Pre-Cambrian Period: The Kaapvaal Craton gneissic granites, buried under the Pongola Supergroup (amphibolites) and sedimentary rocks, are the oldest rocks in the Mkhuze (Lake St. Lucia) and Mfolozi (south of the Lake St. Lucia catchment) catchments (Botha *et al.*, 2013; Nomquphy, 1998).

Jurassic Period: The formation of Gondwana as a product of Pangaea's split, in the early Jurassic, led to rifting and the formation of the south-east African continental margin as well as the launch of the Indian Ocean's evolution. The rifting was initiated by the injection of Karoo magmas. The Pongola Supergroup is overlain by this Permo-Triassic Karoo Supergroup that resulted from Karoo magma intrusion (Botha *et al.*, 2013). The Permo-Triassic Karoo Sedimentary succession is overlain by the Lebombo Group volcanic rocks (amygdaloidal trachy basalts), which is again overlain by Mesozoic and Cenozoic marine deposits (Botha *et al.*, 2013; Nomquphy, 1998). The Lebombo Mountains are made up of lower basaltic (Letaba Formation) and overlying, upper ryholitic (Jozini Formation) lavas. The combined thickness of these two layers exceed 7 000 m (Norman & Whitfield, 2006). The Jozini Formation's pyroclastic and rhyolite volcanic rocks, are 2000 m thick (Botha *et al.*, 2013; Von Roeder, 2014).

Cretaceous Period: The unconform Cretaceous layer is a thick layer, overlying pre-cretaceous lavas and granites. This interface has no influence on the shallow geohydrological regime as it is more than a kilometre below the sea level (Rawlins, 1991). The Mesozoic Zululand Basin beneath Lake St. Lucia, and near wetlands, underwent sedimentation due to the developing continental margin uplift. The uplift led to sedimentation in subsiding rift valleys and accumulation of the Zululand Group's Makitini Formation's sandstone, shales, mudstone and conglomerate - which slightly dips seaward (Botha *et al.,* 2013; Rawlins, 1991; Vaeret *et al.*, 2009; Von Roeder, 2014). Seventy five million years later, erosion of the rift resulted in the removal of 1-3 km thick Karoo Supergroup, deposited on the subsiding continental shelf. For most of the Cretaceous Period, the continental margin was submerged as a shallow continental shelf due to marine transgression and regression cycles (Botha *et al.*, 2013). A hiatus boundary is overlain by the accumulation of the shallow marine Mzinene Formation made up of clayey, fine-grained sandstones and glauconitic siltstones (Botha *et al.*, 2013; Nomquphy, 1998; Rawlins, 1991). The individual cycles of the succession of sandstone and siltstones can be recognised by a layer of light grey-orange sandy limestone concretions (Botha *et al.*, 2013; Rawlins, 1991; Vaeret *et al.*, 2009;). The mid-Cretaceous hiatus distinguishes the Mzinene Formation from the sequential late-Cretaceous, St. Lucia Formation. The St. Lucia Formation is the result of transgression across the Zululand Basin and is predominantly siltstone (Botha *et al.*, 2013).

Since the rifting of East and West Gondwana, a drainage system had begun to develop, and is still an ongoing geomorphologic process. The drainage system flows from the proto-Drakensberg escarpment. The Lake St. Lucia catchment has been dominated by erosion degradation. The development of Lake St. Lucia basin in the late Quaternary Period can be located in Maputuland Group coastal lake, dune and wetland deposits (Botha *et al.*, 2013).

Tertiary Period: During part of the Eocene, the continental margin was flooded (transgression), while regression dominated during the Oligocene. Regression, due to the lowering of the sea level, combined with rhythmical epeirogenic uplift during the late-Miocene and Pliocene (Neogene Period) resulted in a step-like, marine-planed bedrock surface buried under deposits, indicative of the previous higher water level along the shore (Botha *et al.*, 2013). This buried bedrock is the shelly limestone, conglomerates and coarse grained sandstones of the Uloa Formation (Botha *et al.*, 2013; Nomquphy, 1998; Rawlins, 1991; Vaeret *et al.*, 2009).

Quaternary Period: During the last 2.6 million years, Pleistocene and Holocene climate variability led to denudation processes dominating the evolution of the eastern coastal zone. Repetitive base-level changes are ascribed to glacio-eustatic sea-level fluctuations. Estuarine (fossiliferous), flat-lying, partially consolidated sandy deposits of the Port Dunford Formation, accumulated during the late-mid Pleistocene (Botha *et al.*, 2013; Nomquphy, 1998; Rawlins, 1991; Von Roeder, 2014). The Port Dunford Formation has a maximum thickness of 50 m and is made up of yellowish-orange sands, light grey sand, mudstone, lignite clayey sands and corals, largely covered by Aeolian sands (Rawlins, 1991; Vaeret *et al.*, 2009; Von Roeder, 2014). The Port Dunford Formation serves as an aquitard for overlying aquifers. Coastal dune and wetland systems form the Kosi Bay Formation succession, and are presently overlain by the dunes of the KwaMbonambi Formation (Botha *et al.*, 2013; Vaeret *et al.*, 2009; Von Roeder, 2014). The Kosi Bay Formation is partly clay enriched and with a decrease in depth, becomes well-drained along the transition to red sands at the top of the formation (Vaeret *et al.*, 2009). During the last glacial cycles, calcareous dunes have gradually grown to form the Isipingo Formation, reported to be up to 180 m high (Botha *et al.*, 2013; Vaeret *et al.*, 2009; Von Roeder, 2014). Present dune systems (cyclic erosion history) of the eastern shore correlate with periods of global climate variability (Botha *et al.*, 2013). The dune barrier, on the eastern shores, separates Lake St. Lucia from the Indian Ocean. In the Lake St. Lucia area specifically, the dunes do not extend inland further than 1 km (Vaeret *et al.*, 2009).

Lake St. Lucia's basin, in its present state, is the product of an open lagoon formed by marine transgression during the early Holocene Epoch. Five thousand years of combined segmentation, sedimentation and reed swamp encroachment has transformed what once was a lagoon, into a wetland. Transgression dominated at the peak of the mid-Holocene (Botha *et al.*, 2013). It is estimated that by the late-Holocene the lake area had already reduced by 60 %.

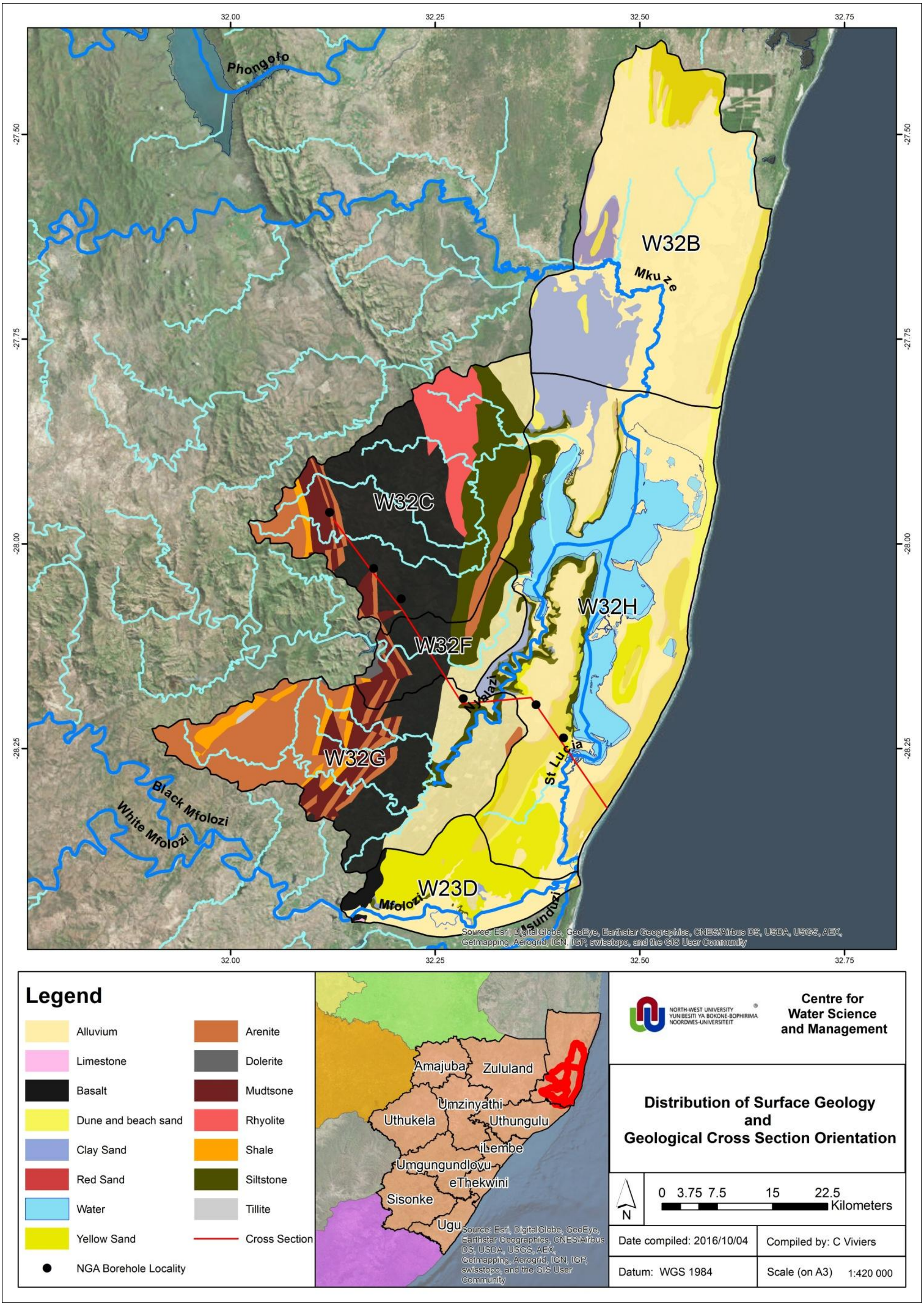

Figure 3:5: Surface geology and cross section locality map (Esri, 2016)

Lake St. Lucia has an average depth of 0.9 m over an area of 350 km^2. The progressively younger shoreline sequence indicates the decrease in water levels as well as the decreasing St. Lucia Lake area associated with sequential regression. The youngest ridge indicates stabilization of the lake close to its present level up to 900 years ago (Botha *et al.*, 2013; Von Roeder, 2014).

Surface Geology Map: In consideration of the literature on the formation of Lake St. Lucia's geological setting, a cross-section of the Lebomo Mountains by Norman and Whitfield (2006), the NGA borehole logs and the surface geology map (1:250 000 Geological Maps) a cross section was constructed (Figure 3:6) along the line in Figure 3:5.

The oldest geological formations outcrop to the west of the study area, while the formations become increasingly younger towards the Indian Ocean/Lake St. Lucia in the east. The Drakensberg Lavas are known as the Letaba Formation forms part of the Lebombo Group (Norman & Whitfield, 2006). In the absence of basement granite outcrops within the study area boundaries, the Karoo Supergroup dominates as the most abundant pre-cretaceous geology. The Karoo Supergroup characterise the sediments outcropping east of the study area, dipping eastwards (Norman & Whitfield, 2006). The oldest surface geological unit in the study area, is the Karoo Supergroup’s Dwyka Group's Tillite, outcropping to the west in quaternary catchment W32G. The tillite outcrops from beneath the overlying, and younger, shale and sandstone (arenite) from the Ecca Group (Norman & Whitfield, 2006). The Beaufort Group's shale and mudstone unconformably overlie the Ecca Group. The Stormberg sediments consist of the Molteno, Elliot and Clarens Formation's sandstones (Norman & Whitfield, 2006).

The sequential lithological group, the Lebombo Group, consists of the Letaba and the Jozini Formations. The basalts characterise the lower Letaba Formation, while the rhyolites characterises the upper Jozini Formation (Norman & Whitfield, 2006). The Letaba basalts coincide with soils dark in colour and rich in clays (Norman & Whitfield, 2006). The basalts are abundant west of the tertiary sediments. The youngest formations of the Karoo Supergroup are the Karoo dolerites (Norman & Whitfield, 2006). The Zululand Group's siltstone and sandstone outcrop west of the quaternary deposits, marking the second youngest geological formation in the study area. The quaternary sands, with varying clay contents, form the eastern boundary of the study area. The distributions of these formations are displayed in Figure 3:5.

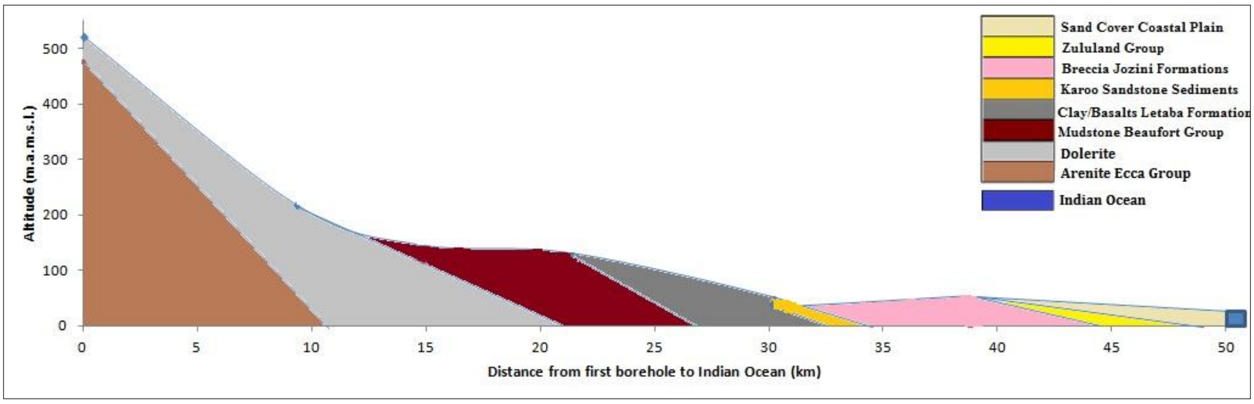

Figure 3:6 Geological cross section along line in Figure 3:5

3.6. Hydrological Setting

Lake St. Lucia is supplied by five rivers namely the Mkhuze River which is most north and the main river draining the area, as well as the Mzinene River, the Hluhluwe River, the Nyalazi River and the Mpate River which are smaller rivers that discharge directly into the lake Figure 3:3. In the south, close to the mouth of Lake St. Lucia, the Msunduze River flows, but does not supply water to Lake St. Lucia directly (Kelbe & Germishuyse, 2010; Rawlins, 1991; Stretch & Maro, 2013). The uMfolozi River only supplies to the Lake St. Lucia Estuary periodically since 1952 (Kelbe *et al.,* 2013b; Rawlins, 1991). The rivers are seasonal, restricted to flow during the wet, summer rainfall seasons, while forming isolated pools in the dry, winter seasons (Stretch & Maro, 2013; Von Roeder, 2014).

In 1952, the uMfolozi (Mfolozi) River was partially separated from the Lake St. Lucia Estuary for consideration of sugarcane farming (Kelbe *et al.,* 2013b; Rawlins, 1991). The uMfolozi River was separated from Lake St. Lucia by depositions of dredge spoil in the natural river course into the St. Lucia Estuary, artificially breaching the uMfolozi River into the Indian Ocean near Maphelane (iSimangaliso Wetland Park, 2016). Hereafter, dredge spoil was periodically deposited in the uMfolozi River, significantly reducing freshwater to Lake St. Lucia from the largest river entering the system. The uMfolozi River is reported to supply 60 % of Lake St. Lucia's fresh water when included in the system (iSimangaliso Wetland Park, 2016.a).

In 2012, research concluded that natural Lake St. Lucia system function, such as permitting the re-join of the uMfolozi River's freshwater into the Lake St. Lucia Estuary, is vital for the system's recovery. By then, the Lake St. Lucia Estuary was already drying up and the system degrading; a strategy to restore the natural function of the system and re-join the uMfolozi River's flow into the Lake St. Lucia system, was implemented (iSimangaliso Wetland Park, 2014). Since 2012, the ecosystem indicators have confirmed compelling recovery, despite receiving lower annual rainfall. Aerial imagery from 2013, still indicate dredge spoil separating the uMfolozi River from the Lake St. Lucia (iSimangaliso Wetland Park, 2014).

In March 2016, the iSimangaliso Newsletter, reported that the uMfolozi River was flowing into the St. Lucia Lake Estuary. The rainfall, which brought hope of repair after 90 % of Lake St. Lucia had dried up, leaving 315 km^2 of the 350 km^2 area exposed, also brought an uMfolozi Sugar Planters (UCOSP) notification, initiating the establishment of the uMfolzi River out to sea again. Excavators were deployed the same day to again separate the uMfolzi River from the Lake St. Lucia Estuary (iSimangaliso Wetland Park, 2016.b).

Sediment loads, especially that from the large Mkhuze River, which drains the Lebombo Mountains, fills the Lake's mouth, forming meandering distributaries. The sandy Eastern Shore contributes to Lake St. Lucia by groundwater and small streamflow (Rawlins, 1991; Stretch & Maro, 2013).

Fluctuations in the water level of Lake St. Lucia will influence groundwater flow rates and quantities (Rawlins, 1991). Water level measurements since 1958 reveal that the water levels fluctuate in response to prevailing winds, tidal motions and other hydrological fluctuations. The result is that the lake surface area varies between 230 and 410 km^2 (Rawlins, 1991). The estimated total area that drains directly into Lake St. Lucia is between 7 575 km^2 and 8 900 km^2 (Kelbe *et al.*, 2013b; Rawlins, 1991). Wetlands increase in occurrence and size closer to Lake St. Lucia and respond directly to climate variation through water depth and wetland size variation (Rawlins, 1991). The absence of rivers on the eastern shoreline, indicate that the recharge must enter the lake through groundwater seepage, and the presence of inter-dunal wetlands indicate a shallow water table (Nomquphy, 1998; Von Roeder, 2014).

There are three DWS river flow monitoring stations in the study area namely, W3H008, W3H014 and W3H015, while the water level in Lake St. Lucia is monitored by DWS estuary station W3T002 (Figure 3:3). The W3H008 station, which monitors the flow of the Mkuze River, and the W3H014 station which monitors the flow of the Mpate River, have more time distributed river flow data that the W3H015 station which monitors flow in the Hluhluwe River.

March is the first month of the year where the water levels of all the rivers and the lake raised from the previous month. The water level increase is ascribed to the March rainfall peak (12.14 %), while the rainfall decreases to half that (6.48 %) in April (Table 3:2). The water levels of the river monitoring stations W3H008 and W3H015 continue to increase in April despite the decrease in rainfall, although the water levels of stations W3H014 and W3T002 decrease. The water levels of all the river monitoring stations decrease in the sequential month. The lake water level rises after a rainfall episode in October, while the increase in river water level is only again visible in January (Table 3:2).

Table 3:2: Average monthly river and lake water level per monitoring station and percentile of annual precipitation for month

	Average monthly river water level per monitoring station			Lake monthly average water level	Percentile of annual rainfall per month
Month	**W3H008**	**W3H014**	**W3H015**	W3T002	**Precipitation (%)**
January	0.190	0.041	-	0.625	13.41
February	0.059	0.043	-	0.690	11.66
March	0.144	0.052	0.089	0.722	12.14
April	0.312	0.026	0.170	0.686	6.48
May	0.296	0.016	0.023	0.700	3.87
June	0.001	0.006	-	0.644	3.60
July	0.010	0.005	0.043	0.644	3.25
August	0.085	0.007	-	0.656	2.97
September	-	0.003	-	0.633	5.76
October	0.010	0.043	-	0.602	12.84
November	-	0.019	-	0.622	12.71
December	-	0.007	-	0.675	11.31
Months for which any data is available	9	12	4	12	12

Under normal (not dry) climate conditions, the major rivers supply the lake with the dominant proportion of the water budget, as the base flow provides less than 10 % of the total water budget (Kelbe & Germishuyse, 2010). The groundwater flow remains consistent while the rainfall and river runoff varies, thus during drought conditions, when river runoff and rainfall contributions may be depleted, the contribution of the groundwater becomes more significant (Kelbe & Germishuyse, 2010). In extreme drought conditions, the groundwater inflow may become the only freshwater supply for the lake (Kelbe & Germishuyse, 2010). In extreme drought conditions, inflow of saline water from the Indian Ocean can result in high salinities (Kelbe & Germishuyse, 2010).

During a rock's formation, the rock's magnetism aligns to that of the Earth's magnetic field. Variation in the Earth's magnetic field during the formation of different rocks, results in variations in the magnetism of the different rocks. A deviation of the magnetic field from the regional, average expected magnetic field, is a magnetic anomaly, and assists in detecting geological structures (McCarthy & Rubidge, 2005). Figure 3:7 indicates the magnetic anomalies dictated on a regional scale through satellite/aerial imagery, indicating the absence of compartmentalization across the aquifer. The boreholes with time series groundwater level data are clustered to the east of the Lake St. Lucia (Figure 3:7).

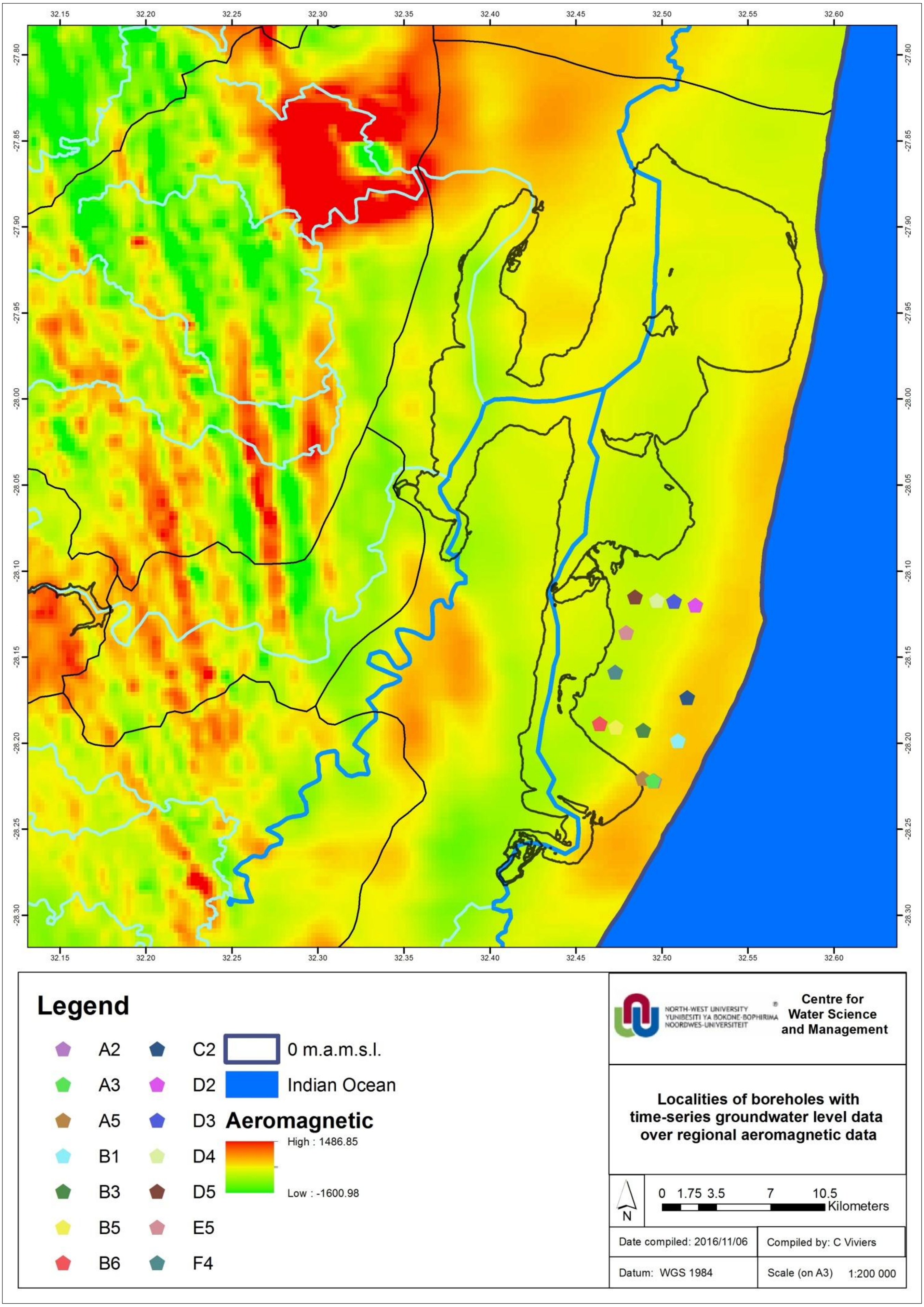

Figure 3:7 Localities of time series boreholes over magnetic regional imagery

The absence of compartmentalisation by confining intrusions is confirmed (Figure 3:7) in addition of the groundwater versus topography correlation, as the time series groundwater level data of the various boreholes all have the same pattern (tendencies). The depth to groundwater level becomes shallower for all boreholes around the end of August 2002; although the last recorded increased precipitation prior to this phenomenon was a month earlier, in July 2002. Boreholes B3 and D4's are exceptions as the groundwater levels do not become shallower in July 2002.

In January 2004, 236.2 mm precipitation only resulted in a regional groundwater level increase (shallower depth to groundwater level) in late March 2004. The 243.6 mm rainfall of March 2005, again only resulted in a regional groundwater level increase in May 2005. A period of no rainfall extending six months from December 2001 till May 2002, resulted in a regional groundwater level deepening below topographic surface by approximately 1 m. The groundwater levels become shallower again by August 2002 in response to gradual increasing precipitation from May till July 2002 (borehole B3 and D3 for example in Figure 3:8).

Boreholes B1 and C2 are situated most east and closest to the Indian Ocean, and have very shallow groundwater levels in comparison to the groundwater levels of boreholes situated further inland. Borehole E5's groundwater level is on average 2 m deeper than the groundwater level of its neighbouring borehole D5. Borehole D2's, situated on the transition zone between the coastal dune shoulder and flat plains, groundwater level has little fluctuation, even in response to precipitation.

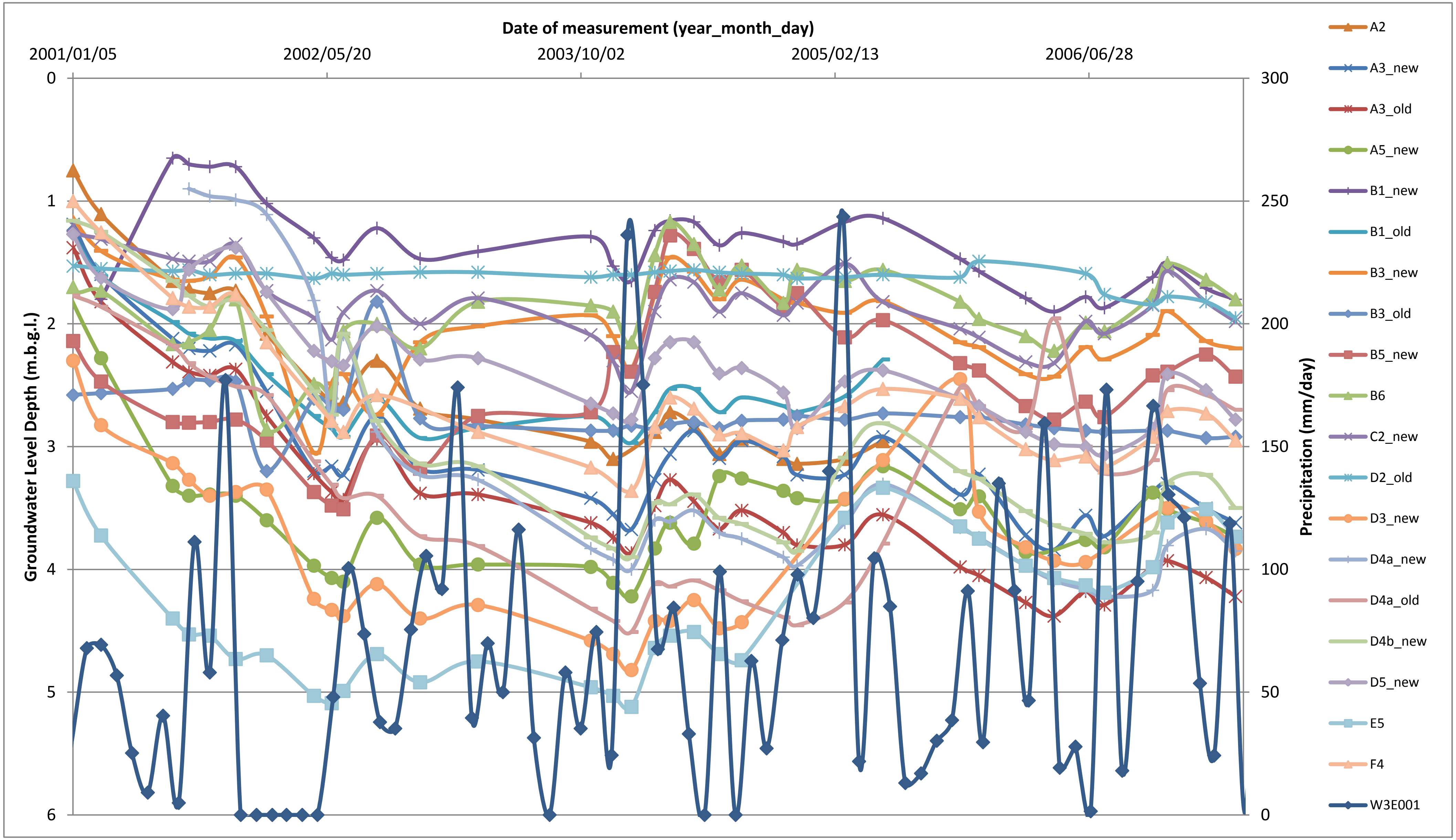

Figure 3:8 Time Series Groundwater Level Data for boreholes in study area (NGA and DWS data)

3.7. Ground- and surface water interaction

The surface waters are extensions of the primary aquifer (Kelbe & Germishuyse, 2010). Along a coastal terrain, ET directly from the groundwater is widespread, because the topography is generally flat and the water table close to the land surface. In these terrains it is common for plant' roots to infiltrate deep enough to transpire groundwater in the absence of a confining layer - causing a significant water loss (Feyen, 2005).

Outside of the study area, to the west, but still within the Lake St. Lucia catchment, secondary aquifers are located within the consolidated Jurassic basalts and rhyolitic rock fractures and fault systems - which are buried under sedimentary rocks. The secondary aquifers release their stored water when the fault or fracture intersects a drainage boundary such as a river/wetland (Kelbe *et al.*, 2013b; Von Roeder, 2014). The contribution of the secondary aquifer to Lake St. Lucia's base flow is neglectable, except during droughts when its contribution to inflow increases more significantly. The primary porosity is crucial for the groundwater dynamics of the whole St. Lucia catchment (Kelbe *et al.*, 2013b; Von Roeder, 2014).

The base flow was calculated for each quaternary catchment using the Harold Method in Aquiworx (See Appendix A).

Table 3:3 Groundwater contributions to river flow according to Herold Method (Baseflow)

Quaternary Catchment	PG Parameter	Decay Parameter	Base flow (Mm^3/a)	Hughes (Mm^3/a)	Pitman (Mm^3/a)	Schultz (Mm^3/a)	V. Tonder (Mm^3/a)
W32B	2.5	0.86	23.424	40.2	20.47	36	28.94
W32C	1.7	0.67	2.309	11.7	2.31	4.8	4.72
W32H	1.3	0.88	26.793	51.05	25.84	43.10	35.8
W32F	2	0.42	3.319	19.15	3.04	6.30	6.81
W32G	1.1	0.77	8.875	23.92	3.37	7.6	8.2
W23D	1.6	0.78	31.773	66.36	29.89	54	44.01

Located within quaternary catchments W32H and W32G, Cretaceous clay stones and siltstones form the aquiclude beneath the Cenozoic, primary aquifer. This aquiclude formed during the Cretaceous Period, when the area was submerged. This hydrological unit has low porosities and thus a low conductivity (Kelbe *et al.*, 2013b). East of the Lebombo Mountains, the coastal plain is made up of Miocene, Pliocene, Pleistocene and Holocene unconsolidated sedimentary deposits that overlies this Cretaceous aquiclude - forming an effective primary aquifer. The primary aquifer is the product of marine succession combined with alluvial and aeolian processes. The resulting hydro-stratigraphical units have varying clay, sand and silt combinations with different hydrological properties (Kelbe *et al.*, 2013b).

The Uloa Mio-Pliocene Formation is buried under Middle to Late Pleistocene estuarine, marine sand, clay and silt off varying thickness. Generally, the Middle to Late Pleistocene sediments have lower porosities, hydraulic conductivities and are less permeable. This results in a partial confining hydro-stratigraphical unit that separates the Cretaceous aquiclude from the overlying Port Dunford sediments, creating a leaky aquifer (Kelbe *et al.*, 2013b). Younger, more permeable sand formations of the Late Pleistocene to Holocene age bury the Middle to Late Pleistocene Port Dunford sediments. The youngest Holocene sediments are usually expected to have the highest porosity, permeability and hydrologic conductivity (Kelbe *et al.*, 2013b).

The water level is shallower in the east, while the water table is deeper below the ground surface to the west in an inland direction. The flow is directed from the west to the east at a relative rapid rate due to the highly permeable soils (Rawlins & Kelbe, 1998; Von Roeder, 2014). The primary aquifer of the study area has an exceptionally shallow water table as supported by the wetlands (Kelbe *et al.*, 2013b). Von Roeder (2014) reports that the groundwater level is usually located one to six meters below the ground surface, but that it may vary.

Groundwater recharge within the St. Lucia primary porosity aquifer occurs dominantly through percolation through the unsaturated zone. The soil water available for recharge is dependent on the rainfall rate and land use (Kelbe *et al.*, 2013b; Von Roeder, 2014). An observed shallow aquifer on the Eastern Shores indicated that a cumulative rainfall event, with a rainfall higher than 10 mm, resulted in an increase of the shallow aquifers' water table that is proportional to the magnitude of the rainfall event (Kelbe & Shezi, 2010). The response time of the water table to the rainfall event increases with increasing depth to water table (Rawlins & Kelbe, 1998).

3.8. Conceptual Model

A conceptual model serves as a tool for simplifying the system while still achieving the intended analysis' purpose. The scenario is simplified and organized as to more readily analyse the complex, dynamic system (Kelbe and Germishuyse, 2010). A conceptual model accounts for measured field data and the interpretation of the dynamics thereof. A conceptual model assists in making modelling repeatable and consequently more scientifically acceptable.

Wetlands and lakes are recharged by rivers, precipitation and groundwater (baseflow), while discharge occurs through rivers, evaporation and baseflow, as well as abstraction to fulfil users' water supply (Kelbe and Germishuyse, 2010). Lake St. Lucia is classified as a coastal lake with direct connection to the ocean through estuaries. Along the shoreline direct seepage to the lake is to be expected and any head differences between the underlying aquifer and the lake, or the rivers that feed the lake, will result in Darcian flow through the bed sediments (Kelbe and Germishuyse, 2010). The main force for groundwater movement is the change of hydraulic head over a certain distance (Darcy's Law). Groundwater moves from higher hydraulic heads towards lower hydraulic heads (Feyen, 2005). Groundwater movement however is not just controlled by the hydraulic gradient, but also by the hydraulic conductivity distribution throughout the geology. Groundwater, in addition to topography and geology, is influenced by recharge - and only together when considering interaction, can the groundwater flow be established (Feyen, 2005).

Along the eastern coastal plain, the groundwater has a low gradient within the primary aquifer, but towards the west inland, the groundwater gradient becomes steeper within the secondary aquifer - groundwater flow rates are thus lower in the primary aquifer (Kelbe *et al.*, 2013b).

The change in storage in the groundwater balance model is the difference between the input and output. Physical boundaries define the spatial extent of water available for abstraction/outflow. Within a hydro-stratigraphic unit, geological and hydrological properties may vary, but are assessed as one uniform unit as based on the dominant averaged properties (Kelbe and Germishuyse, 2010).

Cyrus *et al.* (2011) report that 50 % of the lake system's water is from freshwater inflow, while the remaining 50 % is directly from precipitation.

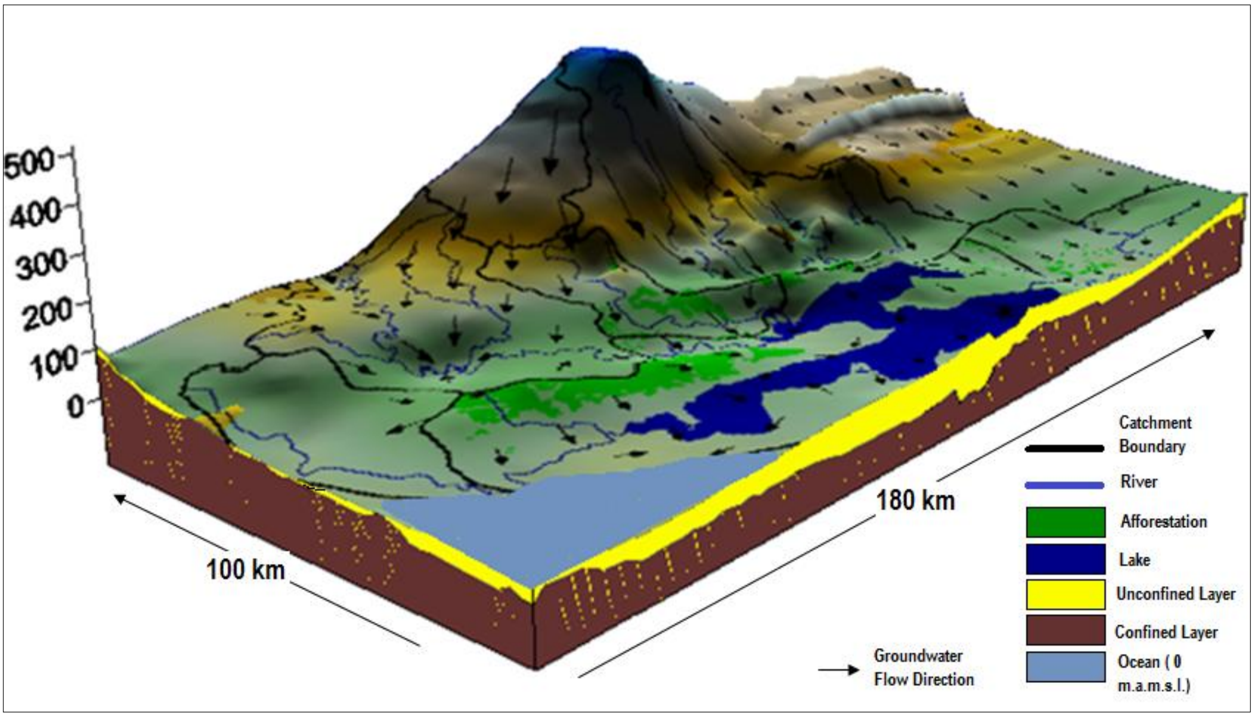

Figure 3:9 Groundwater flow direction, forestry, river and lake locations, and unconsolidated layer over confined layer

The two main hydrostratigraphic units for the Lake St. Lucia regional aquifer is that of the (1) Isipingo, Sibayi and Kosi Bay formation and the (2) Port Dunford Formation. The two hydro-stratigraphical units are not well established and even indistinguishable in many areas. Generally, the water level is near the interface of the two hydrostratigraphical units, forming an unconfined aquifer (Vaert *et al.*, 2009). The aquifer bottom is formed by the impermeable Cretaceous siltstones (Vaert *et al.*, 2009). The Eastern Shores are dominantly covered by highly permeable, well drained sediments without surface runoff apart from rivers mentioned (Vaert *et al.*, 2009). Evaporation and ET occur at rates dependent on the atmospheric demand, and is conceptually modelled at the maximum rate at which the atmosphere is capable of accepting the vapour flux, the PET.

Chapter 4 Method of Investigation

4.1. Analytical Models

Analytical modelling includes selecting the most representative data sets and variables as well as the implementation of the right techniques to format the data. A model is classified as an analytical model when the system is entirely described by mathematical equations - accounting for the interactions between parameters. An exact solution (analytical) model, as for the relevance of the project, is defined as the equations describing the interactions and performance of the system. It describes a collection of measured data, to calculate behaviours and parameter reactions of different elements over a finite time period (Caliri, 2000). In attempt to derive more time variant/transient data as well as limit literature input data (assumptions) for the numerical model, analytical models were used. The SVF method and the CMB method methods were used to calculate groundwater recharge, while ET_0 was simulated using the S&W analytical model.

4.1.1. Saturated Volume Fluctuation Recharge Calculation Method

Time series water level data, is only available across the alluvial/sedimentary deposits, thus the SVF method could only be applied for recharge calculations across this surface geology. The SVF method is a water table fluctuation method (Perkins & Nimmo, 2006). The SVF method is a simulation of an aquifer's water level response, and permits the quantification of aquifer storativity and effective recharge (Adams *et al.,* 2004). The water table fluctuation methods estimate groundwater recharge through analyses of water level fluctuations in observation boreholes (Perkins & Nimmo, 2006). The storage in the saturated zone (groundwater) can be expressed as a system with inputs and outputs as a water budget. The water budget expresses that groundwater storage at depths greater than that of the zero flux plane are increased through recharge and subsurface flow into the area, and decreased through base flow, ET and subsurface flow out of the area (Healy, 2010). As can be seen from the SVF equation (Equation 4:1), the method accounts for inputs in relation to outputs over a specific timeframe of water balance, as well as the change in storage in the systems as caused by this imbalance between inputs and outputs (Adams *et al.*, 2004)

The calendar year 2004, was the most recent year for which most of the monitoring boreholes had the most complete time series water level data. The mean monthly water levels of 15 monitoring boreholes were used to calculated aquifer recharge for the alluvium geology with the SVF method (Figure 4:1).

Equation 4:1 Saturated Volume Fluctuation (Van Tonder & Xu, 2000; Adams *et al.,* 2004)

$$h[i] = h[i-1] + \frac{\%Recharge \times Precip[i]}{Sy} + \frac{Inflow[i] - Outflow[i]}{Sy \times Area} - \frac{Abstract[i]}{Sy \times Area}$$

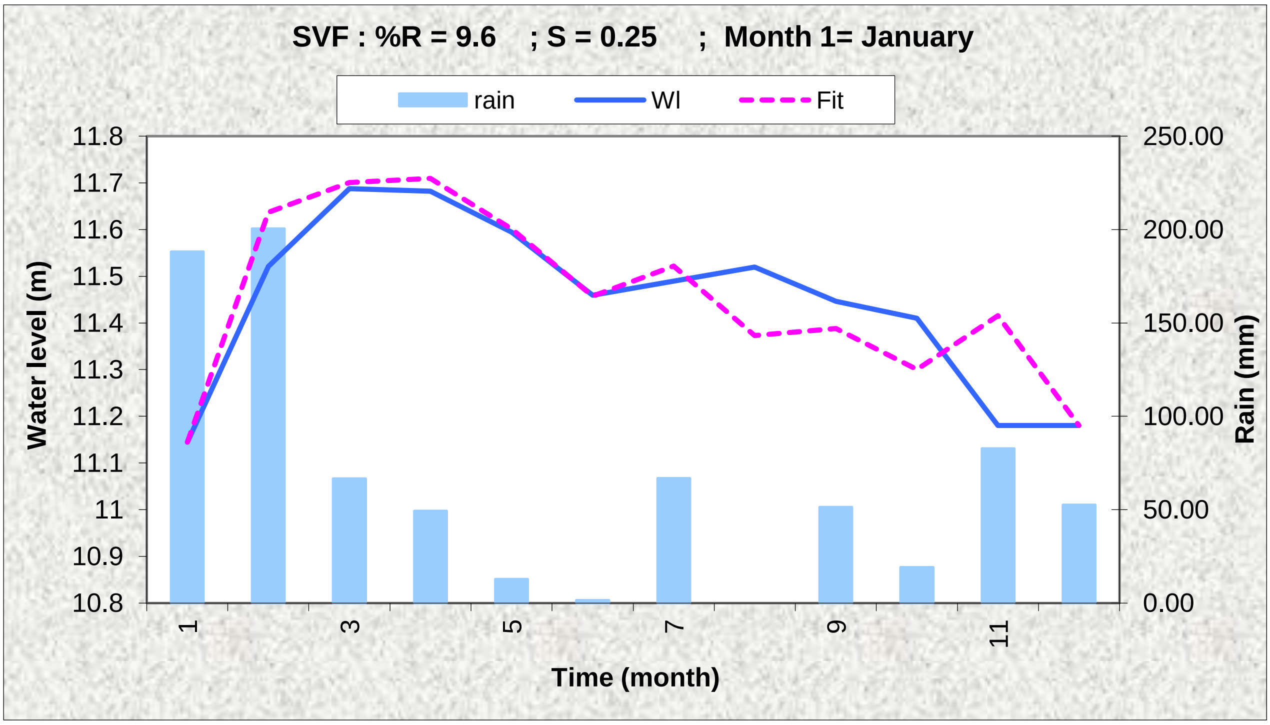

Figure 4:1 SVF Recharge Simulation for Alluvium Surface Geology

<u>**SVF Method assumptions/limitations:**</u>

- The base is an impermeable boundary with no inflow or loss from or to underlying aquifers; base is an aquiclude;
- The simulated recharge is the recharge after ET losses have been accounted for;
- Accuracy dependent of borehole's distribution across relevant study area and
- Aquifer inflow and outflow uncertainty high.

4.1.2. Chloride Mass Balance

The recharges for the rest of the surface geological units were calculated using the CMB-method. The CMB requires little input and is often used as the first recharge quantification due to its simplicity and low cost. The chloride ion is an ideal conservative tracer because it does not participate in oxidizing or reducing reactions with rocks or water, and does not form insoluble precipitates (Adams *et al.*, 2004). The groundwater recharge (Equation 4:2), as based on the CMB method, is calculated as the relationship between the chloride being introduced from rainfall and the chloride in the groundwater. High groundwater chloride concentrations are usually indicative of lower recharge rates (old water and which is not frequently replenished) (Adams *et al.*, 2004).

Equation 4:2 Groundwater's recharge calculation CMB Method (Adams *et al.*, 2004).

$$\% \, Recharge = \frac{Cl \, in \, rainfall \, (mg/l)}{Cl \, in \, groundwater's \, average(mg/l)} \; x \; 100$$

On a local scale, chloride concentrations are expected to decrease with increasing rainfall, while on a regional scale, chloride is expected to increase with increasing precipitation (Adams *et al.*, 2004).

The DWA and National Groundwater Database's (NGA) borehole chemistry data, were filtered for all the available chloride data across the study area. The boreholes with groundwater chloride data, were each assigned to the surface geology it spatially intersects. The average was calculated for the cumulative chloride data per geological unit, in each quaternary catchment. The quaternary catchments' rainfall chloride concentrations were then divided by the average of the available groundwater chloride concentrations for that specific surface geology the borehole is geographically situated in. Consequently, a more accurate recharge value was determined for each quaternary catchment's geological units (Equation 4:3). The calculated groundwater recharge percentile of the MAP, for each geological unit present in each quaternary catchment, is given in Table 4:1.

Equation 4:3 Recharge in m/d (Adams *et al.,* 2004).

$$Recharge \, (m/d) = \frac{\left[\left(\frac{MAP \, in \, mm}{1000}\right) \, x \, \left(\frac{Recharge \, \%}{100}\right)\right]}{365}$$

CMB Method assumptions:

- Precipitation is the only source of chloride for groundwater;
- Chloride is conservative in the system;
- Chloride recycling and concentration is absent within the aquifer;
- Groundwater does not evaporate upstream from the groundwater sampling points and
- Soil and vegetation chloride adsorption is considered neglect able.

The calculated average groundwater recharge values for quaternary catchments W32C and W32D area greater than that of the Groundwater Resource Assessment (GRA) (DWAF, 2006). The GRA data however is the average across a whole quaternary catchment, where these values were derived per geological unit. The average groundwater recharge values for quaternary catchment W32B and W32H are the highest according to the calculated recharge estimations of this study as well as according to the GRA (DWAF, 2006).

Groundwater recharge rates of 18% of the MAP have been reported near the coast while the reported groundwater recharge rates further inland are around 5% (Meyer and Godfrey, 1995).

The average of these two values is 11.5 %, correlating to the recharge values accepted by Bredenkamp *et al.,* (1992) which are between 12 % and 15 % of the annual precipitation. The groundwater recharge values are all between these maximum and minimum literature reported estimations.

Table 4:1 Percentage groundwater recharge per geological unit in each quaternary catchment

Recharge percentage for each geological unit, per quaternary catchment (%)							
	Recharge Method	**W32B (%)**	**W32H (%)**	**W32C (%)**	**W32F (%)**	**W32G (%)**	**W23D (%)**
(DWAF, 2006)	GRA	10.44	8.99	4.26	6.34	6.45	4.11
Arenite	CMB	3.01	3.16	2.45	2.71	2.87	-
Basalt	CMB	-	-	1.29	1.42	1.51	-
Dolerite/Rhyolite	CMB	-	-	2.64	2.91	3.08	-
Mudstone	CMB	-	-	1.58	1.74	1.84	-
Shale	CMB	-	-	0.50	0.56	0.59	-
Siltstone/Tillite	CMB	4.91	5.15	4.00	4.41	4.68	
Alluvial	SVF	9.60	9.60	9.60	9.60	9.60	9.60
Clay-Sand	CMB	3.20	3.36	2.61	9.60	9.60	3.58
Limestone	SVF	9.60	9.60	9.60	9.60	9.60	
Yellow Sand	SVF	9.60	9.60	9.60	9.60	9.60	
Dune Beach Sand	SVF	9.60	9.60	9.60	9.60	9.60	
Red Sand	SVF	9.60	9.60	9.60	9.60	9.60	
Average per quaternary catchment	-	7.39	7.46	5.26	5.95	6.01	6.59

4.1.3. Shuttleworth-Wallace analytical model

The Penman-Monteith Method accounts for aerodynamic and bulk surface resistances, but in addition to the Penman-Monteith Method, the S&W method also accounts for a soil surface resistance (Yang, 2015).

The ET_0 is represented as resistances calculated for the plants and soil in which it is growing (Shuttleworth & Wallace, 1985). The method consists of calculating in-situ climate-related parameters, the aerodynamic -, bulk stomatal -, boundary layer - and surface layer resistances, vegetation parameters and net radiation parameters (Yang, 2015; Zhou *et al.,* 2006). These resistances are then applied to calculating weighting coefficients, the latent soil heat and latent canopy heat (Shuttleworth & Wallace, 1985).

The resistances are used to calculate parameters, again used to quantify weighting coefficients. The potential evaporation of the soil and the ET_0 from the canopy are then multiplied by their respective weighting coefficients. The products (the latent soil heat and latent canopy heat) are summed to quantify total ET_0 as associated with the crop/tree in mm/d (Zhou *et al.,* 2006). The results obtained for the various parameters discussed within this section, is attached as Appendix B.

The great lack of values and research on the tortuosity, the molecular diffusion coefficient, the porosity, the soil moisture content in the first centimetre of the profile and the empirical value above which the soil is able to deliver vapour at a potential rate parameters, for the different soils types, makes it difficult and impractical to use the Choudhury and Monteith method of 1988 to calculate the soil surface resistance (Yang, 2015; Zhou *et al.,* 2006). The soil surface resistance value is therefore taken as 500 s/m, as did Zhou *et al.* (2006) after a literature review on the most acceptable general soil surface resistance.

Net radiation, as the difference between net solar radiation and net loss of energy in long wave radiation to the atmosphere, is included in the quantification of both the soil and canopy potential evaporation (Zhou *et al.,* 2006).

Climate-related parameters

The latent heat of water vaporisation (λ) for the S&W model is calculated as in Equation 4:4. The latent heat of water vaporisation for the S&W model is calculated using the same equation as that of for the Priestley and Taylor (1972) radiations based model. The saturation vapour pressure at a specific recorded temperature, in this case the average daily temperature (T_{mean}), is calculated using Equation 4:5. The saturation vapour pressures (e_s in kPa), is quantified as the average between the e^0 calculated for the minimum and maximum daily temperatures respectively (Equation 4:6).

The slope of the saturation vapour pressure curve is expressed in kPa/°C and calculated using Equation 4:7. The psychometric constant (γ in Equation 4:8 and mean air density at constant pressure (ρ in Equation 4:9) are dependent on the atmospheric pressure (P in Equation 4:10). The calculated P is 101.19 kPa. The specific gas constant (R) is assumed to be 0.287 kJ/kg/K and T_{kv} refers to the air virtual temperature which is the product of the constant 1.01 and the mean daily temperature in Kelvin. The specific heat of moist air (C_p) is assumed as 1.0130 x 10^{-3} MJ/kg/°C, while the ratio molecular weight of water vapour to that of dry air (ε) is assumed as the constant 0.622 (Zhou *et al.*, 2006). The elevation above mean sea level (z) is assumed to be 9 m.a.m.s.l. All together P is expressed in kPa, and so γ in kPa/°C and ρ in kg/m^3. The parameters γ, λ, Δ, e_s, C_p and ρ are related to climate variables, especially to temperature (Zhou *et al.*, 2006).

Equation 4:4 Latent heat of vaporization (Racz *et al.,* 2013)

$$\lambda = 2.501 - (2.361\ x\ 10^{-3})\ T_{mean}$$

Equation 4:5: Saturation vapour pressure at the specific temperature

$$e^0 = 0.6108 \exp(\frac{17.27\ T_{mean}}{T_{mean} + 237.3})$$

Equation 4:6 Saturation vapour pressures

$$e_s = \frac{e^0(T_{\max}) + e^0(T_{\min})}{2}$$

Equation 4:7 Slope vapour pressure curve (Raes, 2009)

$$\Delta = \frac{4098\ (0.6108 \exp(\frac{17.27\ \mathrm{T_{mean}}}{\mathrm{T_{mean}} + 237.3})}{(\mathrm{T_{mean}} + 237.3)^2}$$

Equation 4:8 Psychometric constant (Raes, 2009)

$$\gamma = \frac{\mathrm{C_p\ P}}{\varepsilon\ \lambda} = 0.664742\ \mathrm{x}\ 10^{-3}.\mathrm{P}$$

Equation 4:9 Mean air density at constant pressure

$\rho = \frac{\mathrm{P}}{\mathrm{T_{kv}.R}}$ where $\mathrm{T_{kv}} = 1.01\ \mathrm{x}\ \mathrm{T_{mean\ in\ Kelvin}}$

Equation 4:10 Atmospheric pressure (Raes, 2009)

$$P = 101.3\left(\frac{293 - 0.0065\,z}{293}\right)^{5.26}$$

Aerodynamic Resistances

The aerodynamic resistance between the substrate and the canopy source height is a function of the eddy diffusion coefficient and decay constant, the vegetation's height and the roughness length of the ground as well as LAI (Yang, 2015; Zhou *et al.,* 2006). The aerodynamic resistance between canopy source height and reference level is rather dependent of the friction velocity (dependent of in situ wind speed at reference height) (Shuttleworth & Wallace, 1985; Zhou *et al.,* 2006). The aerodynamic resistance from the soil to canopy (r^s_a in Equation 4:11), and the aerodynamic resistance from the canopy to the reference height (r^a_a in Equation 4:12) are derived with integration of the eddy diffusion coefficients inside and over the canopy.

The vegetation height (h_c) is taken as a constant 30 m for evergreen broadleaf forests (Zhou *et al.,* 2006).

The Eddy diffusivity decay constant of the vegetation (n), is assumed to be 4.25 for vegetation with a height greater than 10 m, such as the case for *Eucalyptus* (Zhou *et al.,* 2006). The Eddy diffusion coefficient at the top of canopy (K_h in Equation 4:13) is expressed in m^2/s, where the Von Karman's constant (κ) is assumed to be 0.41, the friction velocity (u_*) is calculated using Equation 4:14 and the zero plane displacement of the canopy (d_0) is calculated using Equation 4:15 for vegetation with a LAI greater than 4.

The roughness length of a closed canopy (z_{0c}) is assumed to be the product of 0.05 and h_c, for vegetation higher than 10 m. The friction velocity in addition to the κ and d_0 accounts for the reference height 2 m above vegetation (z_a) assumed to be 32 m for *Eucalyptus* trees. The preferred roughness length of the canopy (Z_0 in Equation 4:16) and the wind speed at the reference height (u_a in Equation 2:14) is expressed in m/s. The roughness length of the ground (z_{og}) is assumed to be 0.020 m for quantification of r^s_a, and the preferred zero plane displacement (d_p) is taken as the product of 0.63 and h_c for calculating r^s_a and r^a_a.

Equation 4:11 Aerodynamic resistance from the soil to canopy

$$r^s_a = \frac{h_c \exp(n)}{n.K_h}\, x\, [\exp\left(\frac{-n.z_{0g}}{h_c}\right) - \exp\left\{\frac{-n(Z_0+d_p)}{h_c}\right\}]$$

Equation 4:12 Aerodynamic resistance from the canopy to the reference height

$$r^a_a = \frac{1}{\kappa.u_*}\ln\left(\frac{z_a-d_0}{h_c-d_0}\right)+\left(\frac{h_c}{n\,K_h}\right)[\exp\left\{n\left[\frac{1-(Z_0+d_p)}{h_c}\right]\right\}-1$$

Equation 4:13 Eddy diffusion coefficient at the top of canopy

$$K_h = к. u_*(h_c - d_0)$$

Equation 4:14 Friction velocity

$$u_* = \frac{к. u_a}{\ln\{\frac{z_a - d_0}{z_0}\}}$$

Equation 4:15 Zero plane displacement of the canopy

$$d_0 = \frac{h_c - z_{0c}}{0.3}$$

Equation 4:16 Preferred roughness length of the canopy

$$z_0 = \min\{0.3(h_c - d_0)$$

Equation 4:17 Wind speed at the reference height

$$u_a = \mathrm{u_w} \frac{\ln(\frac{\mathrm{z_b}}{\mathrm{z_{0w}}})}{\ln(\frac{\mathrm{z_b}}{\mathrm{z_0}})} . \frac{\ln(\frac{\mathrm{z_a} - \mathrm{d_0}}{\mathrm{z_0}})}{\ln(\frac{\mathrm{z_w}}{\mathrm{z_{0w}}})}$$

Equation 4:17 is applied to convert the wind speed measurements from the weather stations, to the reference height using a logarithmic profile. The logarithmic profile is in that the internal boundary layer heights over the canopy surface and the weather ground are matched, and a step change in the surface roughness from z_0 to z_{ow} is assumed (Zhou *et al.*, 2006). In the conversion, the height of internal boundary layer (z_b) is calculated using Equation 4:18, where the fetch at the weather stations (F_w) is assumed to be 5 000 m and the roughness length (z_{0w}) is assumed to be 0.005 m. The wind speed observed at the weather station (u_w) is in units m/s and the height of observation (z_w) is assumed to be 10 m.

Equation 4:18 Height of observation

$$z_b = 0.334\, F_w{}^{0.875} z_{0w}{}^{0.125}$$

The turbulent diffusivity is also known as the eddy diffusion coefficient and mechanical dispersion coefficient (Kimura *et al.*, 2012). The turbulent diffusion processes caused by plant canopies contribute to the dispersion of seeds, pollens and even fire sparks from forest fires as well as carbon dioxide, water vapour and other gaseous substances concentrations within and above these plant canopies (Kimura *et al.*, 2012). Due to the complexity of conducting field measurements in tall plant canopies combined with the diversity of conditions in these canopy structures, understanding of transport mechanisms in tall canopies are limited. Since the need to understand the heat-island phenomena as well as dispersion processes grew with the increase in airborne pollutants in urban environments, so did the research (Kimura *et al.*, 2012). Despite the increase in research conducted, little is known about the turbulent diffusivity of tall forest canopies. Estimations made based on length scales and turbulent diffusivity are often in literature, but no explicit data of turbulent diffusivity for tall forest canopies are documented (Kimura *et al.*, 2012). Turbulent diffusivities are important when predicting moisture and temperature changes. The eddy diffusion coefficients are dependent on both the wind velocity as well as the leaf density. The coefficient tends to be larger where the average wind velocity increases, and the anisotropy between the trees tend to decrease as leaf density increases (Kimura *et al.*, 2012).

Bulk stomatal, boundary layer and surface resistances

The bulk stomatal resistance of the canopy (r^c_s) was calculated using both Equation 4:19 and Equation 4:20 independently, while the average between the respective results served as the S&W model input values for the r^c_s parameter. The mean stomatal resistance (r_{ST}) is assumed to be 150 s/m (the minimum recommended for evergreen broadleaf forests by Zhou *et al.* (2005), and the shielding factor (σ_c) is calculated using Equation 4:20. The implementation of the LAI_e, accounts for only the upper canopy leaves which are actively involved during the heat and vapour transfers. The LAI_e is taken as half of the actual calculated LAI where the calculated LAI is greater than 4, as is the case for *Eucalyptus* trees (Shuttleworth & Wallace, 1985 and Zhou *et al.,* 2006).

Equation 4:19 Bulk stomatal resistance of the canopy method 1

$$r^c{}_s = \frac{(r_{ST} \cdot \sigma_c)}{LAI}$$

Equation 4:20 Shielding factor for Equation 4:19

$$\sigma_c = 0.5\ (LAI) + 1$$

Equation 4:21 Bulk stomatal resistance of the canopy method 2

$$r^c{}_s = \frac{r_{ST}}{LAI_e}$$

The bulk resistance of the boundary layer (r^c_a) is calculated using Equation 4:22, where the hydraulic resistance of the concentrated boundary layer (r_b) is calculated using Equation 4:23 and the shielding factor (σ_b) is assumed to be 0.5 for evergreen broadleaf forests. The characteristic canopy leaf width (w_{max}) is assumed to be 0.05 m for evergreen broadleaf forests as by example from Zhou *et al.* (2006). The wind speed at the canopy top (u_h) is calculated with

Equation 4:17, but by replacing the h_c, with z_a. The soil surface resistance *(*r^s_s) is taken as 500 s/m as did Shuttleworth and Wallace (1985) and Federer *et al.* (1996). While there are mathematical formulas for calculating r^s_s, parameters such as the porosity, tortuosity factor and the molecular diffusion coefficient are not known for a great variety of soil types, making the equation impractical to apply.

Equation 4:22 Bulk resistance of the boundary layer

$$r_a^c = \frac{r_{b\,.\,\sigma_b}}{LAI}$$

Equation 4:23 Hydraulic resistance of the concentrated boundary layer

$$r_b = \frac{100}{n}\left(\frac{w_{max}}{u_h}\right)^{0.5}\left[1 - \exp\left(-\frac{n}{2}\right)\right]^{-1}$$

Net radiations over vegetation canopy, substrate soil surface and soil heat flux

The net radiation above the canopy (R_n) is calculated as the difference between the net radiation to the soil surface (R_{ns} in Equation 4:25) and the net loss of long wave radiation energy to the atmosphere (R_{nl} in Equation 4:27) in MJ/m^2/d. The land surface albedo (α) is calculated using Equation 4:26, where the albedo corresponding to the closed canopy (α_m) is assumed to be 0.20 and the albedo corresponding to the bare soil (α_s) is assumed to be 0.1 for evergreen broadleaf forests (Zhou *et al.,* 2006).

The average monthly Direct Normal Irradiation (DNI) and the monthly Global Horizontal Irradiation (GHI) of the National Renewable Energy Laboratory's (NREL) Climatologically Solar Radiation (CSR) model for the specific geological region, was used for the radiation calculations. The solar radiation (R_{solar} in Equation 4:25 and Equation 4:27) is taken as the area's reading from the DNI map and the clear sky solar radiation (R^0_{solar} in Equation 4:27) is taken as the area's GHI map reading in MJ/m^2/d (NREL, 2014).

The NREL data provides monthly average daily total solar resource averaged over surface cells 40 km by 40 km. The data is represented as watt/hours/meters^2/day for each month. The model accounts for cloud cover, atmospheric trace gases and water vapour as well as aerosols present to calculate monthly average daily total insulation on a horizontal surface (NREL, 2014). The data is validated with stations measurements and are generally accurate to 10% of the grid cell's true measurements. The study area is located within NREL's Africa data region 1396314 (NREL, 2014). The DNI (R_{solar}) is an average of 16.88 MJ/m^2/day, which correlates with the Energy Departments' statement that most areas in SA have an average solar-radiation level between 4.5 and 6.5 kWh/m^2/day, which converts to between 16.2 and 23.4 MJ/m^2/day. The SolarGIS maps (2015) indicate a DNI of 1550 KWh/m^2/annum for the immediate area around

Lake St. Lucia which converts to 15.28 MJ/m2/day. The average GHI (R^0_{solar}) for the year, according to the NREL CSR model, is 18.18 MJ/m^2/day. The GHI is 1750 kWh/m^2/annum, which is 17,26 MJ/m^2/day (SolarGIS, 2015). This confirms that the respective monthly CSR solar radiation is viable.

The maximum ($T_{max,K}$) and minimum atmospheric temperatures ($T_{min,K}$) for Equation 4:27 are in kelvin unit. The Stefan-Boltzmann constant (σ) is 4.903 x 10^{-9} MJ/K^4/m^2/d. The actual vapour pressure (e_a in Equation 4:28) is calculated as the average between the e^0 calculated for minimum and maximum temperatures (which is the formula for e_s) multiplied by the mean daily relative humidity (RH_{mean}).

Equation 4:24 Net radiation above canopy

$$R_n = R_{ns} - R_{nl}$$

Equation 4:25 Net radiation to soil surface

$$R_{ns} = (1 - \alpha) R_{solar}$$

Equation 4:26 Albedo of land surface

$$\propto = \propto_m - (\propto_m - \propto_s) \exp(-0.56\, LAI)$$

Equation 4:27 Net loss of long wave radiation energy to atmosphere

$$R_{nl} = \sigma \left(\frac{T^4{}_{\max in\ Kelvin} + T^4{}_{\min in\ Kelvin}}{2} \right) x \left(0.34 - 0.14\sqrt{e_a}\right).(1.35\ \frac{R_{solar}}{R^0{}_{solar}} - 0.35)$$

Equation 4:28 Actual vapour pressure

$$e_a = \frac{(e^0 \text{ x } T_{\max}) + (e^0 \text{ x } T_{\min})}{2}\ x\ \frac{\%\, RH_{mean}}{100}$$

The radiation reaching soil surface ($R^s{}_n$) is calculated using Equation 4:29 where the extinction coefficient of vegetation for net radiation (C_r) is assumed to be 0.5 as also assumed by Stannard (1993) and Mo *et al.* (2004). The soil heat flux (G) is calculated as 0.07 (T_{i+1} - T_{i-1}), where T_{i+1} and T_{i-1} are the mean air temperatures of the previous and next month’s respectively.

Equation 4:29 Radiation reaching soil surface

$$R^s{}_n = R_n \exp(-C_r\, LAI)$$

Vegetation parameters

The LAI is calculated using Equation 4:30, where the maximum leaf area index (LAI_{max}) is assumed to be 7 for evergreen broadleaf forests. *Eucalyptus'* LAI increases with stand development and then stabilizes. The LAI of *Eucalyptus* plantations are influenced by water stress and temperature stress (Battaglia *et al.,* 1997). After canopy closure, forest productivity tends to decrease, supporting the universal tendency of the LAI to decrease with increasing stand age (Martinez-Vilalta *et al.*, 2006).

The maximum fraction of photo-synthetically active radiation ($FPAR_{max}$) is assumed to be 0.950, while the minimum fraction of photo-synthetically active radiation ($FPAR_{min}$) is assumed to be a constant of 0.001 as per example by Zhou *et al.* (2006). The fraction of clumped vegetation (F_{cl}) is assumed to be 0. The ratio of hemispheric reflectance for near infrared light to that for visible light (SR in Equation 4:31) serves as input into quantification of the fraction of photo-synthetically active radiation (FPAR in Equation 4:32) used to determine the LAI. NDVI is taken as 100 % while literature reports 98 % NDVI as 0.689 and 5 % NDVI as 0.0389. The NDVI for water is typically less than 0, bare soils have a NDVI of 0, while vegetation cover has a NDVI greater than 0.1 (Anon, 2002). Dense vegetation typically has a NDVI of 0.7(Zhou *et al.,* 2006). The SR_{min} is taken as 5 % of NDVI population with a constant of 0.039, while a constant of 0.611 is assumed for $SR_{max,}$ 98 % of NDVI population (Zhou *et al.* 2006).

Equation 4:30 Leaf area index

$$LAI = (1 - \mathrm{F_{cl}})\mathrm{LAI_{max}} \frac{\ln(1-\mathrm{FPAR})}{\ln(1-\mathrm{FPAR_{max}})} + \mathrm{F_{cl}}\mathrm{LAI_{max}} \frac{\mathrm{FPAR}}{\mathrm{FPAR_{max}}}$$

Equation 4:31 Ratio of hemispheric reflectance for near infrared light to that for visible light

$$SR = \frac{1 + NDVI}{1 - NDVI}$$

Equation 4:32 Fraction of photo-synthetically active radiation

$$FPAR = FPAR_{min} + (FPAR_{max} - FPAR_{min})\frac{(SR - SR_{min})}{(SR_{max} - SR_{\mathrm{min}})}$$

Simulating ET_0 with the S&W model

The ET_0 is calculated in mm/day, using Equation 4:33. The evaporation from the soil (ET_s) and the transpiration from the tree canopy (ET_c) are calculated with Equation 4:34 and Equation 4:35 respectively. ET_s is then multiplied by the respective bare substrate evaporation weighting coefficient (C_s) and ET_c is multiplied by the closed canopy transpiration weighting coefficient (C_c). The S&W weighing coefficient's input parameters, R_a is calculated as

$(\Delta + \gamma).r^a{}_a$, thus taking the aerodynamic resistance from the canopy reference height into account. Parameter R_c ($(\Delta + \gamma).r^c{}_a + \gamma.r^c{}_s$) accounts for the bulk resistance of both the boundary layer and canopy stomatal, while parameter R_s accounts for the aerodynamic resistance from the soil to the canopy and again the soil surface resistance ($(\Delta + \gamma).r^s{}_a + \gamma.r^s{}_s$).

Equation 4:33 Reference evapotranspiration (S&W)

$$ET_0 = \frac{C_C ET_c + C_s ET_s}{\lambda}$$

Equation 4:34 Evaporation from soil

$$ET_s = \frac{[\Delta\,(R_n - G) + [(24 \text{ x } 3600).\rho.C_p\,(e_s - e_a) - \Delta.r^s{}_a\,(R_n - R^s{}_n)]/(r^a{}_a + r^s{}_a)\,]}{[\Delta + \gamma(1 + r^s{}_s/(r^a{}_a + r^c{}_a)]}$$

Equation 4:35 Transpiration from canopy

$$ET_c = \frac{[\Delta\,(R_n - G) + [(24 \text{ x } 3600).\rho.C_p\,(e_s - e_a) - \Delta.r^c{}_a\,(R^s{}_n - G)]/(r^a{}_a + r^c{}_a)\,]}{[\Delta + \gamma(1 + r^c{}_s/(r^a{}_a + r^c{}_a)]}$$

Equation 4:36 Closed canopy transpiration weighting coefficients

$$C_c = \frac{1}{1 + \{R_c.R_a\}/[R_s(R_c + R_a)]}$$

Equation 4:37 Bare substrate evaporation weighting coefficients

$$C_s = \frac{1}{1 + \{R_s.R_a\}/[R_c(R_s + R_a)]}$$

4.2. Numerical Modelling

Finite Difference Network generation

The finite difference grid consists of 304 rows and 192 columns as displayed in Figure 4:2, where each cell is 400 m by 400 m. The coordinates of the upper left grid cell is 88895.84; -2908219 and the coordinates of the lower right grid cell is 162384.3; -3026900 when using the Transverse Mercator Projection (Longitude 31). The modelled area covered is about 120 km by 80 km. Factors to be considered when determining an adequate groundwater model cell size, include the computational efficiency, suitable representation of the available data and effective simulation of the regional groundwater flow (Zhou and Li, 2011).

A single layer model was developed for the unconsolidated material (primary aquifer). The layer type is confined/unconfined.

The literature review reports that afforestation in the W32 tertiary catchment, is most abundant in quaternary catchments W32H and W32G. The model network includes each of the quaternary catchments surrounding the quaternary catchment W32H. While afforestation is equally abundant in quaternary catchment W32G, the plantations are situated to the east of the quaternary catchment, around the border between quaternary catchment W32H and W32G. The network area thus extends over a greater area than the immediate afforestation areas as the afforestation is not situated near the model boundaries.

Initial groundwater heads, boundaries, sources and sinks as well as other aquifer parameters serve as input into the uncalibrated MODFLOW model.

Boundary conditions

A model boundary serves as the connection between the model area and the active network's boundary and therefore assigning the correct model boundaries are crucial in developing a numerical model into an in-situ site groundwater representation model. Model boundaries require specification as located along the active network's grid and external influences such as rivers and lakes in this case.

The initial groundwater contours simulated indicated the lowest groundwater heads west of the study area, and not to the east of the study area within the proximity of Lake St. Lucia as expected from field observations. A second evaluation of the topography, the geology and the hydrology (the primary elements to account for in selecting hydraulic boundary conditions), brought the steep increase in topography to the west of the study area in consideration with higher precipitation associated with mountainous areas, as well as the fracturing associated with secondary aquifers, into consideration.

Consequently a constant head (Dirichlet) boundary was included to the west of the study area as a recharge area/inflow boundary from the mountain ranges. The constant head boundary to the west of the study area accounts for the flow system which's natural boundary is too great a distance away. The coastline, forming the eastern study area boundary, was accounted for in the model as a constant head boundary of 0 m.a.m.s.l.

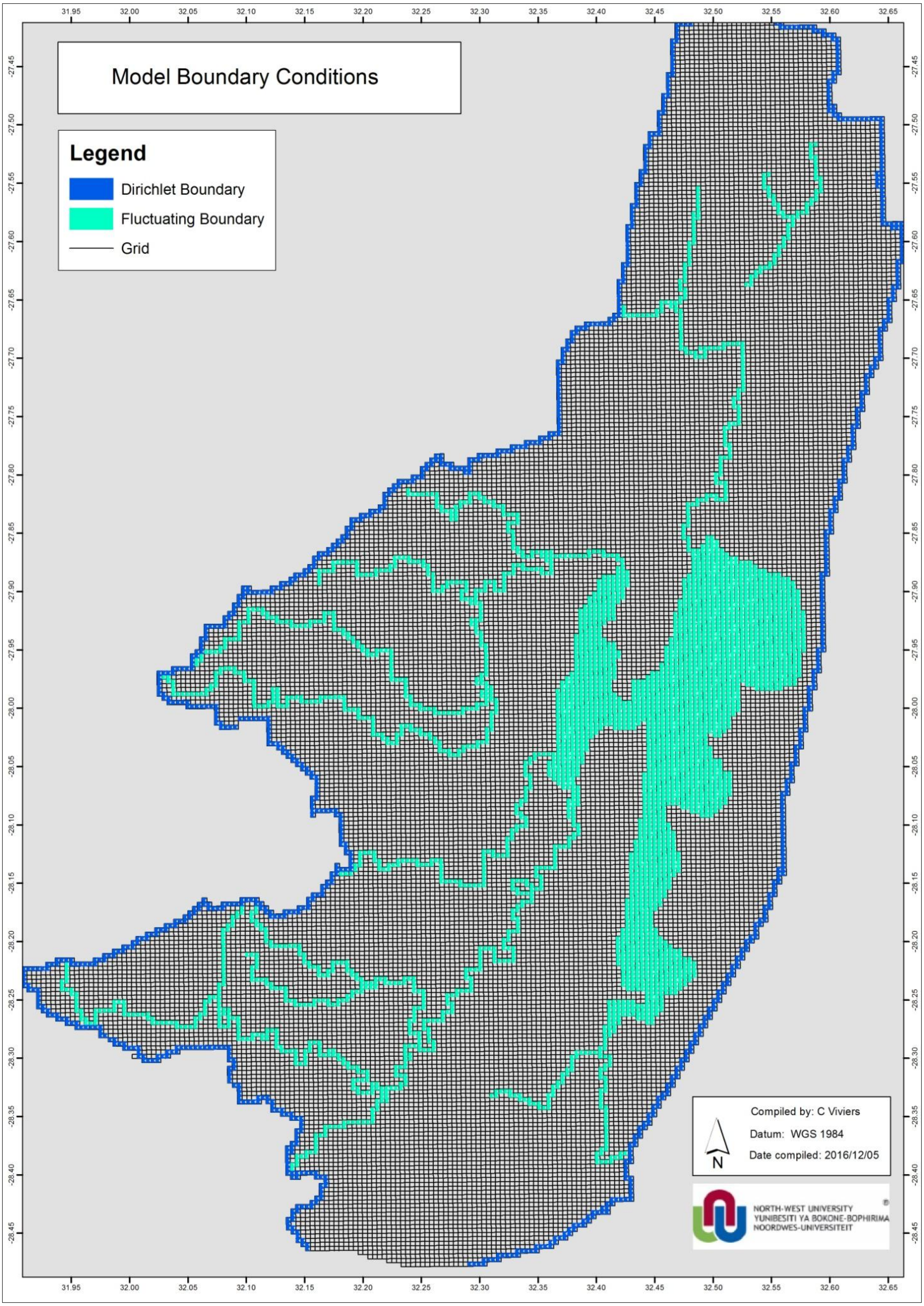

Figure 4:2 MODFLOW grid and boundary conditions

It is most common for rivers and lakes to be simulated as constant head boundaries in MODFLOW simulations. In consideration of the objective to quantify the impact of ET on the streamflow, the rivers and lake were specified as head-dependent, Cauchy, boundaries, a combination of the constant head and specified flux (Neuman) boundary conditions. The Cauchy boundary is most ideal as some river head and lake water level monitoring data is available. The river should be able to react as a losing stream in case the river's hydraulic head is greater than the groundwater hydraulic head in the river's immediate neighbouring grid cells, and vice versa. The lake's water level should also be able to increase (become shallower) in instances where the neighbouring cell's groundwater hydraulic head is greater than the lower hydraulic head of the lake, and vice versa.

Initial hydraulic head

The top of the aquifer layer (topography) is simulated by means of the field interpolation tool in PMWIN. Interpolation input data consisted of 1188 topographic elevation points extracted from Google Earth and was interpolated across the network grid using the Kriging interpolation method. The layer, in consideration of literature and NGA borehole logs, were assumed to be 22 m thick. The interpolated topography (top of layer) served as input for simulating the bottom layer's elevation by subtracting 22 m from the top layer.

The initial groundwater heads were also interpolated across the network grid with available measured groundwater levels as input. A combination of the latest water levels from both NGA and other DWS databases were used as the observation boreholes. The water level, as depth below surface, is subtracted from each borehole's surface topographic height, to calculate hydraulic head. The initial hydraulic heads simulated across the study area, as well as the distribution of the observation boreholes which served as input for the interpolation, are shown in Figure 4:3.

Sources and sinks

In MODFLOW, sources are defined as the aquifer's recharge resources. Recharge resources can be rainfall or recharge from zones with higher hydraulic heads. Zones with higher hydraulic heads, recharge zones, can be another area (typical from mountainous areas), a river or other water bodies and even an overlying or underlying neighbouring aquifer. Initially source input was limited to precipitation recharge as estimated using the SVF and CMB methodology.

Sinks refer to zones from which groundwater leaves the aquifer. Sinks are usually abstraction boreholes, which in this scenario is the boreholes registered in the Water Authorisation and Registration Management System's (WARMS) database. Another sink relevant is the ET. ET is included as the rate results obtained from the S&W model. A sink can also be an area, a water body or an aquifer with a lower hydraulic head to which water discharges.

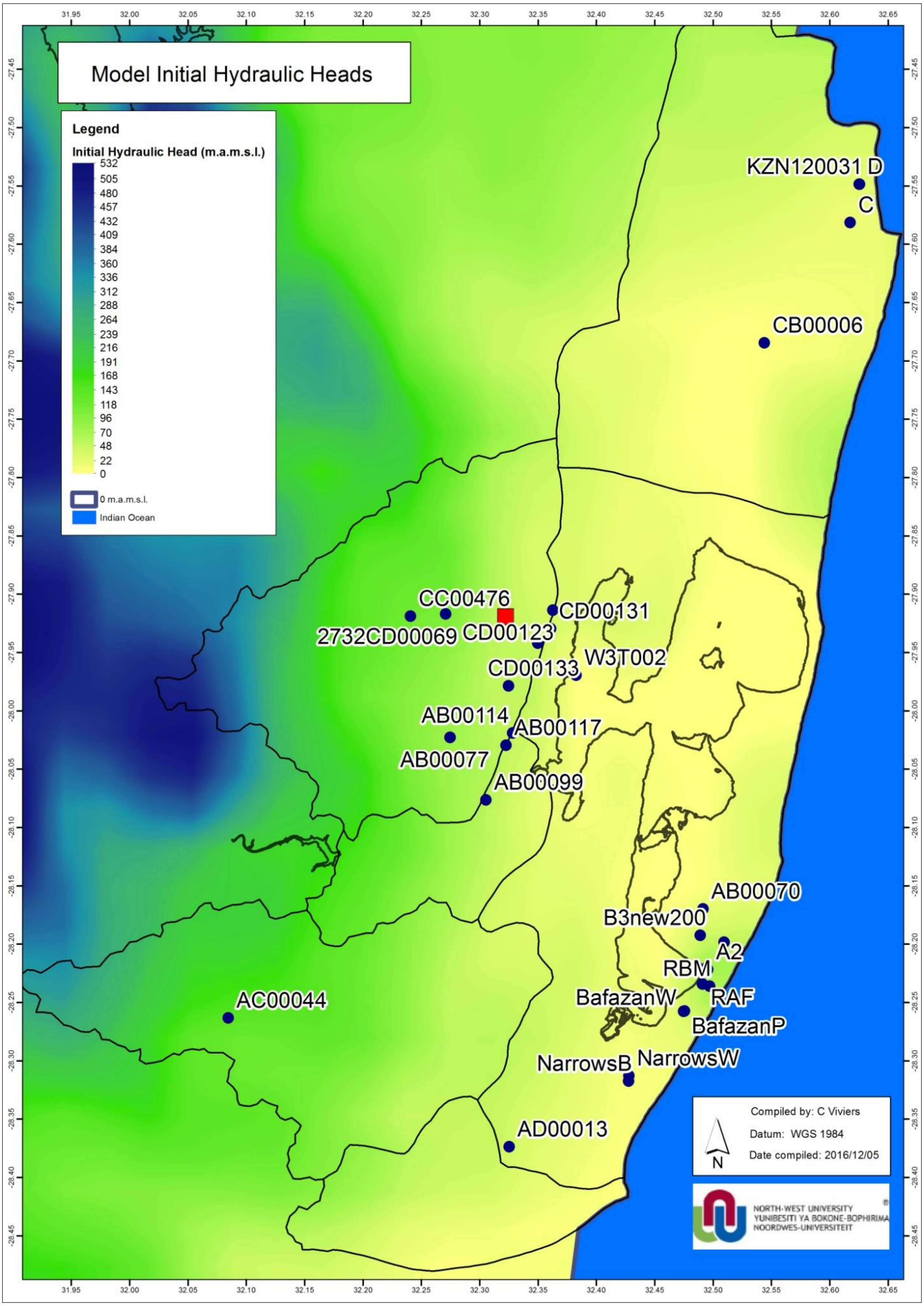

Figure 4:3 Initial regional hydraulic heads and observation borehole localities

Aquifer parameters

The aquifer parameters were simplified by allocating the surface geology into four distinctly characterised aquifers (Figure 4:4) namely the primary aquifer zone, the secondary aquifer (hard rock) zone, the sedimentary zone and Lake St. Lucia. The aquifer parameters per hydrological zone are listed in Table 4:2. The transmissivity is set to constant, calculated as dependent of the hydraulic conductivity.

Table 4:2 Initial hydraulic parameters input data for the different geological units (steady state)

Relevant Zone	Transmissivity (Hydraulic conductivity x Saturated thickness) (m^2/d)	Recharge (m/d)
Primary Aquifer	200	0.00027
Secondary aquifers (hard rock)	5	0.00001
Sedimentary	100	0.00010
Lake St. Lucia	1000	0

Assumptions summary

A mathematical model is implemented to characterise an aquifer system in time and space. Assumptions are part of modelling, whether it an aquifer system or any other dynamic system that is intended to be recreated using mathematical expressions. A numerical groundwater model is simply a representation of a real system – consequently it is an approximation dependent on the available data's accuracy and distribution. Assumption relevant to recreate the complex and dynamic study area, include:

i. The aquifer thickness is uniform across the study area.
ii. The generated/interpolated groundwater hydraulic heads mark the top of the saturated zone (aquifer).
iii. The groundwater levels used for interpolation and calibration are static groundwater levels.
iv. The surface geology map and NGA borehole logs are correct.
v. The hydraulic conductivity/transmissivity, the specific yield and specific storage parameters obtained from historical studies specifically to the study area or just to the lithology type, are considered correct in absence of field analyses. The parameters are consequently submissive to changes during steady state calibration.
vi. The only abstraction boreholes across the study area are those obtained from the WARMS database.

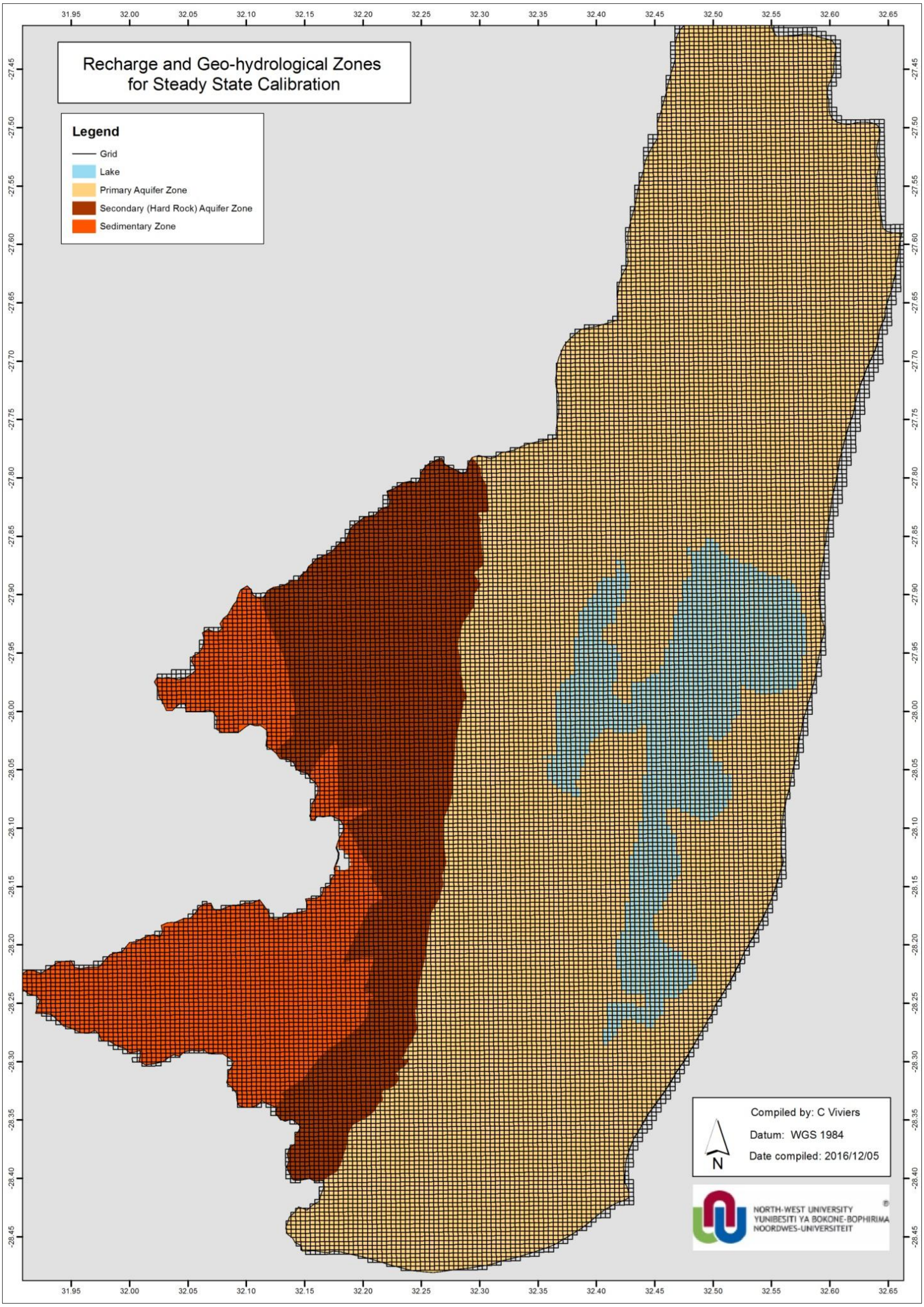

Figure 4:4 Simplified recharge and hydrological zones for steady state calibration

vii. The monthly abstraction quantity, registered in the WARMS database (m^3/year), is equal to the annual registered volume equally divided across the twelve time steps.

viii. The ET rate per time step is equal to the average daily ET rate of the relevant month as calculated using the S&W model.

ix. The quantification of the recharge per groundwater zone, rely on the CMB and SVF simulated recharge estimations per surface geological unit. These estimations are assumed to be correct.

x. Data is obtained in a dynamic environment exposed to anthropogenic disturbances (such as afforestation and borehole abstraction) but applied for calibrating a model in steady state, thus equilibrium is assumed.

xi. The boundary conditions are realistic and assist in recreating the true field environment.

Calibration steady state

As concluded in comparison of Equation 2:19 and Equation 2:20, steady state simulations neglect the storage coefficient when assuming equilibrium conditions and that no inflow or outflow is stored. Consequently, the hydraulic head can be simulated as dependent on the recharge sources, the abstraction sinks, the boundary conditions and the transmissivity input parameters per grid cell. Therefore the parameters available for calibration are lessened by excluding the storage coefficient when simulating steady state. Ranges acceptable for parameter adjustments were set by either the literature or the analytical model results.

Assuming that measured data such as the abstraction rates are more reliable than other modelled/estimated data, the hydraulic conductivity, the groundwater recharge and to a lesser extent the ET and boundary conditions are submissive to alteration. The individual parameters are altered within the viable ranges to obtain an acceptable correlation between the simulated hydraulic heads and the field observed hydraulic heads. One groundwater level, which is higher than the initial hydraulic heads simulated through interpolation of the observations, was excluded from calibration. The hydraulic conductivity and recharge parameters were adjusted to simulate hydraulic heads with a 78 % (Figure 4:5) correlation with the 32 (Figure 4:6) unique groundwater level observations, a correlation considered acceptable as it is greater than 70 %.

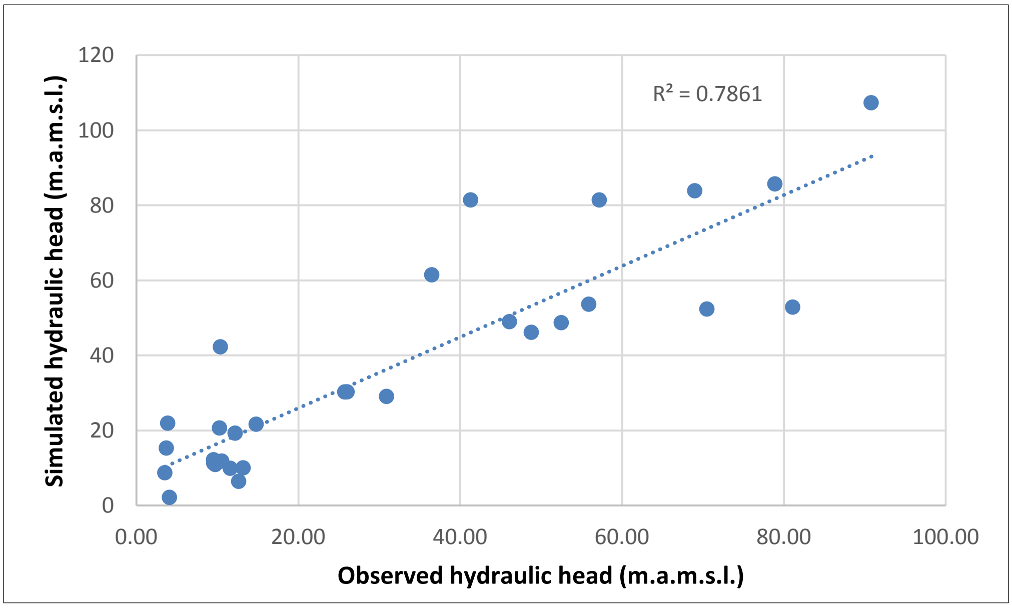

Figure 4:5 Correlation between observed and simulated groundwater hydraulic heads (steady state)

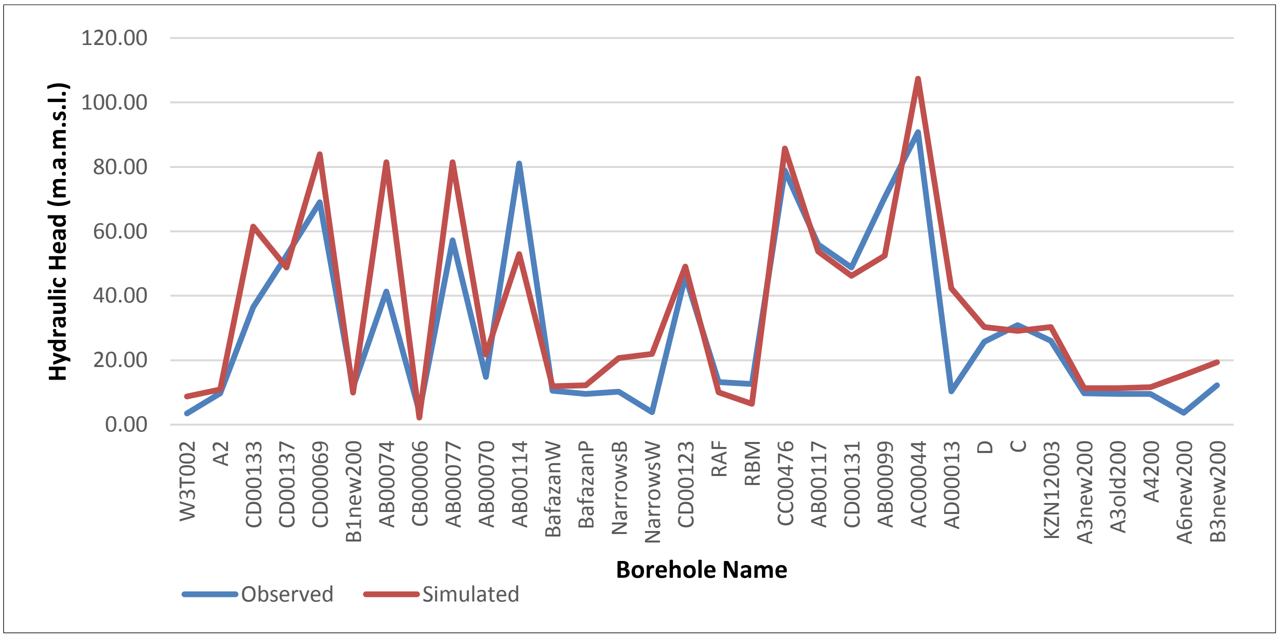

Figure 4:6 Pattern similarity between the hydraulic heads measured and those simulated in steady state calibration

The available groundwater levels were not recorded at a common time or in one season, or even in one year - instead groundwater level recordings differ from seasons or years with variable meteorological and anthropogenic exposures. Groundwater model confidence can be increased by calibrating the simulated groundwater hydraulic heads to time series groundwater hydraulic head data. The calibration is however worthwhile as viable hydraulic conductivity values were achieved during steady state calibration. Transient state calibration is now primarily submissive to the storage coefficient.

Calibration transient state

Transient state calibration was reached by primarily changing the storage coefficient and specific yield, which is included when changing from steady state conditions to transient state conditions as expressed during the literature study by Equation 2:19 and Equation 2:20. The initial steady state hard rocks transmissivities were too low and combined with the steep gradient created by the less permeable formations, inhibited groundwater flow to the down gradient aquifers. Consequently, to smooth the groundwater levels, the sedimentary zone (composed of consolidated sedimentary lithology) and the secondary hard rock aquifer zone were merged for transient state calibration (Figure 4:7).

The calibrated transient state parameters are listed in Table 4:3. The transmissivity and recharge parameters listed in Table 4:3 are those derived during the process of calibrating steady state and are considered less accessible for calibrating transient state. The objective of calibrating MODFLOW in time variant transient state was reached when the simulated hydraulic heads correlated to the field observed hydraulic heads by 83 % (Figure 5:4). During transient state calibration it was concluded that borehole CB00006's groundwater level must be dynamic or a recovering groundwater level.

Table 4:3 Transient state calibrated parameters

Relevant Zone	Transmissivity (Hydraulic conductivity x Saturated thickness) (m^2/d)	Recharge (m/d)	Specific Yield	Storage Coefficient
Primary Aquifer	200	0.00027	0.200	0.1000
Secondary aquifers (hard rock)	5	0.00001	0.009	0.0001
St Lucia Lake	1000	0.00000	0.700	0.7000

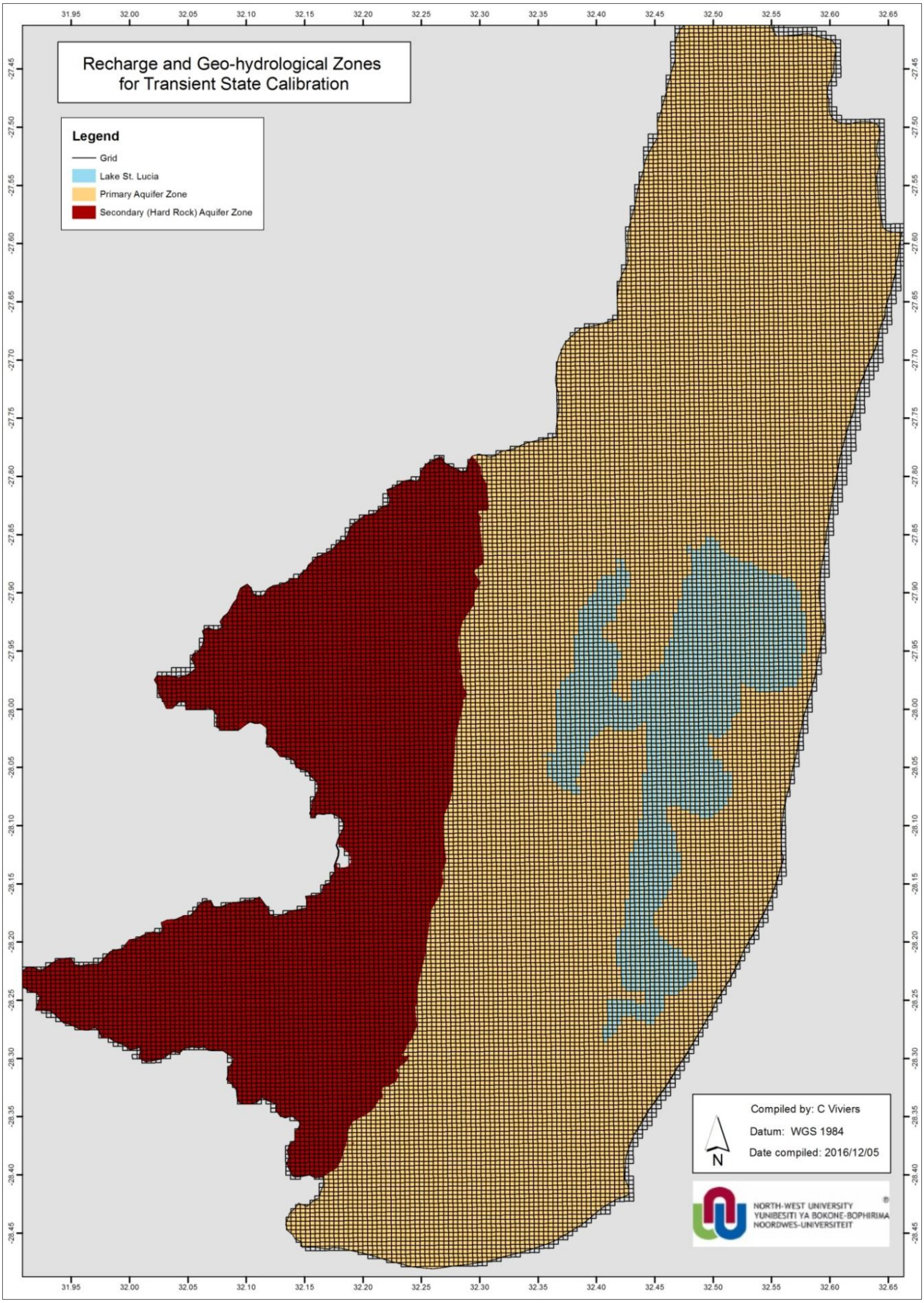

Figure 4:7 Transient state groundwater recharge and geo-hydrological zones

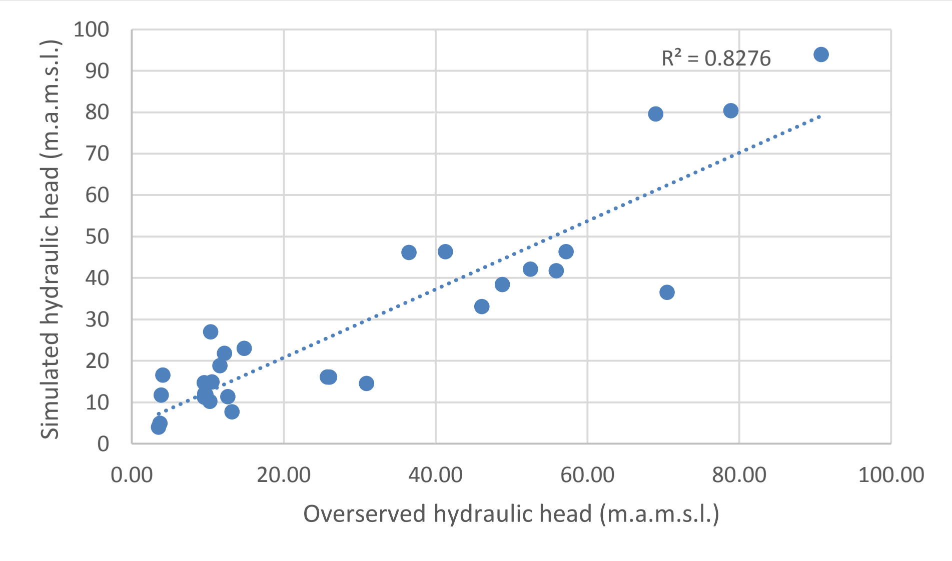

Figure 4:8 Correlation between observed and simulated groundwater hydraulic heads (transient state)

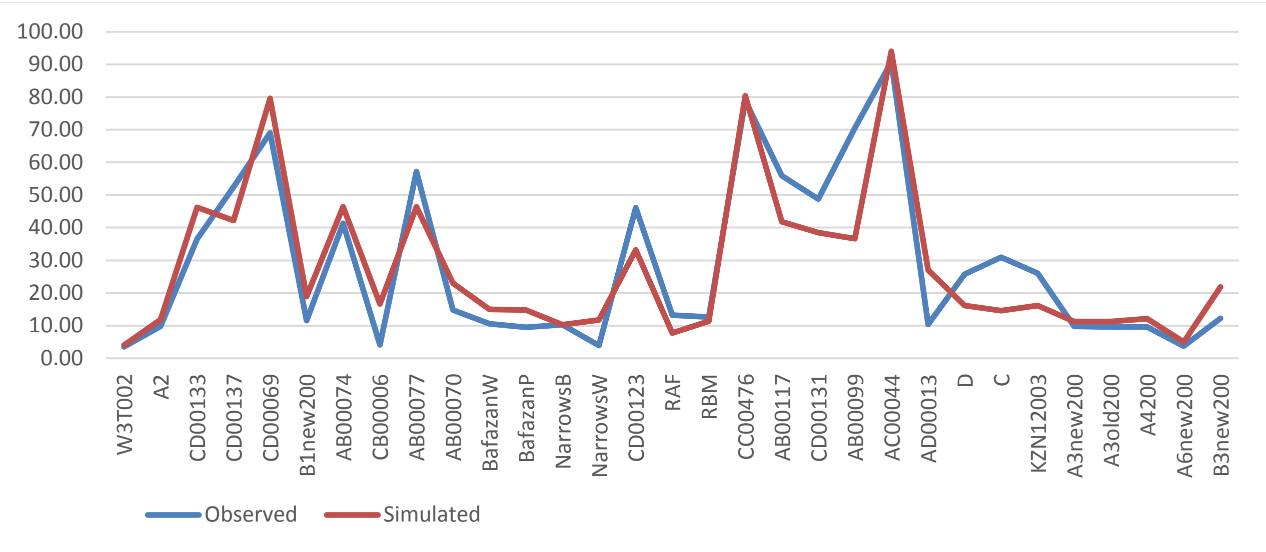

Figure 4:9 Pattern similarity between the hydraulic heads measured and those simulated in transient state calibration

Scenarios

The regional drawdown and the groundwater flow from Lake St. Lucia to the afforested areas situated west and south of the lake was quantified during normal years (the rainfall is the MAP), and during drought circumstances taken as 30 % of the MAP as the only precipitation recharge. The streamflow for 9 different river zones were simulated for years of drought and normal rainfall in the presence and absence of afforestation for six years.

Chapter 5 Results and Discussion

5.1. Shuttleworth and Wallace Model

The ET rate is greatly dependent on the vapour pressure deficit (VPD) and photo-synthetically active radiation as supported by Albaugh *et al.* (2013). The VPD is expressed as e_s - e_a, where e_s and e_a accounts for the minimum and maximum daily temperatures. The simulated ET values to mean daily temperature input, have a correlation of 46 % for 2015 and 31 % for 2014 (Figure 5:1).

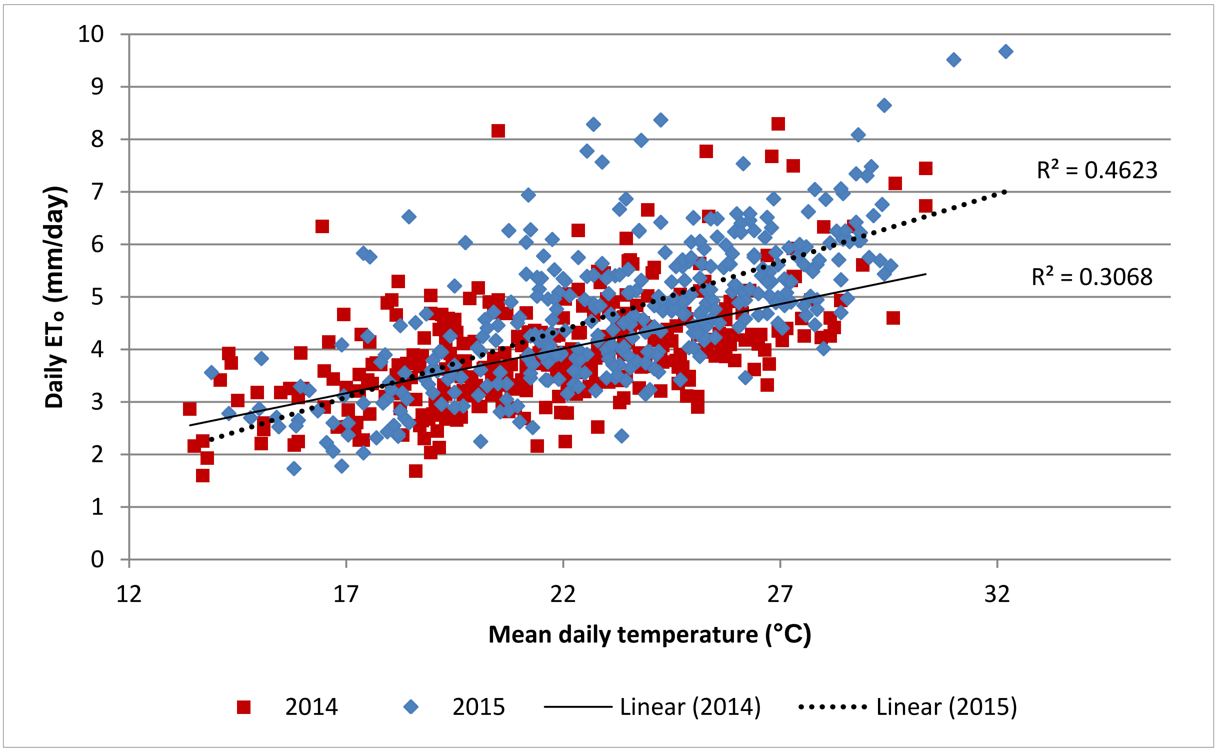

Figure 5:1Simulated ET_o to mean daily temperatures correlation

The 2015 mean daily wind speed to the simulated ET_o correlation, exceeds the correlation between these two parameters for 2014 by 35 % (Figure 5:2). The correlation for the cumulative 2014 and 2015 mean daily wind speed to simulated ET_o, is 35 %.

The S&W maximum daily ET_o for 2014 is 8.30 mm/day in September, and the minimum is 1.59 mm/day in June. The average monthly ET_o reaches a peak in February 2014 from which the monthly average ET_o steadily decrease to below 4 mm/a day from April till August (March's average ET_o is exactly 4 mm/day) (Figure 5:3). The average monthly ET_o steadily increases to an ET_o rate greater than 4 mm/day from November 2014 till January 2015 (average monthly ET_o is 5.4 mm/day).

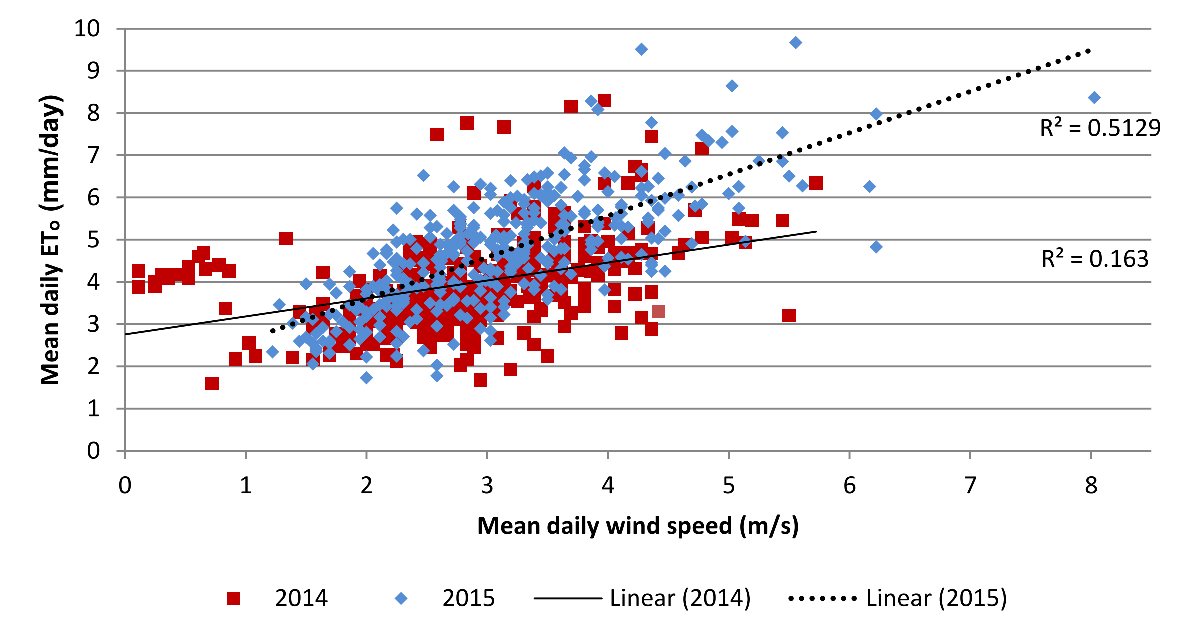

Figure 5:2Simulated ETₒ to mean daily wind speed correlation

The maximum daily ET_o for 2015 is 9.67 mm/day in December, while the minimum daily ET_o is simulated for a day in June at 1.73 mm/day. The average monthly ET_o decreases from March (average monthly ET_o 5.1 mm/day) till July (average monthly ET_o 3.4 mm/day) after which it continues to increase till December. In 2015 only June and July have a mean monthly ET_o less than 4 mm/day compared to 2014 which has an average monthly ET_o less than 4 mm/day from April 2014 till August 2014. The abundant exceeding of 2015 simulated ET_0 rates in comparison to 2014 ET_0 rates can be ascribed to 2015 being the hottest year on record, with higher temperatures than 2014 by a margin of 136 recorded years (Thompson, 2016). The daily simulated ET_0 for both 2014 and 2015 is visible in Figure 5:3.

Albaugh *et al.* (2013) report that from a study conducted during 1992 to 1993, the daily water use of three year old *E. grandis* trees were 7 mm/day on a warm day, and 2.2 mm/day during the winter. A study conducted in the KZN Midlands by Burger (1999), states that during mid-summer 1997, the maximum ET_0 for *Eucalyptus* trees were 8 mm/day.

The maximum average S&W ET_o simulated for 2014 and 2015's individual months' is 6 mm/day, while the minimum average daily ET_o is 3.4 mm/day – both within the ranges provided from Albough *et al* (2013) and Burger (1999). The individual maximum daily S&W ET_o simulated however is 9.7 mm/day, and the minimum 1.6 mm/day. Different *Eucalyptus* species are reported to have an average annual water use rate of 1600 mm/year, and 4.38 mm/day by Coppen *(*2002), while Bosch and Gadow (1990) estimate an annual water use of 1200 mm, at a rate of 3.29 mm/day. Dye (1996) reports that *E. grandis* species specifically have an annual water use of 1231 mm/, with a daily rate of 3.37 mm/day. Calder *et al.* (1997) state that the annual water use for *E. camaldulensis* is 1150 mm/year, while the daily water use is 3.15 mm/day. *E. salinga* has an annual water use of 1084 mm/year (2.97 mm/day) (Von Roeder, 2014), exceeding that of *E. dunnii* which has an annual water use of 629 mm/year (1.72

mm/day) as reported by Dye (2013). The average annual ET_o simulated from S&W for the two years 2014 and 2015 is 1467 mm/year, which is within the ranges provided by literature - greater than the minimum *E. dunnii's* 629 mm/year and the maximum reported by Coppen (2002) which is 1600 mm/year) (no *Eucalyptus* specie distinction is made).

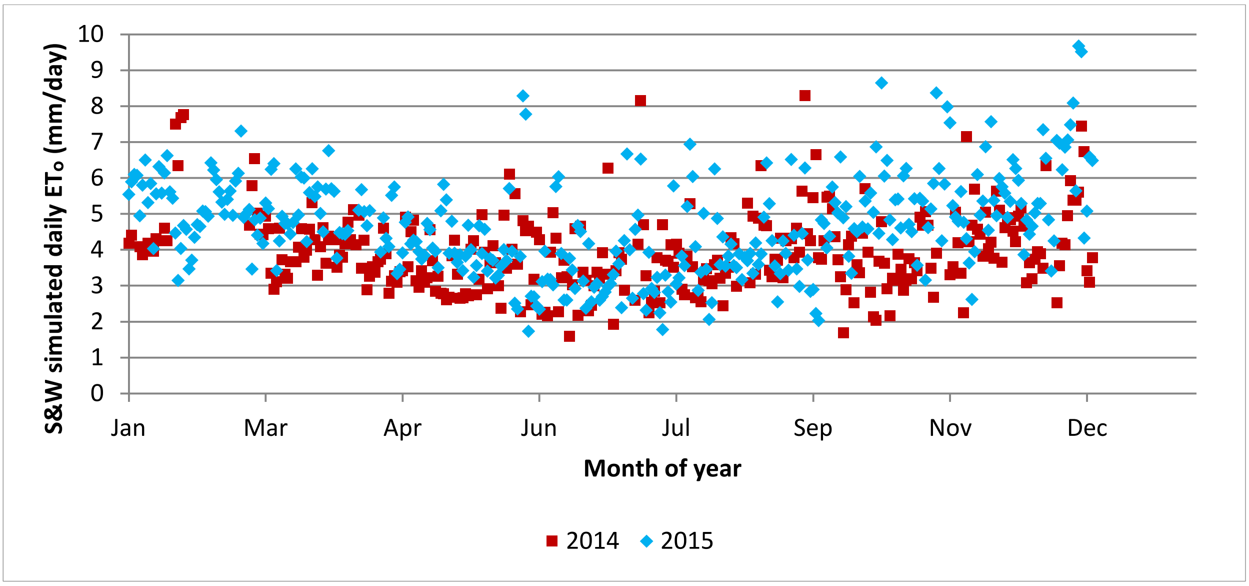

Figure 5:3 S&W daily ET_0 for 2014 and 2015

The 2015 average monthly ET_0 consistently exceed the average monthly ET_0 of 2014, with the exception of February and July for which the month average ET_0 is greater in 2014 than in 2015 (Table 5:1). This can be ascribed to the count of data available from which a monthly average could be calculated. February 2014 only has 5 daily ET_0 readings representing the average across the whole month due to the lack of daily relative humidity readings available for the month, compared to February 2015 which has an average calculated for 28 values (Table 5:1). July 2014 also has 3 recordings less than July 2015. The average monthly temperature and relative humidity is less for 2014, although the average monthly wind speed of July 2014 exceeds than of 2015. It is apparent from the similar correlation between 2015's simulated ET_0 to wind speed and temperature, that S&W is dependent and representative of the variable input parameters and not just temperature for example.

The greatest deviation from the mean ET_0 within a single month is 1.6 mm in June 2015, while the lowest deviation from the mean monthly ET_0 is 0.67 mm in April 2015. Whether the deviation is significant was evaluated using the coefficient of variance (Table 5:1). The variation coefficients are all smaller than 1, indicating low variation within monthly simulated ET_0 rates. This is considered an indication of model stability as great irregularities due to small input parameter differences indicates the model to be representative of only those parameters.

Table 5:1 Average monthly ET_0, data completeness and coefficient of variance

Month	Average Monthly ET_o Rate (mm/day)		Completeness of month's simulated Et_o (%)		Coefficient of Variance	
	2014	2015	2014	2015	2014	2015
January	4.69	5.40	74.19	100	0.27	0.15
February	5.29	5.11	17.86	100	0.16	0.17
March	3.99	5.15	100	100	0.14	0.16
April	3.76	4.50	100	80	0.19	0.15
May	3.51	4.09	100	100	0.25	0.17
June	3.42	3.62	100	100	0.31	0.43
July	3.71	3.45	90.32	100	0.33	0.34
August	3.68	4.03	90.32	100	0.26	0.26
September	4.33	4.32	100	100	0.28	0.29
October	3.64	5.12	100	100	0.25	0.22
November	4.35	5.52	86.67	100	0.23	0.23
December	4.48	6.01	83.87	93.55	0.28	0.26

The total annual S&W ET_0 of 2015 exceeds that of 2014 by 438 mm/annum. The SAWS 684910 station (from which the temperature, wind and humidity data were recorded) is situated in quaternary catchment W32H, but afforestation is also abundant in W32G. The annual 2014 S&W ET_0 is 171 mm less than the annual ET_0 for W32H and 152 mm less than that estimated for W32H by the WRC (2016) (Table 5:2). The annual 2015 S&W ET_0 exceeds the annual ET_0 estimated by the WRC (2016) for quaternary catchment W32H by 267 mm/annum, and by 286 mm for quaternary catchment W32G (Table 5:2). The 2015 daily simulated ET_o values are however 100 % complete for 10 months of the year, while only 6 months of 2014 had 100 % of the values (Table 5:1). The average of both 2014 and 2015's S&W monthly average simulated ET_o were used for MODFLOW ET input. The average monthly total ET_o for 2014 and 2015 has an 85 % correlation to the monthly ET estimated by the WRC (2016) for quaternary catchment W32H and an 84 % correlation to that of quaternary catchment W32G (Figure 5:4). Due to February 2014's incomplete simulated daily ET_o (less than 70 %) it is excluded from averaging and correlation estimations.

ET exceeded MAP by a factor of 1.6 for the southern India study conducted by Calder et al. (1997). The average annual ET_o from that simulated using the S&W model, exceed the MAP calculated from station 684910 by a factor of 1.55, that of station W3E001 by 1.54, that of station W3E002 by 1.51 and by a factor of 2.09 station W3E003. The average annual simulated ET_o thus exceeds the annual average MAP as determined from the weather stations, by a factor of 1.67.

Table 5:2 Monthly and annual S&W simulated and WRC (2016) ET_0

Month	S&W 2014	S&W 2015	W32H (WRC, 2016)	W32G (WRC, 2016)
	mm/month	mm/month	mm/month	mm/month
January	107.94	167.54	161.00	158.00
February	26.46	143.01	133.00	131.00
March	123.65	159.50	129.00	124.00
April	112.70	107.95	98.00	94.00
May	108.81	126.64	83.00	80.00
June	102.59	108.47	64.00	63.00
July	103.90	106.85	75.00	74.00
August	102.95	124.99	98.00	98.00
September	130.04	129.53	116.00	118.00
October	112.79	158.76	139.00	139.00
November	113.17	165.70	143.00	143.00
December	116.43	174.28	167.00	165.00
Total (mm/year)	1261.44	1673.22	1406.00	1387.00

The averages per month from that simulated for 2014 and 2015 were applied as input for MODFLOW (Table 5:3).

Table 5:3 Average monthly ET_o from 2014 and 2015 S&W calculated model applied to MODFLOW

MODFLOW applied ET_o as calculated from S&W	
Month	mm/day
January	5.05
February	5.20
March	4.57
April	4.13
May	3.80
June	3.52
July	3.58
August	3.86
September	4.33
October	4.38
November	4.94
December	5.25

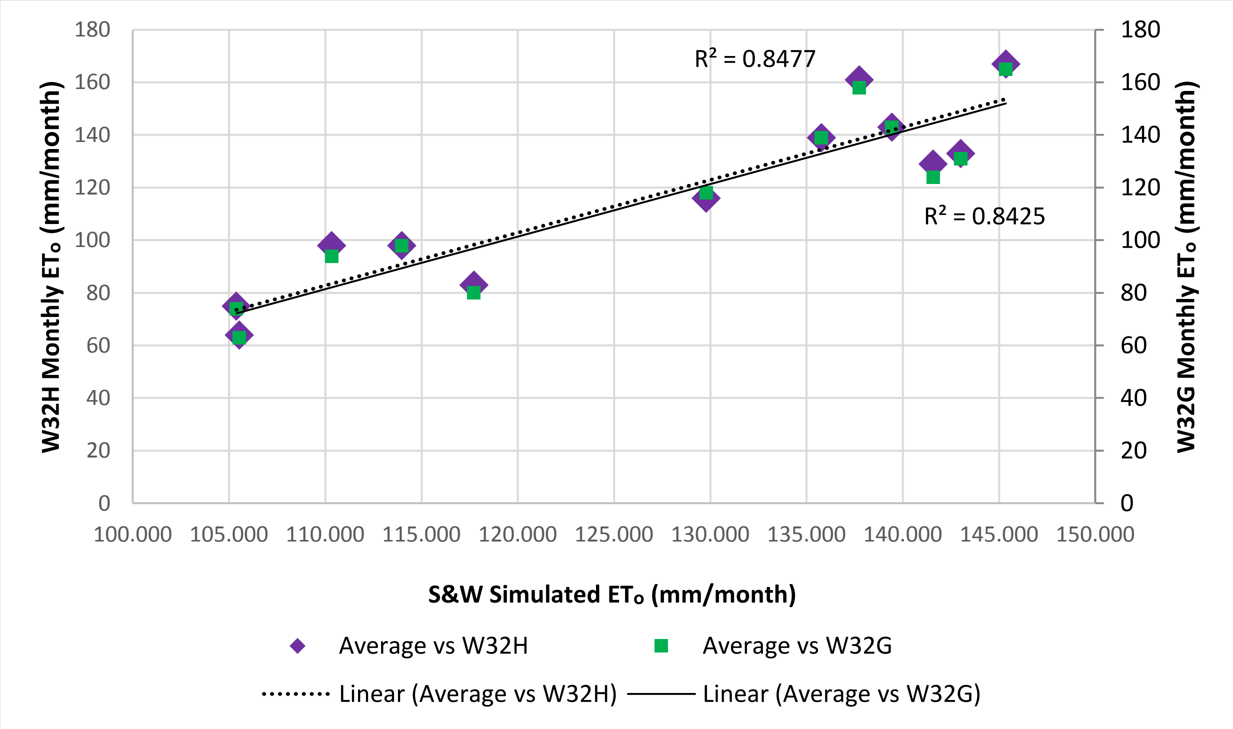

Figure 5:4 Correlation between monthly S&W ET_o and that from WRC (2016) for W32G and W32H

5.2. MODFLOW Numerical Model

ET_o's impact on groundwater drawdown at observation point and regionally

The simulated drawdowns (meters below topographic surface) at observation point A for each of the six years since afforestation, for normal MAP and for drought, are compared in Figure 5:5. The drawdown initially increases 4.3 m greater during drought circumstances than during years with normal rainfall. By year six, the drawdown difference between the drought scenario vs. the normal rainfall scenario, is 7 meters greater. The drawdown continues to increase, without exception for every sequential year - for both normal rainfall and drought scenario's, indicating that the annual ET_o exceeds the annual precipitation. The drawdown increases at a rate 3 % greater per year during drought in comparison to years when receiving the MAP (Figure 5:5). The drawdown is greatest during the first year of afforestation during both drought and normal MAP scenario's.

The increase in drawdown across the study area for 2 years, 4 years and 6 years under normal rainfall circumstances, are displayed in Figure 5:6, Figure 5:7 and Figure 5:8 respectively. The maximum drawdown for each second year increases from 14.1 m two years after afforestation, to 14.7 m four years later and to 15 m six years after afforestation was initiated at the ET rate simulated by S&W.

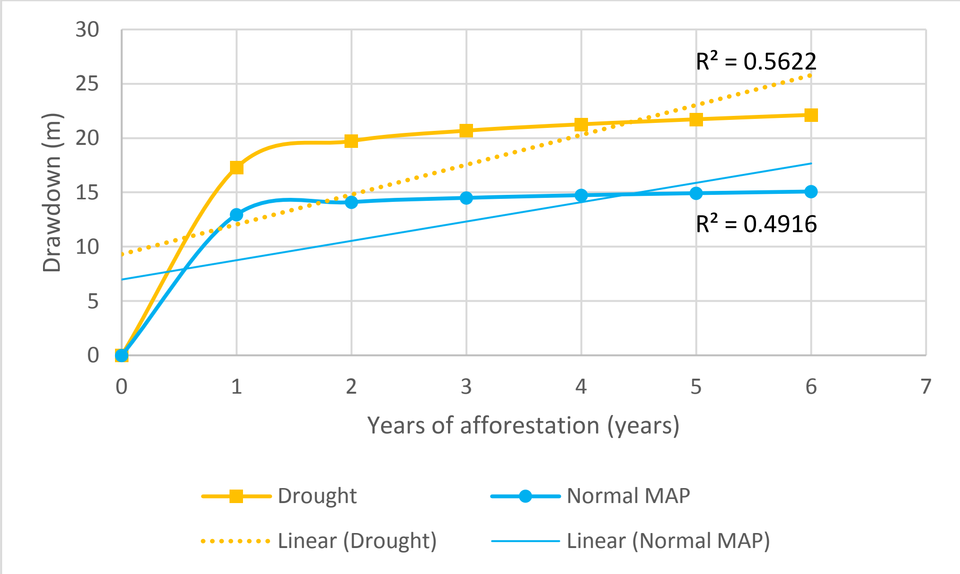

Figure 5:5 Observation point A's drawdown for the normal and drought scenario

The area subjective to drawdown increases significantly with time. The cone of depression from two years of afforestation, does not reach the W32C and W32H quaternary catchment boundary west of Lake St. Lucia (at the W32G, W32D and W32H border). After six years of afforestation, the radius of influence west of Lake St. Lucia has breached the W32C and W32H catchment border. In measuring the cone of depression area formed by change in drawdown, the area of influence west of Lake St. Lucia increases from 154 km^2 to 186 km^2 and again to 212 km^2 every two years of afforestation. The influenced area south-south-west of Lake St. Lucia (at the W32G, W32D and W32H border) increases from 2.6 km^2 after two years of afforestation, to 44 km^2 after four years of afforestation and again to 78 km^2 after six years. These abstraction (drawdown) zones are bordering Lake St. Lucia, and even extend into the lake's boundaries at some localities – consequently, the water flow from the lake to the afforested areas was quantified next.

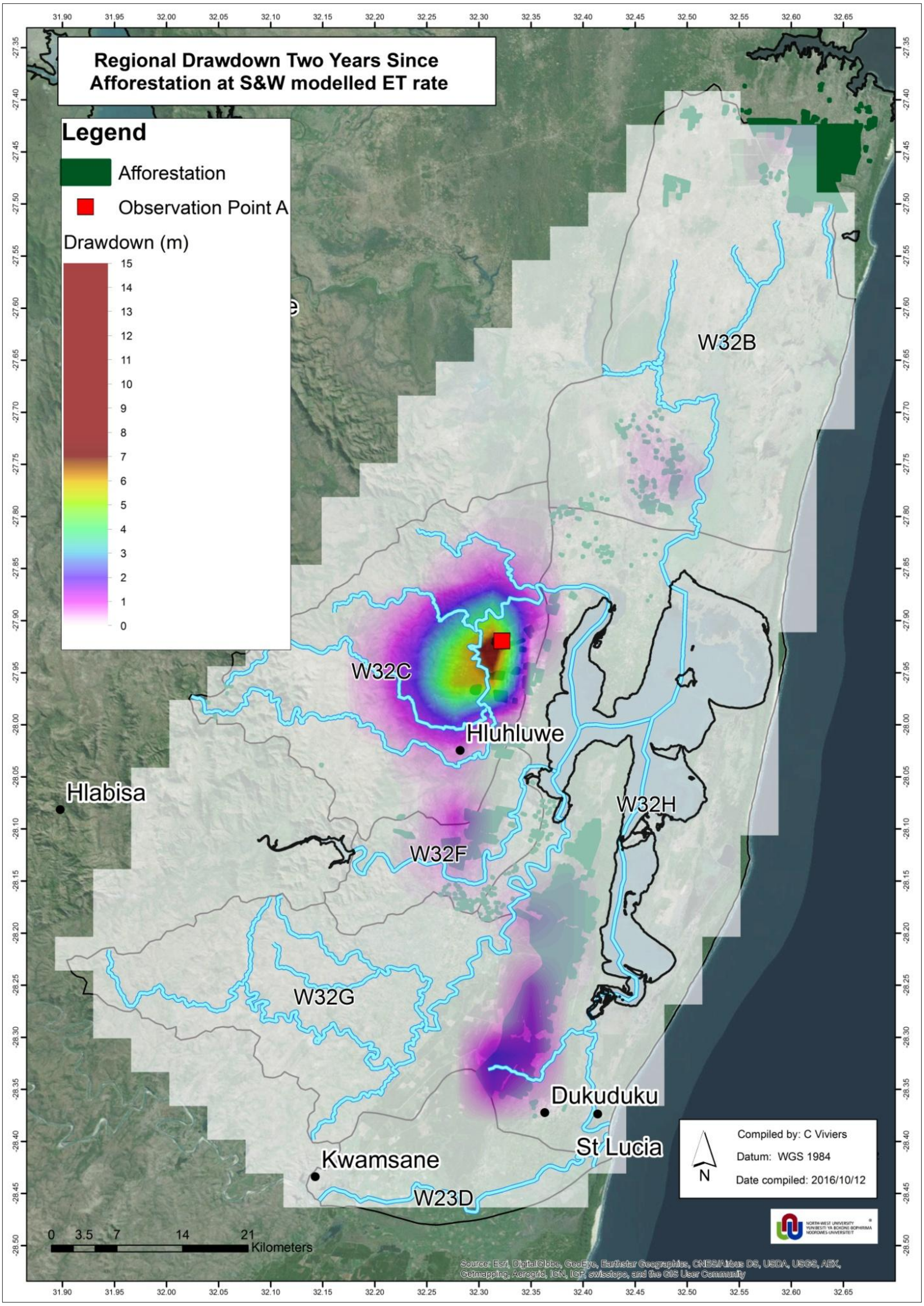

Figure 5:6 Drawdown distributions across study area 2 years since afforestation

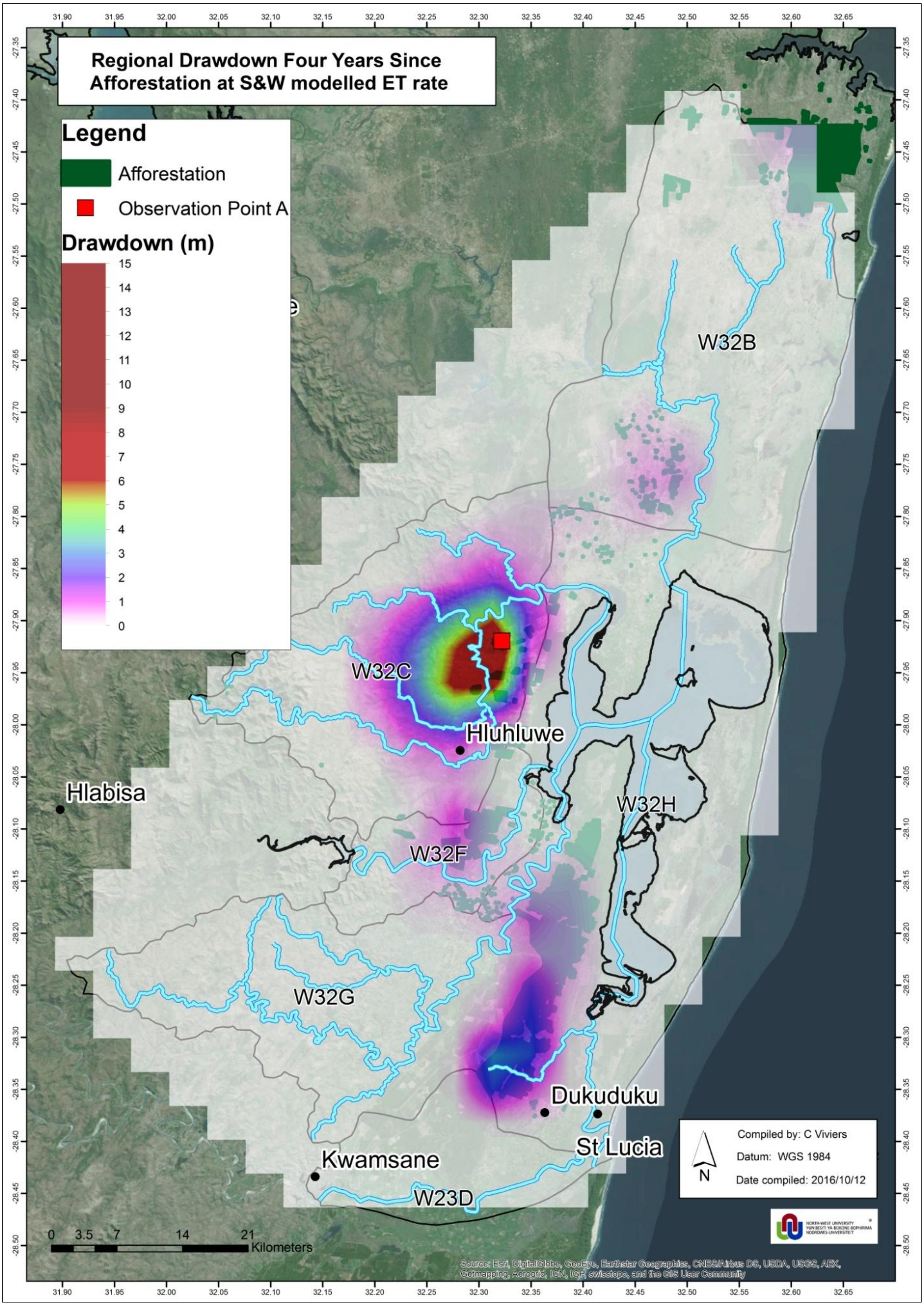

Figure 5:7 Drawdown distribution across study area 4 years since afforestation

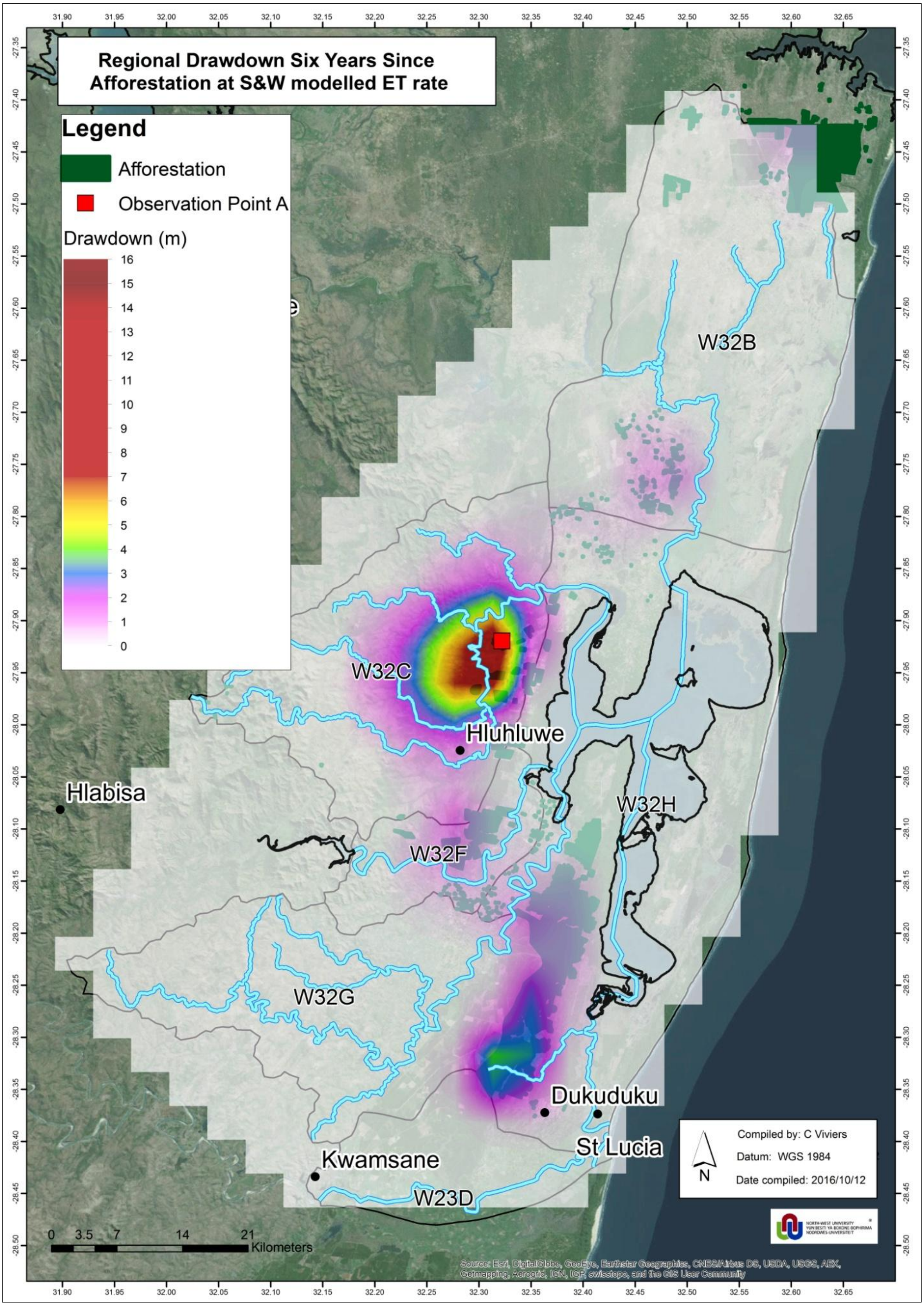

Figure 5:8 Drawdown distribution across study area 6 years since afforestation

ET$_o$'s impact on groundwater flow quantities west and south of lake

Groundwater flowing from the lake, to the afforested areas is less during drought circumstances. The quantities of water flowing from the lake to the afforested area for every sequential year since afforestation are in Table 5:4. The quantities which flow from the lake to the afforested areas, decreases for every year the tree ages, (Figure 5:9) and the extent of decrease for every year is listed in Table 5:5.

Table 5:4 Water flowing from Lake St. Lucia to afforested areas

Water flowing from Lake St. Lucia to afforested areas (m^3/day)							
Years of afforestation at S&W ET$_o$ rate	Normal		Drought (30% of normal rainfall)		Quantity abstracted greater due to absence of drought (without water restrictions)		
	West of Lake	South of Lake	West of Lake	South of Lake	West of Lake	South of Lake	Average over area
1	50162.14	62872.19	47062.95	59399.19	3099.18	3473.00	3286.09
2	50157.56	62839.94	45206.58	57188.17	4950.98	5651.77	5301.37
3	50150.91	62790.87	43892.87	55574.66	6258.04	7216.21	6737.13
4	50142.00	62728.70	42882.90	54312.20	7259.10	8416.50	7837.80
5	50130.86	62657.28	42065.47	53285.45	8065.39	9371.83	8718.61
6	50117.71	62579.75	41379.02	52427.18	8738.70	10152.57	9445.63

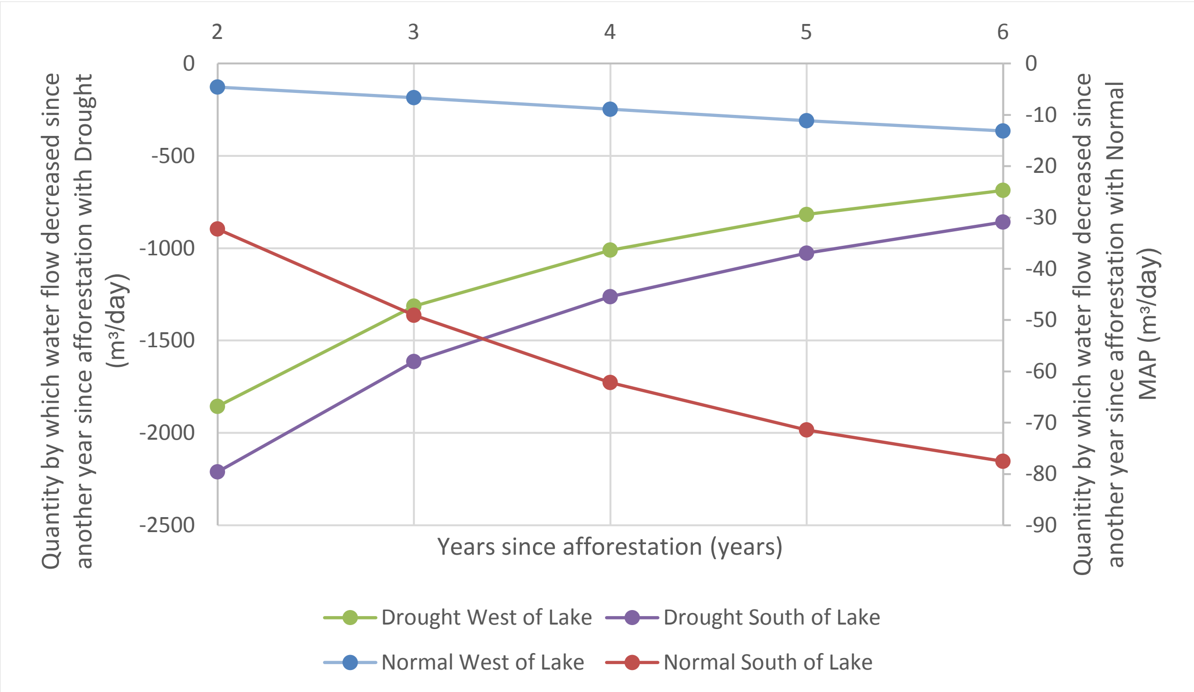

Figure 5:9 Water flow quantity difference for sequential year of afforestation from previous year

During normal circumstances the factor, by which every sequential year's water flow quantity from the lake to the afforested areas decrease, decreases (Table 5:5). The factor by which the difference between the water flow quantity decreased from year 1 to 2, and then again from year 2 to 3, is 1.45 for the area west of the lake and 1.52 for the area south of the lake. The factor by which the difference between the water flow quantity decreased from year 4 to 5, and then again from year 5 to 6, is 1.18 for the area west of the lake and 1.09 for the area south of the lake assuming the area has 6 sequential years without drought and does receive the MAP (Table 5:5).

During drought circumstances the factor, by which every sequential year's water flow quantity from the lake to the afforested areas decrease, increases (Table 5:5). The factor by which the difference between the water flow quantity decreased from year 1 to 2, and then again from year 2 to 3, is 0.71 for the area west of the lake and 0.73 for the area south of the lake. The factor by which the difference between the water flow quantity decreased from year 4 to 5, and then again from year 5 to 6, is 0.84 for the area west of the lake and 0.84 for the area south of the lake assuming the area experiences 30 % of the MAP (Table 5:5). The factor by which the water flow quantity decreases is linear to the age of afforestation (98 % average).

Table 5:5 Factors by which the quantity decreased since the previous year of afforestation

Factor by which the quantity decreased since the previous of afforestation				
Year since afforestation at S&W Et_o S&W rate	Normal		Drought (30% of normal rainfall)	
	West of Lake	South of Lake	West of Lake	South of Lake
3	1.45	1.52	0.71	0.73
4	1.34	1.27	0.77	0.78
5	1.25	1.15	0.81	0.81
6	1.18	1.09	0.84	0.84

ET_o's impact on each streamflow zone

Streamflow for 9 different zones (Figure 5:19), free from afforestation, were quantified for years of drought and of normal MAP. The streamflow of these zones were then also quantified when subjected to the ET rates simulated by S&W - for normal and drought circumstances.

During normal rainfall and drought circumstances, streamflow for zone 1 (Figure 5:10) is not significantly reduced by the afforestation situated west of the streamflow zone. The streamflow is thus most dependent of the rainfall in zone 1, decreasing in reaction to afforestation during drought only by 1 m^3/day streamflow reduction after three years of afforestation.

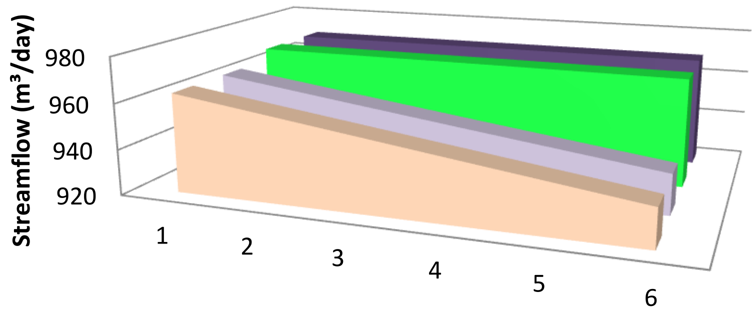

	1	2	3	4	5	6
Drought Afforestation	964	958	953	947	942	937
Drought No Afforestation	964	958	953	948	943	938
Normal Rainfall Afforestation	969	969	969	969	968	968
Normal MAP No Afforestation	969	969	969	969	969	969

Year Zone 1

Figure 5:10 Zone 1 streamflow for scenario's across six years duration

Zones 3, 4 and 5 (which also flow into Zone 2) have streamflows lower than 30 m^3/day irrelevant of precipitation or afforestation. The afforestation is generally situated downstream (to the east) of these river zones. In the absence of afforestation, the streamflow of zone 2 (Figure 5:11) is constant at 28 m^3/day for the six sequential years. Streamflow does however decrease to 25 m^3/day from the first year of afforestation and again to 24 m^3/day from the third year of afforestation when trees mine water at the ET rates simulated by S&W - despite normal MAP. Drought, as was concluded from zone 1 as well, results in a streamflow reduction with time, irrelevant of afforestation.

For zone 2 however, the reduction is 2 m^3/day greater for each sequential year subjected to afforestation. The 2 m^3/day lower streamflow during drought, with afforestation compared to the streamflow during drought without afforestation, concludes that the afforestation's roots are tapping groundwater.

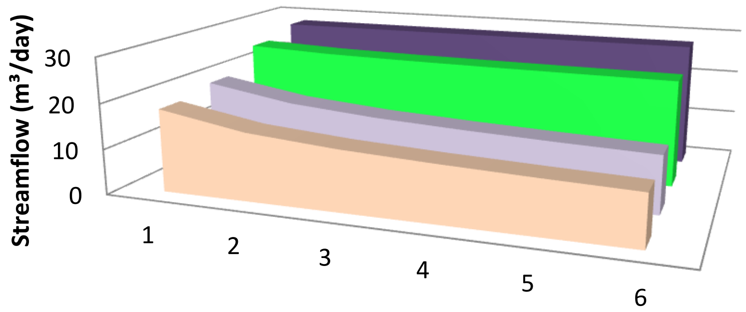

	1	2	3	4	5	6
Drought Afforestation	18	15	13	13	12	11
Drought No Afforestation	20	17	15	14	13	13
Normal Rainfall Afforestation	25	25	24	24	24	24
Normal MAP No Afforestation	28	28	28	28	28	28

Year Zone 2

Figure 5:11 Zone 2 streamflow for scenario's across six years duration

Zone 3 (Figure 5:12) has a constant streamflow decline of 1 m³/day when afforestation mines water, despite normal precipitation. During drought, the streamflow decreases an average 1 m³/day more when subjected to afforestation. Drought decreases the streamflow by halve after six years, irrelevant of afforestation. Zone 3 is more rainfall dependent and little streamflow reduction (1 m³/day) can be ascribed to afforestation's groundwater mining

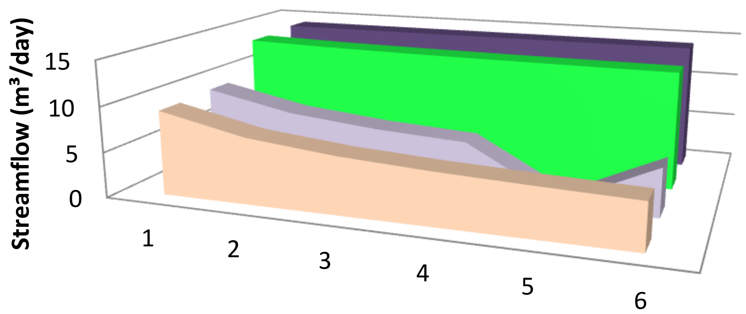

	1	2	3	4	5	6
Drought Afforestation	9	7	6	6	5	5
Drought No Afforestation	10	8	7	6	1	5
Normal Rainfall Afforestation	14	13	13	13	13	13
Normal MAP No Afforestation	14	14	14	14	14	14

Year Zone 3

Figure 5:12 Zone 3 streamflow for scenario's across six years duration

Zone 4 (Figure 5:13) has a streamflow of 5 m³/day during normal rainfall, irrelevant of afforestation, however the streamflow reduces to 3 m³/day during the first year of drought, and reduces further by a factor of 1 after five years of afforestation.

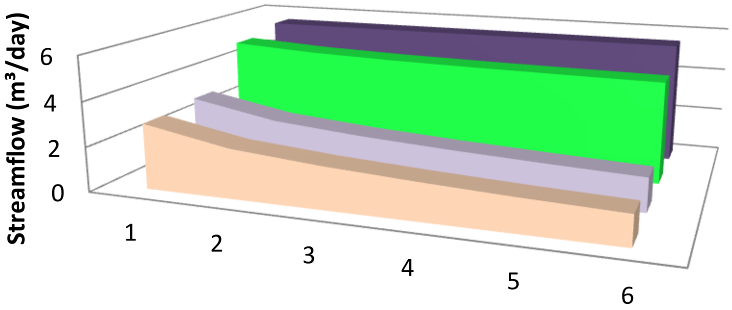

	1	2	3	4	5	6
Drought Afforestation	3	2	2	2	1	1
Drought No Afforestation	3	2	2	2	2	2
Normal Rainfall Afforestation	5	5	5	5	5	5
Normal MAP No Afforestation	5	5	5	5	5	5

Year Zone 4

Figure 5:13 Zone 4 streamflow for scenario's across six years duration

The streamflow of zone 5 (Figure 5:14) is reduced by 1 m³/day under normal rainfall conditions in the presence of afforestation. The streamflow during drought when exposed to afforestation, for zone 5 and zone 6 (Figure 5:15), is only reduced 1 m³/day more than the drought streamflow not subjected to six years of afforestation.

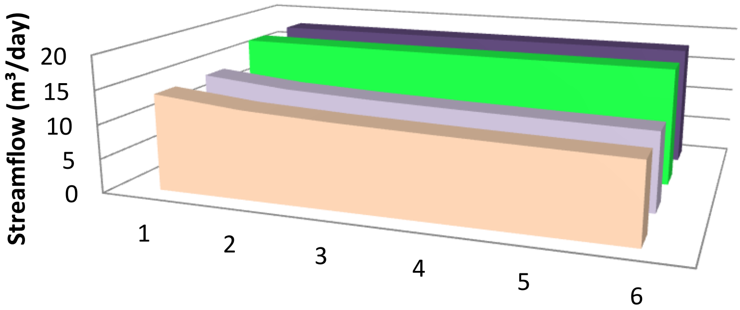

	1	2	3	4	5	6
Drought Afforestation	14	13	12	12	12	11
Drought No Afforestation	14	13	12	12	12	12
Normal Rainfall Afforestation	17	17	17	17	17	17
Normal MAP No Afforestation	18	18	18	18	18	18

Year Zone 5

Figure 5:14 Zone 5 streamflow for scenario's across six years duration

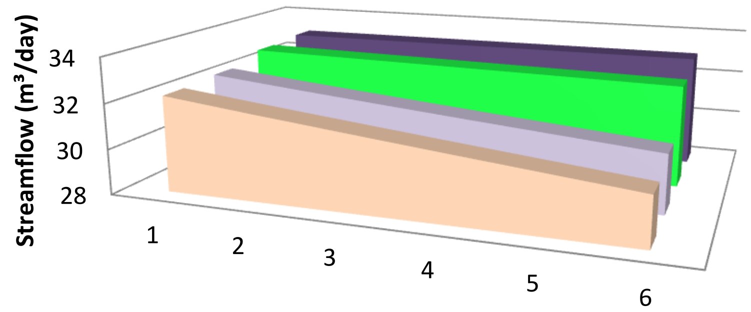

	1	2	3	4	5	6
Drought Afforestation	32	32	31	31	31	30
Drought No Afforestation	32	32	32	31	31	31
Normal Rainfall Afforestation	33	33	33	33	33	32
Normal MAP No Afforestation	33	33	33	33	33	33

Year Zone 6

Figure 5:15 Zone 6 streamflow for scenario's across six years duration

Streamflow zone 7 (Figure 5:16) is subjected to afforestation on the east and west side of the river. Streamflow zone 7 correlates to the area of great drawdown in Figure 5:8. Under normal MAP, the maximum streamflow reduction for zone 7 is 3 m³/day after six years of afforestation - although streamflow reduction is already experienced from the first year of afforestation. Zone 7's streamflow has decreased 20 m³/day by year six of drought irrelevant of afforestation.

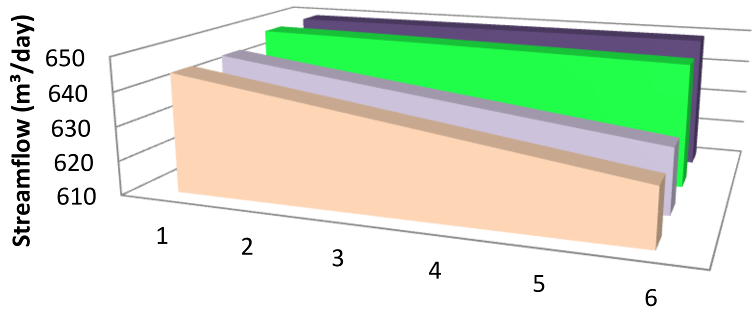

	1	2	3	4	5	6
Drought Afforestation	645	641	638	634	630	627
Drought No Afforestation	645	642	639	635	632	629
Normal Rainfall Afforestation	649	648	648	647	647	646
Normal MAP No Afforestation	649	649	649	649	649	649

Year Zone 7

Figure 5:16 Zone 7 streamflow for scenario's across six years duration

By year six of afforestation, under normal rainfall circumstances, zone 8's (Figure 5:17) streamflow has reduced 14 m³/day, which is 1 m³/day less than that in the absence of 70 % of the precipitation. The streamflow still decreased by 15 m³/day when subjected to drought and afforestation in comparison to the reduction only ascribed to the drought.

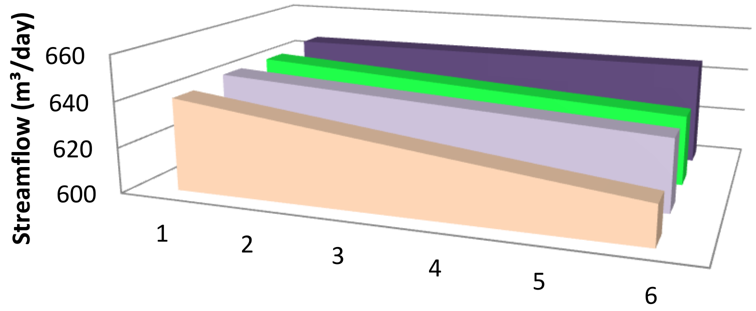

	1	2	3	4	5	6
Drought Afforestation	641	636	631	626	622	617
Drought No Afforestation	643	641	638	636	634	632
Normal Rainfall Afforestation	643	640	638	635	633	631
Normal MAP No Afforestation	645	645	645	645	645	645

Year Zone 8

Figure 5:17 Zone 8 streamflow for scenario's across six years duration

Zone 9 (Figure 5:18) is the river zone that flows from Lake St. Lucia and has a recharge area greater than any other streamflow zone. Zone 9 indicates that six years of afforestation has not decreased the water levels of Lake St. Lucia to the extent that it will reduce zone 9's streamflow. The streamflow does not reduce irrelevant of rainfall and afforestation's presence.

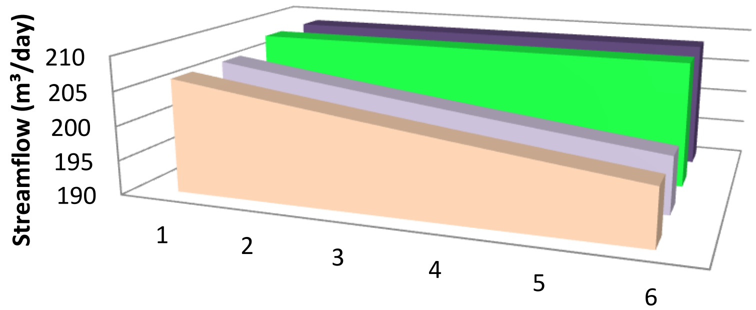

	1	2	3	4	5	6
Drought Afforestation	207	205	203	201	200	198
Drought No Afforestation	207	205	203	201	200	198
Normal Rainfall Afforestation	208	208	208	208	208	208
Normal MAP No Afforestation	208	208	208	208	208	208

Year Zone 9

Figure 5:18 Zone 9 streamflow for scenario's across six years duration

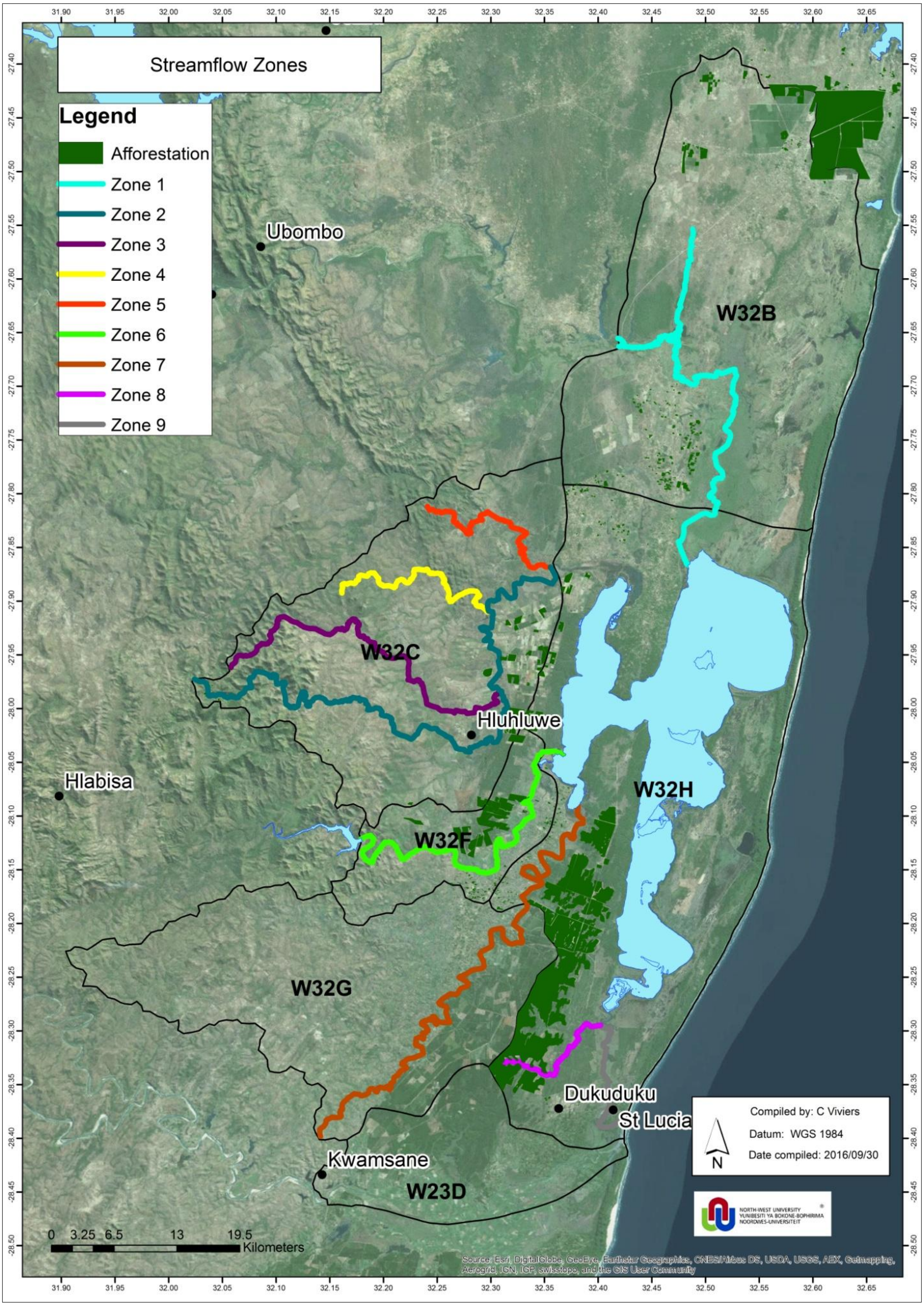

Figure 5:19 Zones for quantification of afforestation's impact on streamflow

The difference between the streamflows subjected to afforestation and not subjected to afforestation's water use after six years, for drought and normal MAP, is in Figure 5:20. The area most impacted by the afforestation, is zone 8 as its streamflow is reduced by more than 14 m^3/d when subjected to six years of afforestation, whether precipitation is normal or 70 % less than the MAP. The difference between the streamflow impacted and not impacted by afforestation simulated for normal rainfall periods, is greater than the difference between the streamflow impacted and not impacted by afforestation during drought in zone 2. The streamflow reduction ascribed to afforestation's impact is generally constant and not significantly greater due to drought, but adds to the steamflow reduction from the drought.

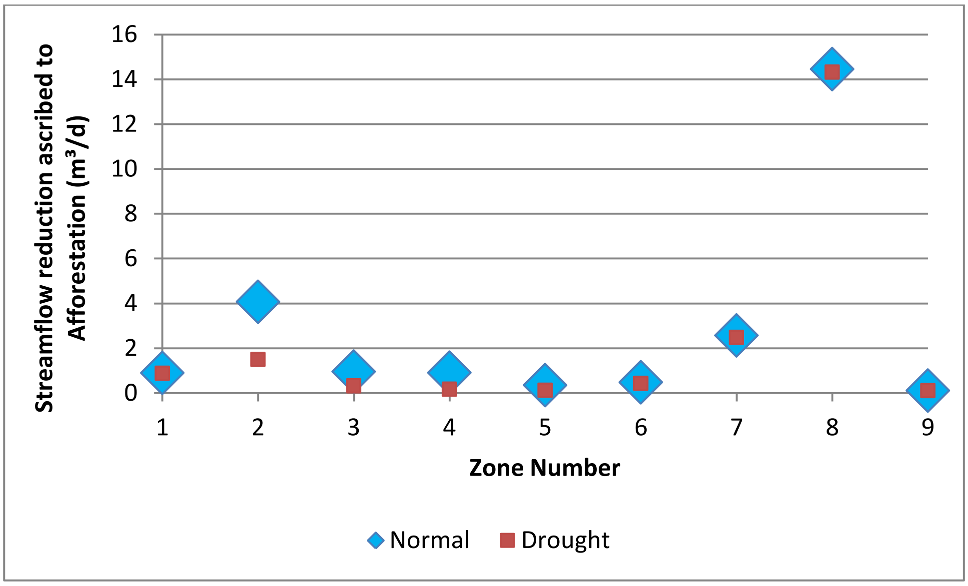

Figure 5:20 The difference between streamflow subjected to afforestation and not subjected to afforestation (sixth year of afforestation)

Chapter 6 Conclusions

6.1. Shuttleworth - Wallace Analytical Model

The individual maximum daily S&W ET_o simulated is 9.7 mm/day, and the minimum 1.6 mm/day. The maximum average daily ET_o for 2014 and 2015 months' as simulated using the S&W model, is 6 mm/day, while the minimum average daily ET_o is 3.4 mm/day – both within the ranges provided from Albough *et al.* (2013) and Burger (1999).

The total annual S&W ET_0 of 2015 exceeds that of 2014 by 438 mm/a. The average annual ET_o simulated from S&W for the two years 2014 and 2015 is 1467 mm/year, which is within the ranges provided by literature - greater than the minimum *E. dunnii's* 629 mm/year and less than the maximum reported by Coppen (2002) which is 1600 mm/year (no *Eucalyptus* specie distinction was made). The continuous greater simulated ET_o for 2015 compared to 2014, can be ascribed to (1) the lack of relative humidity recordings for February 2014, and (2) 2015 being the hottest year on record, with higher temperatures than 2014 by a margin of 136 recorded years (Thompson, 2016).

The average monthly total ET_o for 2014 and 2015 has an 85 % correlation to the monthly ET estimated by the WRC (2016) for quaternary catchment W32H and an 84 % correlation to that of quaternary catchment W32G.

The average annual ET_o from that simulated using the S&W model, exceed the study area's MAP calculated from station 684910 by a factor of 1.55, that of station W3E001 by 1.54, that of station W3E002 by 1.51 and by a factor of 2.09 station W3E003. The average annual simulated ET_o thus exceeds the annual average MAP as determined from the weather stations, by a factor of 1.67. The S&W model quantified viable time variant data comparable to literature data, and with little variance within monthly simulated ET_o. This was achieved despite the application of numerous constant and literature reported parameters.

Recommendations:

- Improve the value's accuracy by increasing the scope - model more years' daily ET_o to quantify the monthly average from.
- Use more complete datasets for simulating daily ET_o as this influenced the weight of individual estimations.
- Decrease constant, no- transient input parameters with field recorded parameters - leaf area or tree height measurements for example.

- Extend the model to quantify ET_o per age class specifically. S&W is very sensitive to tree height and can be adjusted to quantify the change in ET_o as the tree ages by simulating it for tree ages' height.
- In-situ field ET recordings can assist in model calibration to site specifically.

6.2. Numerical Modelling

Drawdown increases at a 3 % greater rate per year during drought in comparison to years with normal MAP. The extent of drawdown is greatest during the year since afforestation and then decreases. The drawdown continues to increase, without exception for every sequential year - for both normal rainfall and drought scenarios, correlating to the results from S&W that the annual ET exceeds the annual precipitation.

The maximum drawdown for each second year, when receiving MAP, increases from 14.1 m two years after afforestation, to 14.7 m four years later and to 15 m six years after afforestation was initiated at the ET rate simulated by S&W. The area subjective to drawdown increases significantly with time. The cone of depression since two years of afforestation, does not reach the W32C and W32H quaternary catchment boundary west of Lake St. Lucia (at the W32G, W32D and W32H border). After six years of afforestation, the radius of influence west of Lake St. Lucia has breached the W32C and W32H catchment border.

The factors by which the quantity of groundwater flow from the lake to the afforested area's flow for every sequential year decrease, decreases when receiving the MAP - but increases when experiencing drought. After six years of afforestation, the impact of afforestation, only considering normal rainfall circumstances, decreased streamflow most by 14.45 m^3/day at zone 8. Zone 8 has afforestation along the whole western streamflow zone boundary. Zone 2 is reduced by 4 m^3/day and zone 7's streamflow is reduced by 3 m^3/day when subjected to forestry's water needs - irrespective of receiving the MAP. Zones 4 and 9's streamflow do not reduce when receiving normal rainfall and is subjected to afforestation. Streamflow zone 4 has no afforestation situated along it. Zone 9 flows out of Lake St. Lucia which is recharge by regional groundwater, precipitation and the inflow from the other streamflow zones; zone 9 does not have reduced streamflow even when subjected to drought and afforestation. The streamflow reduction ascribed to afforestation's impact is generally constant and not significantly greater due to drought, but adds to the steamflow reduction from the drought.

Recommendations:

The following actions are recommended to improve the research results:

- Hydrocensus and groundwater monitoring data collection.
- More extensive river flow monitoring stations are needed.
- In-situ pump tests for quantification of model parameters (transmissivity and storativity).
- Quantification of the difference between afforestation's impact when the Lake St. Lucia mouth is open to the Indian Ocean in comparison to when it is closed.
- From most to least impacted, Zone 8's streamflow decreases the most (14 m^3/d), while Zone 2's streamflow decreases by 4 m^3/d and Zone 7 by 3 m^3/d. Drawdown is also the greatest between Zone 7 and 8 as well as along Zone 2.

  It is recommended that all afforestation within 3 kilometres of these river zones and the lake be removed to limit the drawdown curve's extent to not reach the river zones/lake boundary.

Bibliography

Adams, S., Titus, R. and Xu, Y. 2004. Groundwater recharge assessment of the basement aquifers of central Namaqualand. Water Research Commission Report No. 1093/1/04 (ISBN: 1-77005-214-3). 19 p.

Albaugh, J. M., Dye, P. J. and King, J. S. 2013. *Eucalyptus* and water use in South Africa. *International Journal of Forestry Research*. 2013(1): 1-11 p.

Allen, R. G., Pereira, L. S., Raes, D. and Smith, M. 2006. Crop Evapotranspiration-Guidelines for computing crop water requirements. *FAO Irrigation and Drainage* Paper 56(4): 1-5 p.

Anon. 2002. Normalised Difference Vegetation Index. [Available on the Internet:]. http://www.met.rdg.ac.uk/~swsgrime/artemis/ch3/ndvi/ndvi.html. [Date access: July 2015].

Battaglia, M., Cherry, M. L., Beadle, C. L., Sands, P. J. and Highston, A. 1997. Prediction of lead area index in Eucalypt plantations: effects of water stress and temperature. *Tree Physiology.* 18(1): 521 – 528 p.

Benyon, R.G., Theiveyanathan, S. and Doody, T. 2006. Impacts of tree plantation of groundwater in south-eastern Australia. *Australian Journal of Botany* 54(10): 181 - 192 p.

Bernardo, A., Reis, G.G., Reis, M.G.F. and Harrison, R. 1998. Effect of spacing on *Eucalyptus camaldulensis, E. pellita* and *E. urophylla* plantations in south-eastern Brazil: Growth & biomass. *Forest Ecology and Management.* 104(3):1-13 p.

Bilal, H., Nisa, S. and Ali, S.S. 2014. Effects of exotic *Eucalyptus* plantation on the ground and surface water of district Malakand, Pakistan. *International Journal of Innovation and Scientific Research*. 8(2): 229 - 304 p.

Blaney, H.F. and Criddle, W.D. 1950. Determining water requirements in irrigated area from climatologically irrigation data. Unite States Department of Agriculture, Soil Conservation Service. 96(1): 48 p.

Bosch, J. and Gadow, K. 1990. Regulating afforestation for water conservation in South Africa. *South African Forestry Journal.* 153(1): 41 - 54 p.

Botha, G. A., Haldorsen, S. and Porat, N. 2013. Geological History (*In* Perissinotto, R., Stretch, D. D. and Taylor, R. H ., *ed.* Ecology and conservation of estuarine ecosystems Lake St Lucia as a Global Model England:Cambridge University Press. 47 – 51 p.).

Bredenkamp, D.B., Notha, L.J. and Venter, D. 1992. St Lucia Lake: Geohydrology and related aspects. Department of Water Affairs and Forestry Report No. GH3776. 2 - 6 p.

Burger, C. 1999. Comparative evaporation measurements above commercial forestry and sugarcane canopies in the KwaZulu-Natal Midlands. University of Natal. (Dissertation – M.Sc.) 64 p.

Calder, I. R. 2007. Forests and water-ensuing forest benefits outweigh water costs. *Forest Ecology and Management*. 251(2007): 110 – 120 p.

Calder, I. R. Rosier, P.T.W., Prasanna, K.T. and Parameswarappa, S. 1997. *Eucalyptus* water use greater than rainfall input-a possible explanation from southern India. *Hydrology and Earth Sciences.* 1(2): 249 - 256 p.

Caliri, G. V. 2000. Introduction to Analytical Modelling. (In Proceedings of the 26th International Computer Measurement Group Conference. 31-36 p.).

Campbell, B. M. and Moll, E. J. 1977. The Forest communities of Table Mountain. *Vegetatio*. 34(2): 105 – 115 p.

Camp Dresser and McKee (CDM). 2001. Evaluation of integrated surface and groundwater modeling tools. *Water Resources Research and Development Program*. Report No. J:\9998\28039

Clulow, A. D., Everson, C. S. and Gush, M. B. 2011. The long-term impact of *Acacia mearnsii* trees on evaporation, streamflow and groundwater resources. Pretoria: Water Research Commission Report No. 505: 67 and 86.

Coppen, J. 2002. *Eucalyptus*: The genus *Eucalyptus*. London: CRC Press. 122.

Cyrus,D., Jerling, H., MacKay, F. and Vivier, L. 2011. Lake St. Lucia, Africa's largest estuarine lake in crisis: Combined effects of mouth closure, low levels and hyersalinity. *South Africa Journal Science.* 107(3):1 - 13 p.

Department of Agriculture, Forestry and Fishery (DAFF). 2016. South African Forestry and Statistics [Available on the Internet:] http://www.forestry.co.za/statistical-data/ [Date of access: 12 October 2016].

Department of Agriculture, Forestry and Fishery (DAFF) 2014. Report on commercial timber resources and primary roundwood processing in South Africa 2011/2012. Pretoria: Government Printer. 9 – 24 p.

Department of Agriculture, Forestry and Fishery (DAFF). 2011. State of the forests report. Pretoria: Government Printer 2007 – 2009. 1 - 39 p.

Department of Water Affairs (DWA). 2014. South African Forestry and Forest Products Industry Facts. Pretoria: Government Printer. 198 – 201 p.

Department of Water Affairs (DWA). 2010. Groundwater Strategy. Pretoria: Government Printer. 8 - 18 p.

Department of Water Affairs and Forestry (DWAF). 2000. Water conservation and demand management strategy for the forest sector in South Africa. Pretoria: Government Printer. 10 – 30 p.

Department of Water Affairs and Forestry (DWAF). 2006. Groundwater Resource Assessment II - Task 3aE Recharge. Pretoria: Government Printer. 122 p.

Dye, J. P. 2013. A review of changing perspectives on *Eucalyptus* water-use in South Africa. *Forest Ecology and Management*. 301(1): 51 – 57 p.

Dye, J. P. 1997. The determination of the relationship between transpiration rate and declining available water for *Eucalyptus grandis*. Pretoria: Water Research Commission Report No. RP 441/1/97. 1 - 20 p.

Dye, J.P. 1996. Response of *Eucalyptus grandis* trees to soil water deficits. *Tree Physiology*. 16(1): 233 - 238 p.

Dye, J. P., Jacobs, S. and Drew, D. 2004. Verification of 3-PG growth and water-use predictions in twelve *Eucalyptus* plantation stands in Zululand, South Africa. *Forest Ecology and Management.* 193(2004): 197 – 218 p.

Dye, J. P. and Jarmain, C. 2004. Water use by black wattle (*Acacia mearnsii*): implications for the link between removal of invading trees and catchment streamflow response. *South African Journal of Science*. 100 (1): 40 – 44 p.

Dye, J. P., Olbrich, B. and Everson, C. 1995. The water use of plantation forests and montane grassland in summer-rainfall forestry regions of South Africa. *Proceedings of the seventh South African National Hydrological Symposium.* South Africa: Grahamstown.

Dye, J. P., Poulter, A. G., Soko, S. and Maphanga, D. 1997. The Determination of the relationship between transpiration rate and declining available water for Eucalyptus grandis. Pretoria: Water Research Commission Report No. RP 441/1/97. 124 - 130 p.

Eijkelkamp (Agrisearch Equipment). 2009. Evaporation Pan. Operating Instructions. Netherlands. [Available on the Internet:] http://www.kean.edu/~csmart/Hydrology/Lectures /Evaporation_pan. [Date of access: 19 July 2015].

Environmental Systems Research Institute (ESRI). 2016. Landsat Imagery: Change Matters Viewer. [Available on the Internet:] http://www.esri.com/software/landsat-imagery/viewer. [Date of access: 24 September 2016].

Federer, C. A., Vorosmarty, C. J. and Fekete, B. 1996. Intercomparison of methods for potential evapotranspiration in regional or global water balance models. *Water Resource Research*. 32(1): 2315 – 2321 p.

Feyen, L. 2005. Large scale groundwater modelling. European Commission: Joint Research Centre. Report No, EUR/22124/EN. Italy. [Available on the Internet:] https://core.ac.uk/download/pdf/38609353 [Date of access: 24 October 2016].

Freeze, R.A. and Witherspoon, P.A. 1967. Theoretical analysis of regional groundwater flow: 2. Effect of water table configuration and subsurface permeability variation. *Water Resources Research.* 3(2):623 - 634 p.

Haely, R. W. 2010. Water-budget Methods (In Haely, R.W. ed. Estimating Groundwater Recharge. New York: Cambridge University Press. 15 - 28 p).

Haitjema, H.M. and Mitchell-Bruker, S. 2005. Are water tables a subdued replica of the topography? Groundwater. 43(6):781 - 786 p.

Hesch, W. 2009. Conceptual model development for MODFLOW and FEFLOW models. *Feflow Conference Schlumberger Water Services*. [Available on the Internet:] http://novametrixgm.com/pdfs/brochures/FEFLOW_Conference_HydroGeoBuilder_final.pdf [Date of access: 12 November 2016].

iSimangaliso Wetland Park. 2014. iSinmagaliso to remove Lake St Lucia dredger spoil. iSinmangaliso Newsflash. [Available on the Internet:] isimangaliso.com/newsflash/isimangaliso-to-remoe-lake-st-lucia-dredger-spoil/ [Date of access: 2 November 2016].

iSimangaliso Wetland Park. 2016.a. iSimangaliso signs historic contract to restore Lake St Lucia. iSinmangaliso Newsflash. [Available on the Internet:] isimangaliso.com/newsflash/isimangaliso-signs-historic-contract-to-restore-lake-st-lucia/ [Date of access: 2 November 2016].

iSimangaliso Wetland Park. 2016.b. Lake St Lucia's lifeline cut off. iSinmangaliso Newsflash. [Available on the Internet:] isimangaliso.com/newsflash/lake-st-lucias-lifeline-cut-off/ [Date of access: 2 November 2016].

Jovanovic, N., Bugan, R. D. H., Isreal, S., Dzikiti, S., Kapangaziwiri, E., Le Maitre, D., Rozanov, A., Stander, M., Mikes, D., May, F., Jarmain, C. and Everson, C. 2012. Reducing uncertainties of evapotranspiration and preferential flow in the estimation of groundwater recharge. Water Research Commission Report No. RP 1909/1/12. 9 - 31 p.

Karisson, E. and Pomade, L. 2004. Methods for estimating potential and actual evapotranspiration. Department of Water Resources Engineering: 2 – 11 p.

Katerji, N. and Rana, G. 2006. Modelling evapotranspiration of six irrigated crops under Mediterranean climate conditions. *Agricultural and Forest Meteorology.* 138(2006): 146 - 155 p.

Kelbe, B. and Germishuyse, T. 2010. Groundwater/surface water relationships with specific reference to Maputuland. Pretoria: Water Research Commission Report No. RP 1168/1/10.

Kelbe, B. E. and Shezi, W. 2010. Groundwater recharge and discharge for shallow primary aquifers in Maputuland: Case study 5. (*In* Kelbe, B. and Germishuyse, T. *ed.* Groundwater/surface water relationships with specific reference to Maputuland. Pretoria: Water Research Commission Report No. RP 1168/1/10)

Kelbe, B.E., Taylor, R.H. and Bate, G.H. 2013a. The linkage between hydrological and ecological drivers: Mgobezeleni Studies. Pretoria: Water Research Commission Report No. K5/2259/1/1.

Kelbe, B. E., Taylor, R. H. and Haldorsen, S. 2013b. Groundwater Hydrology. (*In* Perissinotto, R., Stretch, D. D.and Taylor, R .H. *ed.* Ecology and conservation of estaurine ecosystems Lake St Lucia as a Global Model. New York: Cambridge University. 151 – 167 p.).

Kienzle, S. and Schulze, R. 1992. A simulation model to assess the effect of afforestation on groundwater resources in deep sandy soils. *Water South Africa.* 18(4): 265 – 272 p.

Kim, N.W., Chung, I. M., Won, Y. S. and Arnold, J. G. 2008. Development and application of the integrated SWAT-MODFLOW model. *Journal of Hydrology.* 356(1): 1 – 16 p.

Kimura, S., McKibbin, R., Ogawa, J., Kiwata, T., Komatsu, N. and Nakamura, K. 2012. Leaf area index and topographical effects on turbulent diffusion in a deciduous forest. *Res. Lett. Inf. Mathematical Science*. 16(1): 1 – 22 p.

Kumar, C.P. 2002. Groundwater flow models. *National Institute of Hydrology*. [Available on the Internet:] http://www.angelfire.com/nh/cpkumar/publication/flowmodels.pdf [Date of access: 12 November 2016].

Le Maitre, D. C., Van Wilgen, B. W., Gelderblom, C. M., Bailey, C., Chapman, R. A. and Nel, J. A. 2002. Invasive alien trees and water resources in South Africa: case studies of the costs and benefits of management. *Forest Ecology and Management.* 160(2002): 143 – 159 p.

Le Maitre, D., Scott, D. and Colvin, C. 1999. A review of information on interactions between vegetation and groundwater. *Water South Africa.* 25(2): 137 – 152 p.

Le Maitre, D.C. and Versfeld, D. B. 1997. Forest evaporation models: relationship between stand growth and evaporation. *Journal of Hydrology,* 193(1): 240 – 257 p.

Lu, J., Sun, G., McNulty, S. G. and Amatye, D. M. 2003. Modelling actual evapotranspiration from forested watersheds across the South-Eastern United States. *Journal of the American Water Resources Association*. 2145(1): 887 – 896 p.

Mallory, S. 2002. Overview of the water resources of the Usutumhlathuze Water Management Area. Pretoria: Government Printer. 1 – 34 p.

Martinez-Vilalta, J., Vanderklein, D. and Mencuccini, M. 2006. Tree height and age-related decline in growth of Scots Pine (*Pinus sylvestris L*.). *Ecophysiology Oecologi*. 10(1): 1 – 16 p.

McCarthy, T. and Rubidge, B. 2005. The story of earth and life: A southern Africa perpective on a 4.6 billion-year-journey. 134 p. Cape Town: Struik Publishers.

Meadows, D. G. 1999. Hybrids allow Sappi and Mondi to increase production of Pine and Eucalypts. *Tappi Journal*. 82(7): 60 – 67 p.

Meyer, R. and Godfrey, L. 1995. Characterization and mapping of te groundwater resources, Kwazulu Natal Province. Pretoria: DWAF.

Mo, X., Liu, S., Lin, Z. and Zhao, W. 2004. Simulating temporal and spatial variation of evapotranspiration over the Lushi basin. *Journal of Hydrology.* 285(1): 125 – 142 p.

National Renewable Energy Lapboratory (NREL). 2014. Solar: monthly and annual average direct normal (DNI), global horizontal (GHI), latitude tilt, and diffuse data and GIS data at 40km resolution for Africa from NREL. Region 1396314. [Available on the Internet:] http://en.openei.org/datasets/dataset/solar-monthly-and-annual-average-direct-normal-dni-global-horizontal-ghi-latitude-tilt-and-d/resource/dd3f22a5-9e51-462f-9ce3-fd390be15a1f?inner_span=True. [Date access: 10 August 2015].

Nisbet, T. 2005. Water Use by trees Information Note. Forestry Commission. [Available on the Internet:] http://www.forestry.gov.uk/pdf/FCIN065.pdf/$FILE?FCIN065.pdf [Date of Access: 28 September 2016].

Nomquphy, V. W. 1998. Geohydrological studies of the western shores of Lake St Lucia. KWA-DLANGEZWA: University of Zululand (Dissertation – B.Sc. Hons) 13 - 84 p..

Norman, N. and Whitfield, G. 2006. Geological Journeys: A traveller's guide to South Africa's rock and landforms. Cape Town: Struik Nature. 164-165 p.

Pandey, P. K., Dabral, P. P. and Pandey, V. 2016. Evaluation of reference evapotranspiration methods for the north-eastern region of India. *International Soil and Water Conservation Research*. 4(1): 52 – 63 p.

Perkins, K. and Nimmo, J. 2006. Applicability of the Darcian Method for recharge estimation. USGS. [Available on the Internet:] http://www.rcamnl.wr.usgs.gov/uzf/DarcianRecharge/. [Date of Access: 13 June 2016].

Prietsley, C.H.B. and Taylor, R.J. 1972. On the assessment of the surface heat flux and evapotranspiration using large-scale parameters. Monthly Weather Review. 100(2): 81 - 83 p.

Racz, C., Nagy, J. and Dobos, A. C. 2013. Comparison of several methods for the calculation of reference evapotranspiration. *Acta Silv. Lingn. Hung*.9 (2013): 9 - 24 p.

Raes, D. 2009. Evapotranspiration from a reference surface. *Food and Agriculture Organization of the United Nations Reference Manual.* 3(1): 1 - 38 p.

Ramirez-Builes, V. H. and Harmsen, E. W, 2011. Water vapour flux in agroecosystems methods and models review. (*In* Labedzki, L. *Ed*. Evapotranspiration. Croatia.InTech. 3 - 30 p.).

Rao, L. Y., Sun, G., Ford, C. R. and Vose, J. M. 2011. Modeling potential evapotranspiration of two forested watersheds in the Southern Appalachians*. American Society of Agricultural and Biological Engineers.* 54(6): 2067 – 2078 p.

Rawlins, B.K. and Kelbe, B.E. 1998. Groundwater modelling of the impact of commercial forestry on an ecologically sensitive coastal lake. (*In* Wheater, H. and Kirby, C. *ed.* Hydrology in a changing environment. England: John Wiley and Sons Ltd. 65 - 88 p.).

Rawlins, B.K. 1991. A geohydrological assessment of the behaviour and response of the Zululand coastal plain to both environmental influences and human activity. University of Zululand. (Dissertation – M.Sc.) 1 - 35 p.

Scott, D. F. and Lesch, W. 1997. Streamflow responses to afforestation with *Eucalyptus grundis* and *Pinus putu* and to felling in the Mokobulaan experimental catchments*. South African Journal of Hydrology.* 199(1): 360 – 377 p.

Shuttleworth, J. W. and J. S. Wallace, 1985. Evaporation of sparse crops-an energy combination theory.Journal of the Royal Meteorological Society. 111(3): 839 - 885 p.

Singh, S. K., Verma, C. L. and Sharma, D. K. 2014. Plant height model for *Eucalyptus* plantations for bio-drainage use. International Journal of Research in Engineering and Technology. 3(6): 250 – 259 p.

Smith, M., Allen, R. and Pereira, L. 1996. Revised FAO methodology for crop-water requirements. [Available on the Internet:] http://www.fao.org/docrep/X0490E00.htm [Date of Access: 13 June 2016].

SolarGIS. 2015. Direct Normal irradiation. [Available on the Internet:] http://solargis.info/doc/free-solar-radiation-maps-DNI. [Date of access: 2 July 2015].

South Africa. 1998. National Water Act (NWA) 36 of 1998. Pretoria: Government Gazette 1998(398):19182.

South African Pulp and Paper Industries (Sappi). 2005. Species Selection (*In* Sappi *ed* Tree Farming Guidelines for private growers. 1 - 21 p.).

South African Pulp and Paper Industries (Sappi). 2012. *Eucalyptus* trees. (*In* Sappi *ed* Frequently asked questions about: *Eucalyptus* trees. 1 - 5 p.).

Stannard, D. I. 1993. Comparison of Penman-Monteith, Shuttleworth-Wallace, and modified Priestly-Taylor evapotranspiration models for wildland vegetation in semiarid rangeland. Water Resource Research. 29(5): 1379 – 1392 p.

Stretch, D. D. and Maro, A. Z. 2013. Catchment Hydrology (*In* Perissinotto, R., Stretch, D. D. and Taylor, R. H, *ed* Ecology and conservation of estaurine ecosystems Lake St Lucia as a Global Model. New York: Cambridge University. 77 – 86 p.).

Thompson, A. 2016. 2015 Shatters Hottest Year Mark; 2016 Hot on its Heels? Climate Central [Available on the Internet:] http://www.climatecentral.org/news/2015-hottest-year-2016-could-surpass-19929 [Date of access: 1 Sept 2016].

Toth, J. 1963. A theoretical analysis of groundwater flow in small drainage basins. *Journal of Geophysical Research*. 68(16): 4795 - 4812 p.

United States Geological Survey (USGS). 1997. Modeling ground-water flow with MODFLOW and related programs Transpiration [Available on the Internet:] https://pubs.usgs.gov/fs/FS-121-97/fs-121-97.pdf [Date of access: 2 November 2016]

United States Geological Survey (USGS). 2016. Transpiration - The Water Cycle. [Available on the Internet:] http://www.water.usgs.gov/edu/watercycletranspiration.html. [Date of access: 2 May 2016].

Vaeret, L., Kelbe, B., Haldorsen, S. and Taylor, R. H. 2009. A modelling study of the effects of land management and climate variations on groundwater inflow to Lake St. Lucia, South Africa. *Hydrogeology Journal*. 17(1): 1949 – 1967 p.

Valerio, A.M. 2000. Modeling groundwater-surface water interactions in an operational setting by linking riverware with MODFLOW. University of Michigan. (Dissertation - M.Sc.)

Van Tonder, G. Xu, Y. 2000. A guide for the estimation of groundwater recharge in South Africa. *Water South Africa*. 27(3): 341 - 343 p.

Von Roeder, M. A. B. 2014. The impact of *Eucalyptus* plantations on the ecology of Maputaland with special reference to wetlands. Technische Universität München (Dissertation – M.Sc.) 1 - 70 p.

Vorosmarty, C. J. Federer, C. A. Schloss, A. L.1998. Potential evaporation functions compared on US watersheds: possible implications for global-scale water balance and terrestrial ecosystem modelling. *Journal of Hydrology.* 207(1): 147 – 169 p.

Water Research Commission (WRC). 2016. Water Resources of South Africa, 2012. [Available on the Internet:] http://waterresourceswr2012.co.za/ [Date of access: 12 June 2016].

Weitz, J. and Demlie, M. 2014. Conceptual modelling of groundwater-surface water interactions in the Lake Sibayi Catchment, Eastern South Africa. *Journal of African Earth Sciences.* 99(1): 613 – 624 p.

Wels, C., Mackie D. and Scibek, J. 2012. Guidelines for groundwater modelling to assess impacts of proposed natural resource development activities. British Columbia Ministry of Environment Water Protection and Sustainability Branch. Report No. 194001. Canada. [Available on the Internet:] http://www.env.gov.bc.ca/wsd/plan_protect_sustain/groundwater/groundwater_modelling_guidelines_final-2012.pdf, 11.2.2015 [Date of access: 12 November 2016].

Wonn, H. T. and O'Hara, K. L. 2001. Height: diameter ratios and stability relationships for Northern Rocky Mountain tree Species*. Western Journal of Applied Forestry.* 6(2): 87 – 94 p.

Xu, C. Y. and Singh, V. P. 2002. Cross comparison of empirical equations for calculating potential evapotranspiration data from Switzerland. *Water Resource Management.* 16(3):197-219 p.

Yang, Y. 2015. Evapotranspiration over heterogeneous vegetated surfaces. *Models and applications.* University of Tsinghua. (Dissertation – Ph.D.)

Zahid, D.M. Nawaz, A. 2007. Comparative Water Use Efficiency of *Eucalyptus camaldulensis* versus *Dalbergio sissoo* in Pakistan. *International Journal of Agriculture and Biology.* 9(4): 540 - 543 p.

Zahn, G. A. and Neethling, B. A. 1926. Notes on the exotic trees in the Cape Peninsula. *South African Journal of Science*. 26(1): 211 – 234 p.

Zhou, M.C., Ishidaira, H., Hapuarachchi, H. P., Magome, J., Kiem, A. S. and Takeuchi, K. 2006. Estimating potential evapotranspiration using Shuttleworth–Wallace model and NOAA AVHRR NDVI data to feed a distributed hydrological model over the Mekong River basin. *Journal of Hydrology*. 327(1): 151 – 173p.

Zhou, Y. and Li, W. 2011. A review of regional groundwater flow modeling. *Geoscience Frontiers*. 2(2): 205 - 214 p.

Appendix A

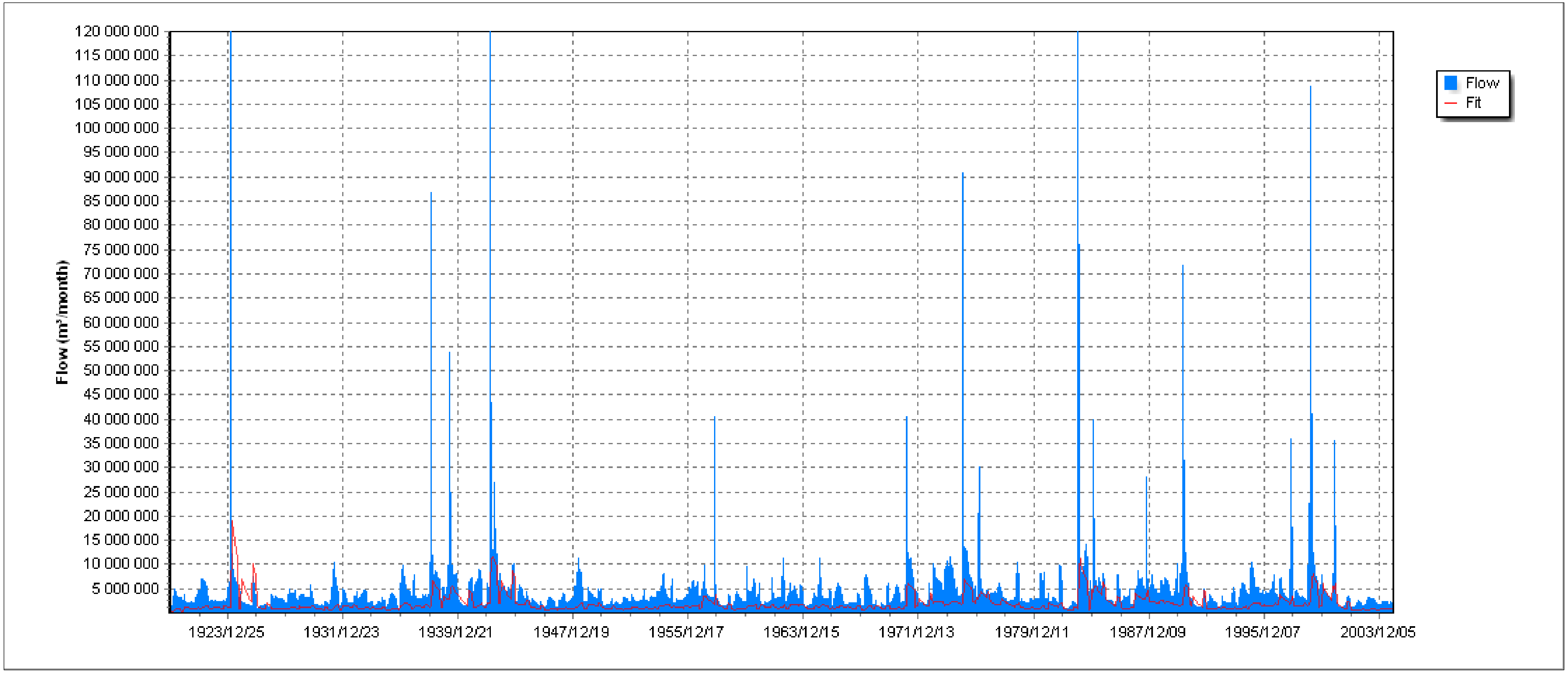

Catchment W32B Base flow Quantification using the Herold Method

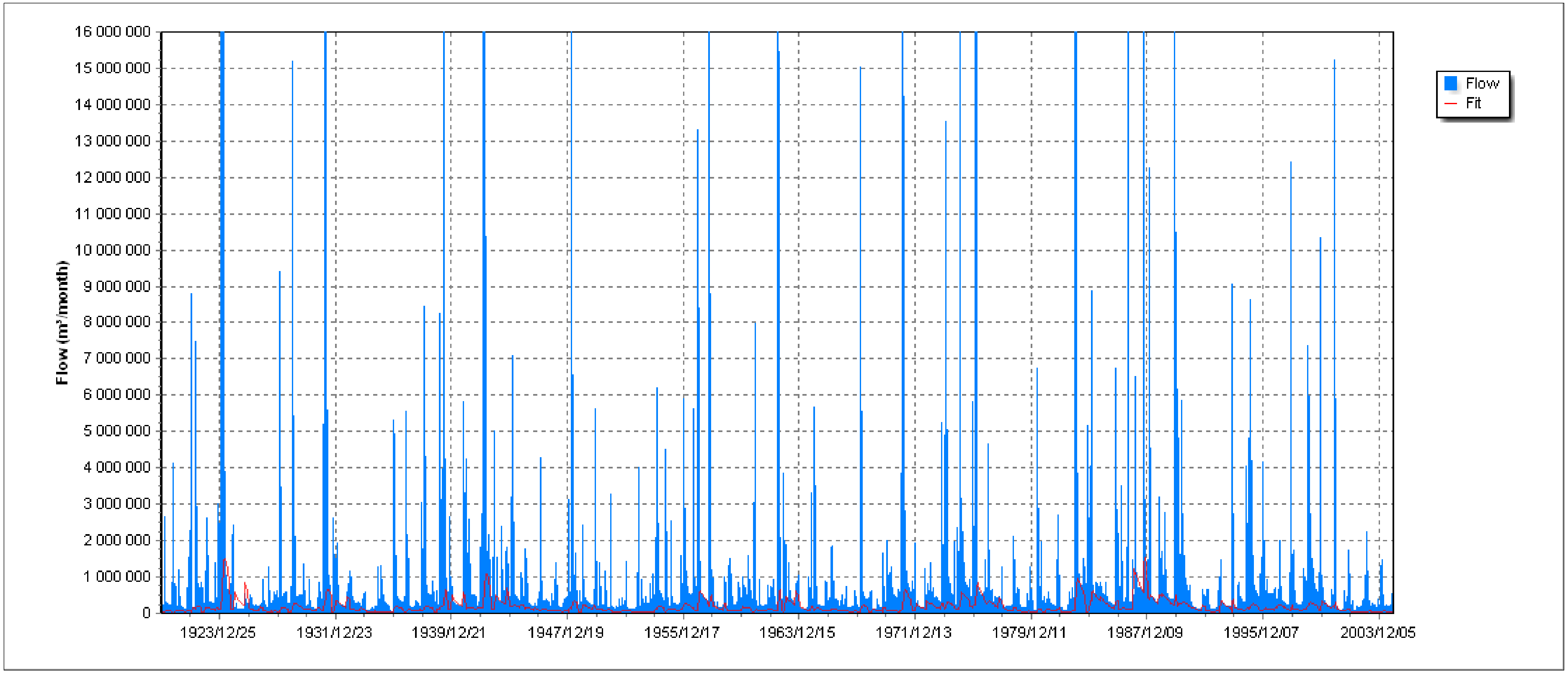

Catchment W32C Base flow Quantification using the Herold Method

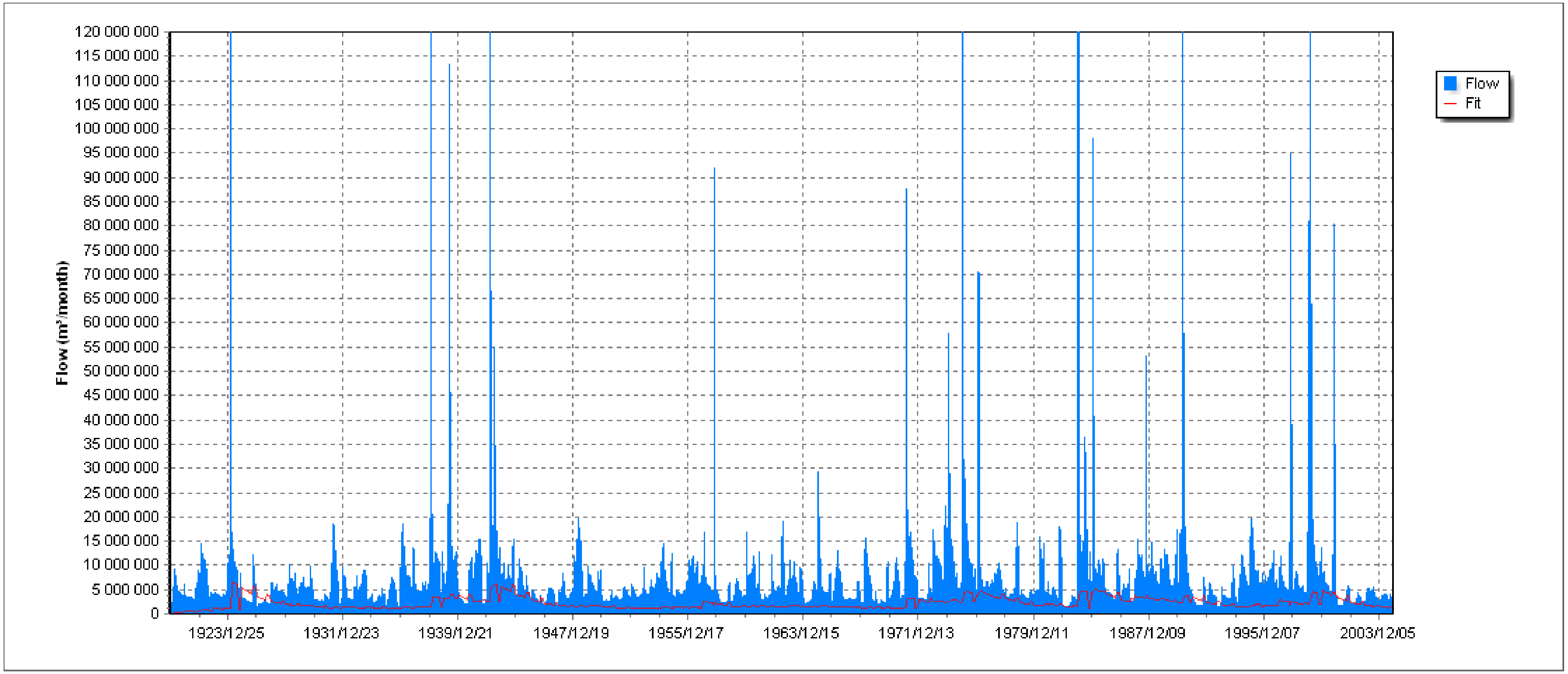

Catchment W32H Base flow Quantification using the Herold Method

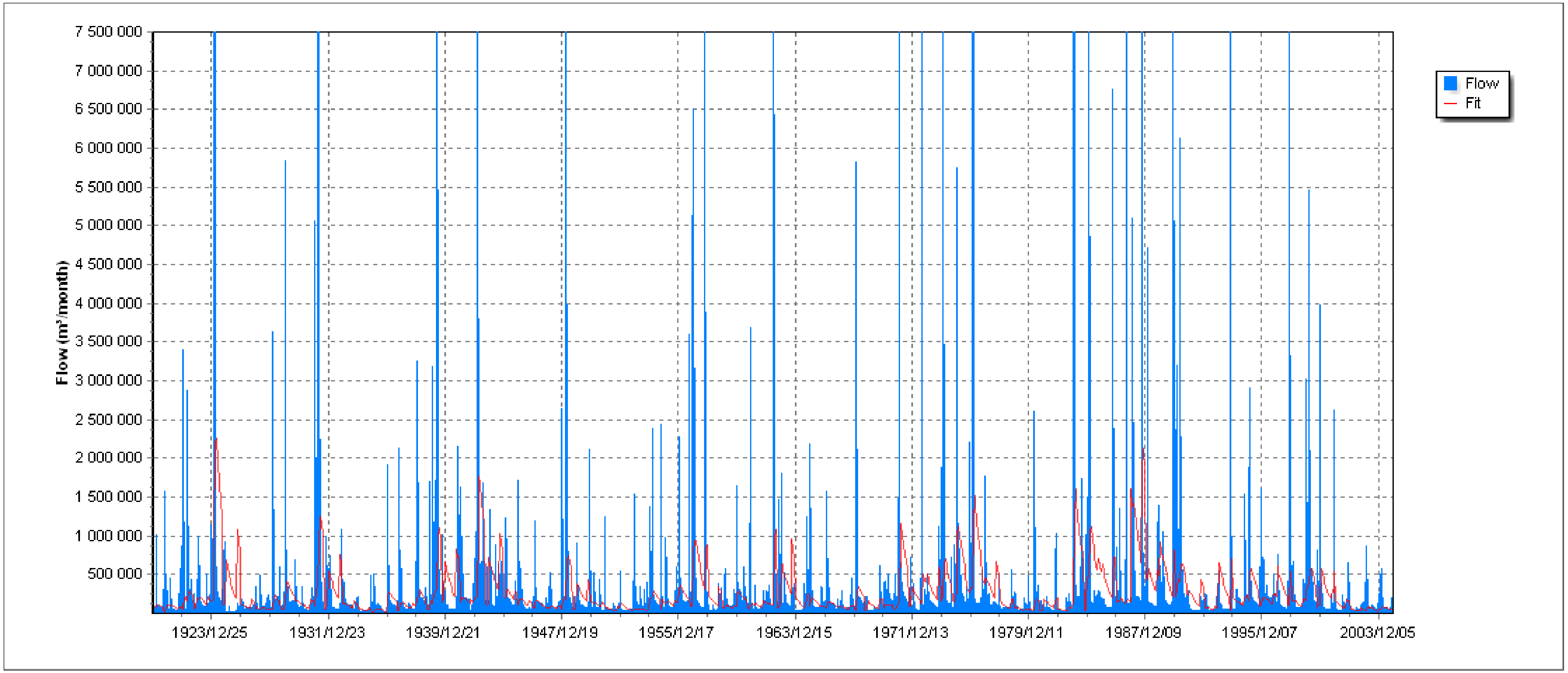

Catchment W32F Base flow Quantification using the Herold Method

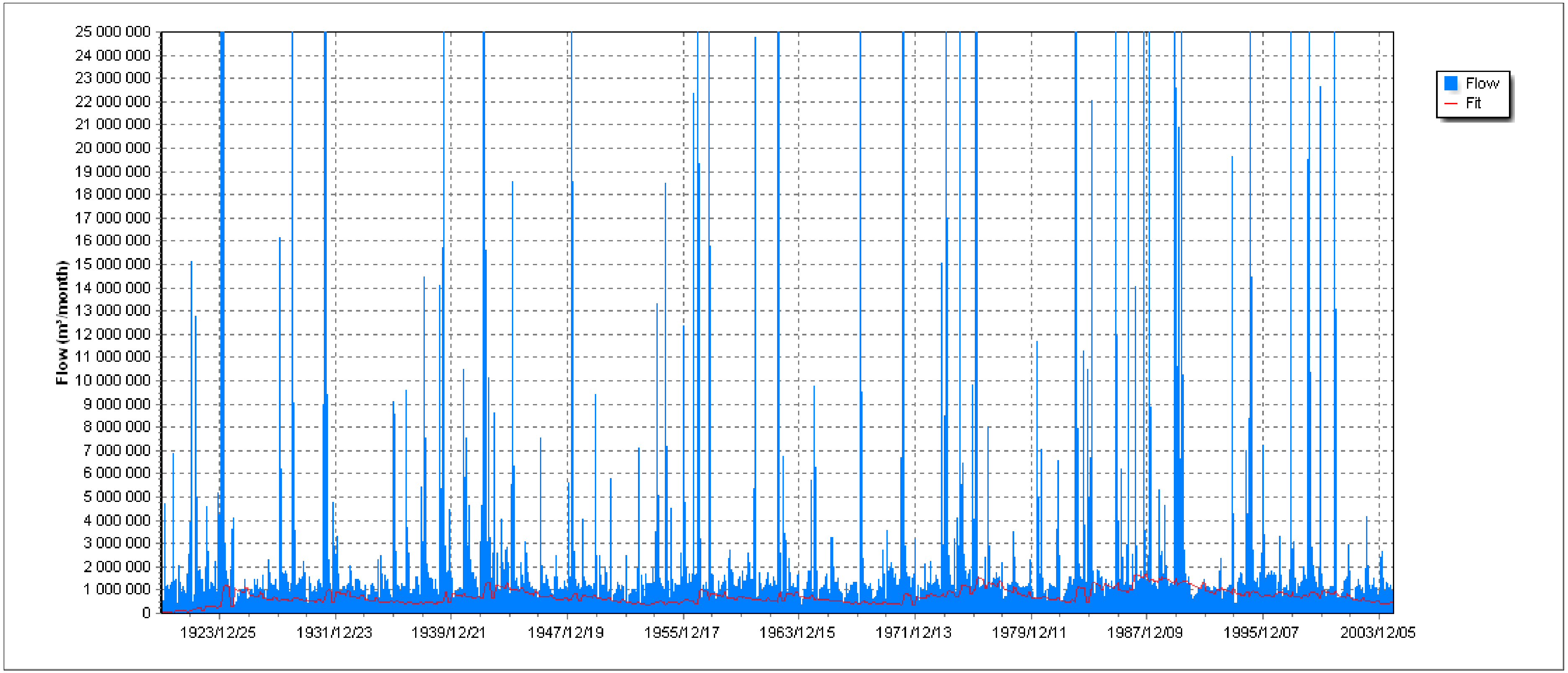

Catchment W32G Base flow Quantification using the Herold Method

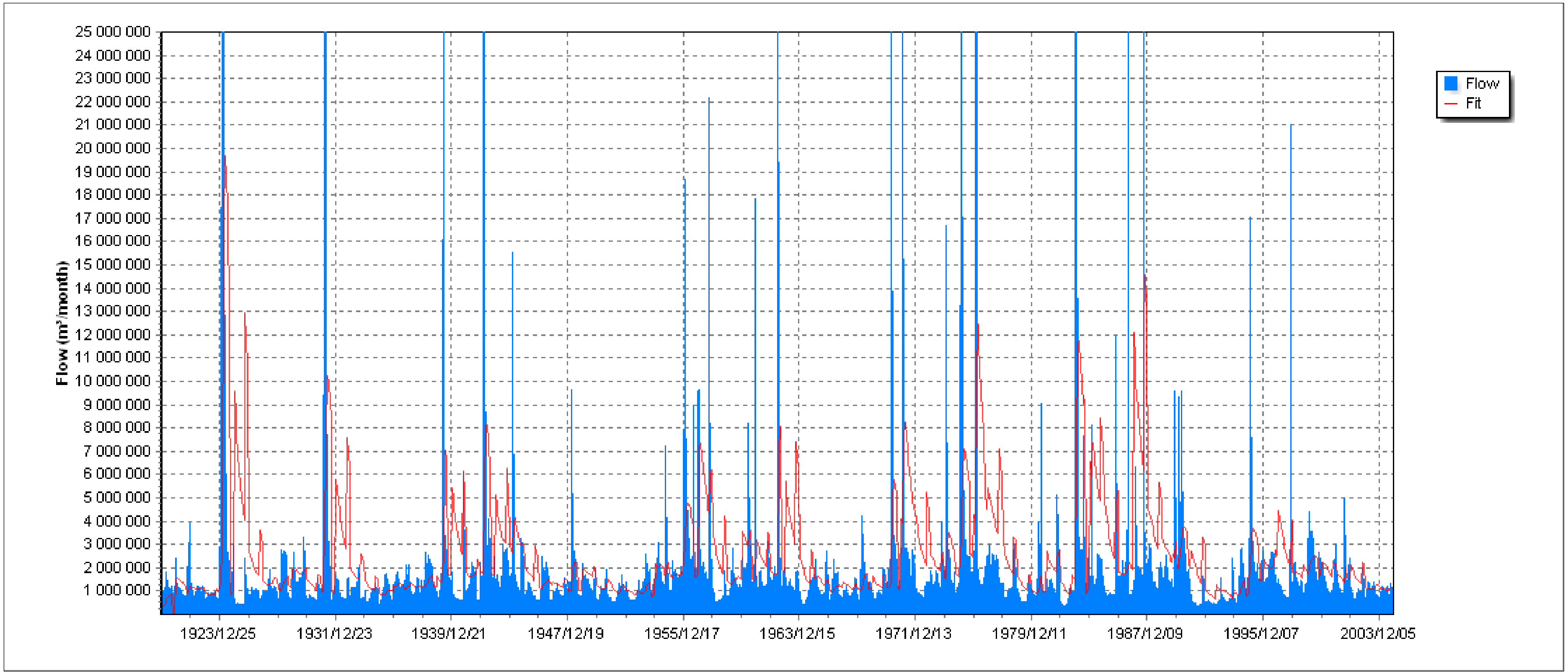

Catchment W23D Base flow Quantification using the Herold Method

Appendix B

Climate Related Parameters									
	Average daily temperature	Latent heat of water vaporisation	Saturation vapour pressure at the specific temperature	Saturation vapour pressure	Actual vapour pressure	Slope of saturation vapour pressure curve	Mean air density at constant pressure	Psychometric constant	Air Virtual Temperature
	T_s	λ	e°	e_s	e_a	Δ	ρ	γ	T_{kv}
Date	°C	MJ/kg	kPa	kPa	kPa	kPa/°C	kg/m³	kPa/°C	K
2014/01	26.12	2.44	3.39	3.51	2.62	0.20	1.17	0.07	302.11
2014/02	25.26	2.44	3.22	3.36	2.39	0.19	1.17	0.07	301.24
2014/03	25.21	2.44	3.22	3.35	2.70	0.19	1.17	0.07	301.19
2014/04	22.19	2.45	2.70	2.85	2.21	0.16	1.18	0.07	298.15
2014/05	20.39	2.45	2.41	2.58	1.95	0.15	1.19	0.07	296.32
2014/06	18.20	2.46	2.13	2.40	1.67	0.13	1.20	0.07	294.11
2014/07	17.80	2.46	2.06	2.26	1.53	0.13	1.20	0.07	293.71
2014/08	19.63	2.45	2.30	2.48	1.80	0.14	1.19	0.07	295.56
2014/09	21.20	2.45	2.54	2.71	1.92	0.16	1.19	0.07	297.14
2014/10	20.16	2.45	2.38	2.49	1.86	0.15	1.19	0.07	296.09
2014/11	23.24	2.45	2.87	3.01	2.24	0.17	1.18	0.07	299.20
2014/12	24.52	2.44	3.12	3.28	2.47	0.19	1.17	0.07	300.49
2015/01	26.57	2.44	3.49	3.64	2.71	0.21	1.17	0.07	302.56
2015/02	26.12	2.44	3.41	3.58	2.68	0.20	1.17	0.07	302.11
2015/03	26.30	2.44	3.44	3.63	2.65	0.20	1.17	0.07	302.29
2015/04	23.40	2.45	2.89	3.08	2.23	0.17	1.18	0.07	299.36
2015/05	23.12	2.45	2.84	3.05	2.27	0.17	1.18	0.07	299.09
2015/06	18.98	2.46	2.21	2.48	1.71	0.14	1.20	0.07	294.90
2015/07	18.80	2.46	2.19	2.39	1.73	0.14	1.20	0.07	294.72
2015/08	20.02	2.45	2.37	2.57	1.83	0.15	1.19	0.07	295.95
2015/09	21.73	2.45	2.64	2.82	2.02	0.16	1.18	0.07	297.68

2015/10	23.68	2.45	2.95	3.15	2.17	0.18	1.18	0.07	299.65
2015/11	23.50	2.45	2.92	3.12	2.12	0.18	1.18	0.07	299.46
2015/12	26.72	2.44	3.54	3.74	2.56	0.21	1.16	0.07	302.72
Count 2014	370.00	370.00	370.00	370.00	347.00	370.00	370.00	370.00	370.00
Count 2015	373.00	373.00	373.00	373.00	373.00	373.00	373.00	373.00	373.00

Aerodynamic Resistances						
	Wind speed observed at the weather station	Wind speed at the reference height	Friction Velocity	Eddy diffusion coefficient at the top of canopy	Aerodynamic resistance	Aerodynamic resistance
Date	u_w	u_a	u_x	K_h	r^s_a	r^a_a
	m/s	m/s	m/s	m²/s	s/m	s/m
2014/01	0.65	0.27	0.07	0.15	6235.20	186.82
2014/02	2.77	1.17	0.31	0.64	768.08	23.01
2014/03	2.63	1.11	0.29	0.60	835.69	25.04
2014/04	2.63	1.11	0.29	0.60	827.55	24.80
2014/05	2.78	1.17	0.31	0.64	796.14	23.85
2014/06	2.45	1.03	0.28	0.56	1035.86	31.04
2014/07	2.95	1.24	0.33	0.68	747.88	22.41
2014/08	3.11	1.31	0.35	0.72	751.26	22.51
2014/09	3.58	1.51	0.40	0.82	605.13	18.13
2014/10	3.35	1.41	0.38	0.77	646.71	19.38
2014/11	3.19	1.35	0.36	0.73	695.12	20.83
2014/12	3.16	1.33	0.35	0.73	676.27	20.26
2015/01	3.24	1.36	0.36	0.74	665.19	19.93
2015/02	3.07	1.29	0.34	0.71	719.85	21.57
2015/03	2.84	1.20	0.32	0.65	753.41	22.57
2015/04	2.62	1.10	0.29	0.60	836.24	25.06
2015/05	2.61	1.10	0.29	0.60	836.37	25.06
2015/06	2.31	0.97	0.26	0.53	994.80	29.81
2015/07	2.67	1.12	0.30	0.61	869.05	26.04
2015/08	2.99	1.26	0.33	0.69	736.61	22.07
2015/09	3.34	1.41	0.37	0.77	689.69	20.67
2015/10	3.58	1.51	0.40	0.82	597.16	17.89
2015/11	4.07	1.71	0.46	0.93	555.62	16.65
2015/12	3.82	1.61	0.43	0.88	567.79	17.01
Count 2014	370.00	370.00	370.00	370.00	362.00	362.00
Count 2015	373.00	373.00	373.00	373.00	373.00	373.00

Bulk stomatal, boundary layer and substrate soil surface resistance						
	Bulk resistance of canopy stomatal	Relative Humidity	Wind speed at top of canopy	Hydraulic resistance of the concentrated boundary layer	Bulk boundary layer resistance of canopy	Substrate soil surface resistance
Date	r^c_s	RH	u_h	r_b	r^c_a	r^s_s
	s/m	%	m/s	s/m	s/m	s/m
2014/01	83.55	74.58	0.21	16.51	1.69	200.00
2014/02	83.55	71.40	0.91	6.33	0.65	200.00
2014/03	83.55	80.48	0.86	6.58	0.67	200.00
2014/04	83.55	77.57	0.87	6.55	0.67	200.00
2014/05	83.55	75.74	0.91	6.41	0.66	200.00
2014/06	83.55	69.93	0.81	7.16	0.73	200.00
2014/07	83.55	68.23	0.97	6.21	0.64	200.00
2014/08	83.55	72.20	1.03	6.18	0.63	200.00
2014/09	83.55	71.33	1.18	5.61	0.57	200.00
2014/10	83.55	74.84	1.10	5.80	0.59	200.00
2014/11	83.55	74.29	1.05	5.99	0.61	200.00
2014/12	83.55	75.34	1.04	5.94	0.61	200.00
2015/01	83.55	74.45	1.07	5.88	0.60	200.00
2015/02	83.55	74.75	1.01	6.09	0.62	200.00
2015/03	83.55	73.03	0.94	6.27	0.64	200.00
2015/04	83.55	72.25	0.86	6.58	0.67	200.00
2015/05	83.55	74.39	0.86	6.59	0.67	200.00
2015/06	83.55	69.43	0.76	7.14	0.73	200.00
2015/07	83.55	72.55	0.88	6.67	0.68	200.00
2015/08	83.55	71.06	0.98	6.17	0.63	200.00
2015/09	83.55	72.30	1.10	5.94	0.61	200.00
2015/10	83.55	68.84	1.18	5.58	0.57	200.00
2015/11	83.55	67.63	1.34	5.35	0.55	200.00
2015/12	83.55	69.03	1.26	5.43	0.56	200.00
Count 2014	376.00	347.00	370.00	362.00	362.00	376.00
Count 2015	376.00	373.00	373.00	373.00	373.00	376.00

Net radiations							
	Solar radiation	Clear sky solar radiation	Net solar radiation	Net loss of long wave radiation energy to atmosphere	Net radiation over vegetation cover	Radiation reaching soil surface	Soil heat flux
Date	R_{solar}	R^0_{solar}	R_{ns}	R_{nl}	R_n	R^s_n	G
	$MJ/m^2/d$	$MJ/m^2/d$	$MJ/m^2/d$	$MJ/m^2/d$	$MJ/m^2/d$	$MJ/m^2/d$	°C
2014/01	19.72	23.93	15.90	3.42	12.49	1.09	-0.0042
2014/02	18.27	22.06	14.74	3.70	11.04	0.96	0.0057
2014/03	17.76	19.35	14.33	3.82	10.51	0.91	-0.0052
2014/04	18.83	16.67	15.19	5.80	9.39	0.82	-0.0144
2014/05	19.25	13.98	15.53	7.97	7.56	0.66	0.0059
2014/06	16.86	12.01	13.60	8.75	4.84	0.42	-0.0210
2014/07	17.99	12.83	14.51	9.09	5.42	0.47	-0.0095
2014/08	16.95	15.24	13.67	6.37	7.30	0.63	0.0198
2014/09	14.78	17.54	11.92	4.25	7.67	0.67	0.0007
2014/10	13.17	19.97	10.62	2.93	7.69	0.67	0.0138
2014/11	15.00	22.02	12.10	2.83	9.27	0.81	0.0073
2014/12	14.09	22.85	11.36	2.24	9.12	0.79	-0.0306
2015/01	19.72	23.93	15.90	3.32	12.59	1.09	0.0020
2015/02	18.27	22.06	14.74	3.36	11.37	0.99	0.0009
2015/03	17.76	19.35	14.33	3.95	10.38	0.90	-0.0086
2015/04	18.83	16.67	15.19	5.87	9.32	0.81	-0.0137
2015/05	19.25	13.98	15.53	7.39	8.13	0.71	-0.0018
2015/06	16.86	12.01	13.60	8.74	4.85	0.42	-0.0179

2015/07	17.99	12.83	14.51	8.62	5.89	0.51	-0.0145
2015/08	16.95	15.24	13.67	6.33	7.34	0.64	0.0402
2015/09	14.78	17.54	11.92	4.13	7.78	0.68	0.0001
2015/10	13.17	19.97	10.62	2.77	7.85	0.68	0.0073
2015/11	15.00	22.02	12.10	2.97	9.13	0.79	-0.0021
2015/12	14.09	22.85	11.36	2.22	9.14	0.79	-0.0607
Count 2014	376.00	376.00	376.00	347.00	347.00	347.00	365.00
Count 2015	376.00	376.00	376.00	373.00	373.00	373.00	371.00

Total evapotranspiration and S&W parameters										
	Model Parameters			Canopy transpiration weighting coefficient	Bare substrate evaporation weighting coefficient	Evaporation from soil	Transpiration from canopy	Latent heat transfer ET	Simulated evapo-transpiration
Date	R_a	R_c	R_s	C_c	C_s	ET_s	ET_c	λET	ET_o
	-	-	-	-	-	mm/day	mm/day	mm/day	mm/day
2014/01	50.07	6.10	1704.69	0.99	0.20	0.58	11.43	11.44	4.69
2014/02	5.95	5.81	232.40	0.99	0.50	0.20	12.99	12.92	5.29
2014/03	6.47	5.81	249.55	0.99	0.49	0.20	9.76	9.74	3.99
2014/04	5.69	5.78	223.64	0.99	0.52	0.16	9.23	9.20	3.76
2014/05	5.09	5.75	203.44	0.99	0.54	0.13	8.65	8.61	3.51
2014/06	6.07	5.75	236.04	0.99	0.52	0.11	8.45	8.40	3.42
2014/07	4.36	5.72	179.18	0.99	0.58	0.11	9.18	9.12	3.71
2014/08	4.71	5.74	190.83	0.99	0.57	0.13	9.08	9.02	3.68
2014/09	3.98	5.74	166.51	0.99	0.60	0.13	10.69	10.62	4.33
2014/10	4.13	5.74	171.39	0.99	0.59	0.12	8.98	8.92	3.64
2014/11	4.99	5.78	200.10	0.99	0.55	0.16	10.70	10.64	4.35
2014/12	5.09	5.79	203.60	0.99	0.54	0.16	10.99	10.94	4.48
2015/01	5.42	5.81	214.74	0.99	0.53	0.22	13.23	13.18	5.40
2015/02	5.76	5.81	226.00	0.99	0.52	0.21	12.51	12.46	5.11
2015/03	6.07	5.82	236.49	0.99	0.50	0.21	12.60	12.55	5.15
2015/04	6.04	5.79	235.20	0.99	0.50	0.18	11.05	11.00	4.50
2015/05	5.97	5.79	232.85	0.99	0.51	0.16	10.04	9.99	4.09
2015/06	6.05	5.75	235.45	0.99	0.51	0.12	8.93	8.88	3.62
2015/07	5.23	5.74	208.25	0.99	0.54	0.12	8.51	8.46	3.45

2015/08	4.64	5.75	188.31	0.99	0.56	0.13	9.95	9.89	4.03
2015/09	4.62	5.76	187.98	0.99	0.57	0.14	10.63	10.57	4.32
2015/10	4.35	5.77	178.82	0.99	0.58	0.16	12.60	12.52	5.12
2015/11	4.02	5.76	167.78	0.99	0.60	0.16	13.60	13.51	5.52
2015/12	4.62	5.80	188.14	0.99	0.57	0.19	14.74	14.64	6.01
Count 2014	362.00	362.00	362.00	362.00	362.00	330.00	330.00	330.00	330.00
Count 2015	373.00	373.00	373.00	373.00	373.00	368.00	368.00	368.00	368.00